POLITECNICO DI MILANO

School of Industrial and Information Engineering

Master of Science in Energy Engineering

Development of a Stationary and a Preliminary Dynamic Model for Proton Exchange Membrane (PEM) Electrolyzer

Supervisor:

Prof. Stefano Campanari

Co-supervisor:

Ing. Paolo Colbertaldo

Master of Science Thesis submitted by:

Vasileios Botsis Matricola: 873403

Academic Year 2018 – 2019

Extended Abstract

1. Introduction

One of the main and most representative effects of climate change is global warming, which mostly depends upon the increased level of greenhouse gases (GHG) in the atmosphere. These gases include CO_2, CH_4 and other compounds that are released both naturally and from human activities. The CO_2 released to the atmosphere is mainly produced during the combustion of fossil fuels (e.g., coal, oil, natural gas). Considering the increase of TPES by almost 2.5 times between 1971 and 2016 [1], CO_2 emissions have been doubled. A robust solution to overcome the climate change effects was introduced with the use of clean sources of energy (e.g. solar, wind) to generate electricity, especially, to cover the growing demand of energy in a sustainable way. In the path towards the increase of the share of renewables in the energy map, new challenges are arising concerning storing and utilization of the surplus energy, system operation, distributed generation management, energy supply reliability, and future integration with an automotive sector based on the electric vehicles. The problem which arises with renewables is that they present significant challenges to grid operators, including intermittent output and a mismatch between peak output and peak demand, which can result in grid instability, negative pricing, and wasteful curtailment. The traditional way to store electricity for non-residential application is pumped hydro storage but this way is not always available. In small scale power plants, batteries are the most used but can be characterized as unsustainable, due to the toxic materials and the recycling process. An alternative way of storage is through water electrolysis, which can also be used to produce H_2 with a sustainable way. Aiming at the decarbonization and the reduction of CO_2 setting as a goal the environmental sustainability, it can be easily understood that water electrolysis is widely agreed to be the most interesting source of sustainable hydrogen for the future, an advantaged is the integration with renewable energy sources [9]. The three main technologies which lead to the classification of electrolyzers are: AEC, PEMEC, SOEC [10]. From them PEMEC has a comparative advantage due to the fact that can operate under different pressures at the two side of the electrolyzer, which will facilitate hydrogen storage. PEMEC solid electrolyte enables a more compact design and operation at differential pressures is feasible and it can be combined with application of a variable power load due to its faster response in dynamic systems [16].

Table 1.1 indicates that PEMEC is still required to characterize and improve both in terms of models and experimental analysis. The study of PEM electrolyzers, both in term of stack and system, have been addressed by scientists only over the last 15 years. There have been numerous experimental studies investigating different aspects of PEMEC operation [10, 28]. The current thesis presents a numerical model that describes a PEM electrolysis stack under a zero-dimension approach in both steady state and dynamic conditions. The aim is to simulate the operation of a commercial PEM electrolyzer that was experimentally tested, featuring a nominal power of 60 kW_{AC} manufactured by Proton On Site.

Advantages	Disadvantages
Current density: High **Voltage efficiency:** High **Load range:** Good partial load range **System Design:** compact **Degree of Purity:** High gas purity **Dynamic:** high dynamic operation **Response:** rapid system response	**Technology:** New and partially established **Cost:** High cost of components **Catalyst type:** Noble catalyst **Corrosion:** acidic environment **Durability:** comparatively low **Stack:** Below MW range **Membrane:** limited and costly **Commercialization** is in near term

Table 1.1: Advantages & disadvantages of PEMEC

2. Water Electrolysis

Electrolysis is historically known as an electrochemical process for splitting water into hydrogen and oxygen. The overall chemical reaction involved can be written as:

$$2H_2O \rightarrow 2H_2 + O_2 \quad (1)$$

The chemical reaction in eq.1, thermodynamically speaking, is not expected to occur. This means that a form of energy must be provide in order to propagate it. So, a more correct form of this equation can be seen in eq.2:

$$H_2O_{(l)} + 237.2 \ + 48.6 \ \rightarrow H_{2(g)} + 1/2O_{2(l)} \quad (2)$$

The energy of 237.2 kJ/mol refers to the electricity that must be provided from an external source, while the 48.6 kJ/mol refers to the additional heat [18]. In the electrochemical water electrolysis, the cell is separated into two different areas where two different electrochemical reactions occurred. Where oxidation of the species occurs, here water is split into O_2 and H^+ this is called anode (+) and for simplicity it is called oxygen evolution reaction (OER). Where reduction occurs, here where H_2 is formed, this is called cathode (-) and for simplicity it is called hydrogen evolution reaction (HER). When an electrolytic cell operates at constant temperature and pressure, the required energy for the water electrolysis reaction is determined by the process enthalpy change ΔH. For this reaction to take place, part of the energy provided by electric power. This part corresponds to the Gibbs' free energy change ΔG. The rest is thermal energy Q and equals to the product of the process temperature T and the entropy change ΔS. The following expression shows the relation among these thermodynamic magnitudes.

$$\Delta G = \Delta H - Q = \Delta H - T\Delta S \quad (3)$$

The ideal work consumed from a water electrolyzer can be extracted by eq.3 and it is called the reversible work Wrev or reversible potential difference Erev (Open circuit voltage, OCV) when eq.4 is applied. The Erev is the lowest required voltage for the electrolysis to take place. This voltage can be calculated as a function of Gibbs free energy as:

$$E_{rev} = \frac{\Delta G_R}{zF} \quad (4)$$

Where z is the numbers of electrons that participate in the reaction, in this case z=2 and F is the Faraday's constant which represents the charge on one mole of electrons (96,485 C/mol). A better way to describe eq.4 is to refer E^o_{rev} which stands for the cell voltages under standard conditions (Pressure (P), Temperature (T): Constant). The latter can be explained because even if a system works under constant T, P if the operation conditions change, then the equilibrium potential also will be changed. At standard temperature and pressure (298.15 K and 1 atm), ΔG_R^o =237.21 kJ/mol, ΔS^o= 0.1631 kJ/mol K, and ΔH^o= 285.84 kJ/mol. By substituting ΔG_R^o and ΔH^o in eq.3 and eq.4 the E^o_{rev} = 1.229 V.[28], [29], without having an external heat source, the entire energy for the reaction to take place ΔH^O_R must be delivered by electrical energy. Hence, the voltage required is higher than E^o_{rev} and is called the thermoneutral voltage E^o_{th} at standard state.

$$E_{th} = \frac{\Delta H_R^O}{zF} = 1.481 \quad (5)$$

The equilibrium potential difference as it was mentioned previously, is a function of temperature at STP. Moreover, the E_{eq} is depending also on the activities (α_i) of the species. eq.6 shows this depends and it known as Nernst's equation[28].

$$E_{rev} = \ E^o_{rev} \ - \frac{RT}{2F} \ln\left(\frac{p_{H_2} p_{O_2}^{0,5}}{\alpha_{H20}}\right) \quad (6)$$

Where p_{H2} and p_{O2} are the partial pressure of hydrogen and oxygen, respectively. One other important relation for the electrochemical cells is Faraday's equation:

$$i = \frac{n_e F Q_i}{A_{cell}} \quad (7)$$

Where n_e is the electrons moles per hydrogen moles for water the value is 2, i is the current density (A/cm^2), Qi (mol/s) is the molar mass flow of the species (which later will be used with letter F_i) and Acell (cm^2) is the area of the cell. Faraday's equation is very important when the cell or stack is being modelled on the part of mass balance [28].

3. Modelling of PEM Electrolyzer

The working principle of PEM, reactions on each electrode and thermodynamics of the cell need to be known to better understand the PEM electrolyzers. The electrolysis cell is a reaction medium composed of membrane

electrode assembly (MEA), the electric current collectors, the gas distribution layers (GDL) and the gaskets. A typically schematic representation of the parts of a single electrolysis cell is given in Figure 3.1. The electrolysis cell is a reaction medium composed of membrane electrode assembly (MEA), the electric current collectors, the gas distribution layers (GDL) and the gaskets. A typically schematic representation of the parts of a single electrolysis cell is given in Figure 3.1. To model PEMEC, the current work developed a semi-empirical model in zero dimension, first for steady state and second for dynamic state. This is done considering the interactions between various subgroups of the model on the anode, the cathode, voltage calculation, mass transport phenomena and thermal energy balance. For the latter an extended literature review was done, to identify values and ranges for the parameters that are involved in the mass balance, electrochemical and energy balance equations of PEMEC. Although the modelling work aims at generality, some features need to be specified to select the proper equations and assumptions. Moreover, the experimental data that will be used for validation comes from experimental work performed by researchers of the Department of Energy of Politecnico di Milano that inevitably involves a PEMEC system made by Proton On Site company. Hence, it is relevant to detail some characteristics of the tested device in Table 3.1.

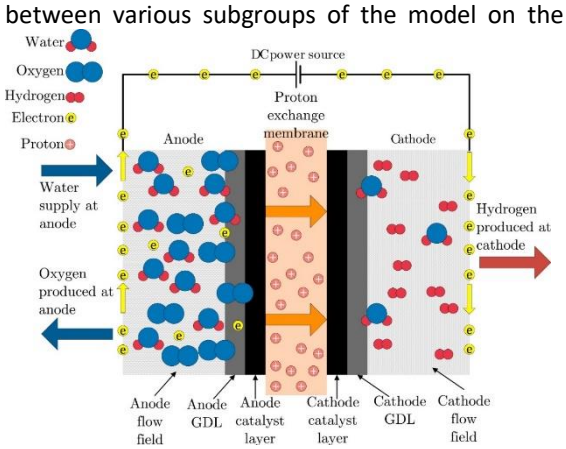

Figure 3.1: Schematic representation of a PEM electrolyzer

Table3.1: List of main technical characteristics of the considered device by Proton On Site

Parameter	Value
Nominal power	60 kW
Number of stacks	1
Outlet H2 flow rate	10 Nm_3/h
Nominal H2 delivery pressure	30 barg
H2 delivery purity	99.9998 %
Expected specific consumption	68.9 kWh/kgH2
Number of cells	65
Active area per cell	213,67 cm^2
Nominal voltage	137 V
Nominal current density	1.9 A cm^{-2}

- **Mass balance**

In the anode side water is oxidized and oxygen produced according to, eq 8,9 and 10 where Fin and F^{out} are anode inlet and outlet molar flow rates of O_2, H_2O and H_2 respectively, F^{gen} is the molar flow rate of oxygen generation at the anode, F^{cons} is the molar flow rate of water consumed at the anode and F^{mem} is the molar flow rate of membrane water. The terms of F^{gen} , F^{cons} are computed with eq. 7. The inlet flow rate of oxygen is zero. The term F^{perm} stands for the cross penetration of the O2 that potentially can travel through the membrane.

$$\frac{dN_{O_2}}{dt} = F_{O_2}^{in} - F_{O_2}^{out} + F_{O_2}^{gen} - F_{O_2}^{perm} \quad (8)$$

$$\frac{dN_{H_2O}}{dt} = F_{H_2O}^{in} - F_{H_2O}^{out} - F_{H_2O}^{cons} - F_{H_2O}^{mem} \quad (9)$$

$$\frac{dN_{H_2}}{dt} = F_{H_2}^{perm} - F_{H_2}^{out} \quad (10)$$

This phenomenon was reviewed by Ito et al. [8] and they computed F^{perm} as:

$$F_{O_2}^{perm} = \frac{K_{p,O_2}\ A_{cell}\ (y_{O_2}^{mean_{an}} P_{mean}^{an} - y_{O_2}^{out_c} P_c)}{(t_{mem} + t_{el}^{an} + t_{el}^{c})} \quad (11)$$

Where $K_{P,O2}$ [mol/(m s Pa)] is the permeability coefficient for O_2. Kim et al.[77] , suggest that this flow is significantly lower than the H_2 due to the size of the molecules, so they neglect it. Nevertheless, in the current study for the validity of the model it is included it and it is handled as a fixed parameter; its value is obtained from the literature ($1.62 \cdot 10^{-16}$ mol/m s Pa) [78]. Similarly, with the O_2, H_2 permeability can be written as:

$$F_{H_2}^{perm} = \frac{K_{p,H_2}\ A_{cell}\ (y_{H_2}^{out_c} P_C - y_{H_2}^{mean_{an}} P_{mean}^{an})}{(t_{mem} + t_{el}^{an} + t_{el}^{c})} \quad (12)$$

The $K_{P,H2}$ [mol/(m s Pa)] is again a small value but according to [78], [77] , [32] this value is twice than the value of the oxygen permeability, so the assumption is $3 \cdot 10^{-16}$ mol/m s Pa. Nevertheless, flows are very small compared to the others flows, and they do not have a significant role in the performance of the model. To compute the

vapor fractions yi that appear in eq. 11,12 it was used the library of Aspen Customer Modeler given the pressures and the temperature combine with the assumption that the gas behaves as Ideal. P^{an}_{mean} is the mean pressure of the anode side. For the zero-dimension model that was followed in the current study it has been assumed that the Pin, inlet pressure on the anode side, is decreasing linearly with a slope 0.1 (10% pressure drop). Moreover, it was assumed that the total composition of the flows in the outlet of the anode side (zi) is equal to the mean values of the same parameter.

In the cathode side protons are reduce to H_2. The mass balances of H_2, H_2O, O_2 are:

$$\frac{dN_{H_2}}{dt} = F_{H_2}^{in} - F_{H_2}^{out} + F_{H_2}^{gen} - F_{H_2}^{perm} \quad (13)$$

$$\frac{dN_{H_2O}}{dt} = F_{H_2O}^{in} - F_{H_2O}^{out} + F_{H_2O}^{mem} \quad (14)$$

$$\frac{dN_{O_2}}{dt} = F_{O_2}^{perm} - F_{O_2}^{out} \quad (15)$$

The F^{perm} are calculated with eq.11 and 12 while the values F^{in} for both the water and the hydrogen are equal to zero. For the F^{mem} which appears on eq. 9 and 14, is calculated based on:

$$F_{H_2O}^{mem} = F_{H_2O}^{diff} + F_{H_2O}^{eo} - F_{H_2O}^{pe} \quad (16)$$

Where F^{diff} is the molar flow rate of water due to diffusion from anode to cathode, F^{eo} is the molar flow rate of water from anode to cathode due to electro-osmotic drag and F^{pe} is the molar flow rate of water from the cathode to the anode due to the pressure effect. The electro-osmotic drag is directly related to the flux of hydrated protons migrating from the anode to the cathode through the membrane and so the molar flow rate can be expressed as:

$$F_{H_2O}^{eo} = \frac{n_{eo} I}{F} \quad (17)$$

Where the n_{eo} is the electro-osmotic drag coefficient [mol_{H2O} /mol $_{H3O+}$]. Gorgun et. al [80] used a correlation, based on Dutta S, Shimpalaee S, Zee JWV (2001) paper, which depending on the arithmetic mean of water content in the membrane between cathode and anode.

$$n_{eo} = 0.0029\lambda_m^2 + 0.05\lambda_m - 3.4e^{-19} \quad (18)$$

Where λ_m is the degree of hydration [mol_{H2O}/mol_{so-3}] of the membrane and it depends on the water activity α_w on the interfaces of the membrane. Measuring the water content, λ, of membrane in contact with liquid water, Zawodzinski et al. [81] reported λ values of 17 and 22 of Nafion membrane in contact with liquid water at 30 and 80 °C, respectively. For the current model a λ_m equal to 21 was adopted. For this value n_{eo} is equal to 2.33. Moreover in [83] the value of their model is 5. For the current model the values of 2.33 and 5 was chosen, to be tested. The flow through the membrane due to diffusion is expressed by a Fick's law relation between the two membrane interfaces (anode and cathode):

$$F_{H_2O}^{diff} = \frac{AD_w}{t_{mem}} (C_{H2O,mem}^{an} - C_{H2O,mem}^{c}) \quad (19)$$

Dw [m^2 /s] which is the diffusion coefficient of water in the membrane and the C_{H2O} are the two concentration of water in the anode and the cathode interface (the "mem" subscription) respectively. In the [68, 84, 85] they introduce D_w as a function of temperature and λ:

$$D_w = D_\lambda \exp\left[2416\left(\frac{1}{T_{amb}} - \frac{1}{T_{op}}\right)\right] \quad (20)$$

Where D_λ is the value $1.25 \cdot 10^{-10}$ m^2/s for $\lambda > 4.5$. For the concertation of the water in the membrane interface, it was applied the diffusion of water in the GDL, considering the porosity (0.3) of GDL, and the H_2O/H_2 and H_2O/O_2 mixtures. For the calculation of F^{pe} Darcy's law was used:

$$F_{H_2O}^{pe} = K_{Darcy} A_{cell} \frac{\rho_{H2O,C} \left(P_c - P_{mean,an}\right)}{\mu_{H2O} * t_{mem}} \quad (21)$$

Where K_{Darcy} is the membrane permeability (m2) to water, μH2O is the viscosity of water and ρH2O is the density of water in the cathode side. The value of K_{Darcy} is obtained by the literature 1.58·10-18 m^2.[6, 72, 77, 79].

- **Electrochemical relations**

For the electrochemical relations of the cell it was consider the equation that introduces the potential of the cell with respect to the over potentials that are introduced at the system.

$$Vcell = E_{rev} + \eta_{ohmic} + \eta_{act} + \eta_{diff} \quad (22)$$

E_{rev} is calculate with eq.6. η_{act} is the activation over potential and it is calculated using Butler-Volmer equation both for anode and cathode:

$$i_{el} = i_{o,el} \{exp\left[\frac{a_{el} zF\eta_{el}}{RT}\right] - exp\left[\frac{(1 - aa_{el})zF\eta_{el}}{RT}\right]\} \quad (23)$$

Where $i_{o,el}$ and α_{el} are the exchange current density and the transfer coefficient, respectively. Both are obtained by the literature and proper values on their range were obtained.

Table 3.2: Exchange currents and Transfer coefficient from literature

Paper	$i_{o,el}$ (an/c) [A/cm^2]	α_{el} (an/c) [-]
[83]	an: 10^{-7}, c: 10^{-1}	αan = 0.8, αc = 0.25
[67]	an: $2{\cdot}10^{-7}$, c: $2{\cdot}10^{-3}$	αan = 2, αc = 0.5
[3]	an/c: range [10^{-13} -10^{-6}]	αan = range [0.18- 0.42]
[63]	an: 10^{-7}, c: 10^{-3}	αan = 0.5, αc = 0.5
[69]	an: 10^{-6}, c: (-)	αan = (-), αc = (-)
[61]	an: 10^{-7}, c: 10^{-3}	αan = 0.5, αc = 0.5
[58]	an: range [10^{-9}- 10^{-12}], c: 10^{-3}	αan = range [0.1- 0.6], αc = 0.5

The ohmic overpotential (η_{ohm}) is calculated by the summation of the resistance on the membrane and the electrodes both in anode and cathode applied Ohm's law. For the electrode resistance (R_{el}), it was assumed that the material was graphite /carbon with a porosity 0.3 and a resistivity 7.5 μΩ cm [18, 72, 83, 90]. For the membrane resistance (R_{mem}) the value of conductivity was calculated according [93]:

$$\sigma_{mem} = (0.005139\lambda - 0.00326) \exp\left[1268\left(\frac{1}{303} - \frac{1}{T}\right)\right] \quad (24)$$

Where λ is 21. For the diffusion overpotential it was obtained a correlation base on a value of a limited current density (i_L) with a value of 6.2 A/cm^2 [74]:

$$\eta_{diff} = \frac{RT}{\alpha_{an}\, neF} \ln\left(\frac{i_L}{i_L - i}\right) \quad (25)$$

- **Energy Balance**

For the energy balance the model adopts a zero-dimension thermal capacitance model which represents a simplified approximation of the thermal models.

$$c_{th} \frac{d(T)}{d(t)} = \dot{E}_{in} - \dot{E}_{out} + P_{el} + \dot{Q}_{loss} \quad (26)$$

Where Cth equals to 50.1 [kJ/K] is the global thermal capacity of the stack, and it was calculated assuming reasonable geometrical and materials values. The Q_{loss} is the loss of heat due to free convection and radiation. Pel is the electrical input, E_{in} and E_{out} is calculated by the species enthalpy enters and leaving the stack.

4. Stationary Model results

Before showing the results, an analysis on experimental data was performed obtained by a commercial PEM electrolyzer system build by Proton On Site company. The experimental data of the current density, the voltage and the temperature were chosen to be tested. With this analysis, it was able to obtain suitable average values that were used for the calibration of the current model. Moreover, the analysis shows that the real system has a lot of perturbation in terms of current density, voltage and temperature when the electrical power varies. Moreover, an analysis was performed to the experimental production of H_2 compared to the theoretical H_2 production. The values that were obtained and were depicted as the red point in Figure 4.1, are represented in Table 4.1. With these values the calibration of the stationary model was performed to the parameters that show the greatest variation on Vcell when they change. To do so, a sensitivity analysis was performed on the different parameters which were categorized according to their physical representation. Their values and ranges were obtained from the literature review, when the model was set up (see. Table 4.2)

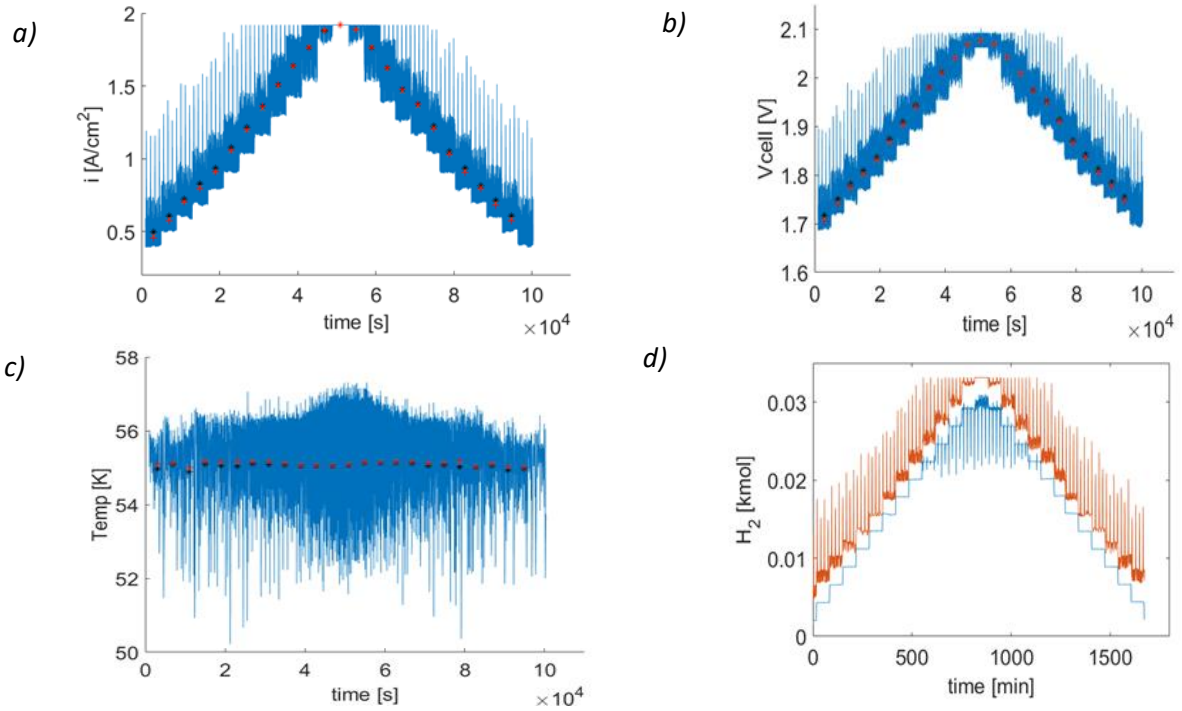

Figure 4.1: a) depicts the variation of current density over one day, b) depicts the variation of cell voltage over one day, c) depicts the variation of operation temperature over one day, d) depicts the cumulative H_2 production between theoretical (orange) and experimental (blue). The dots in a, b and c represents different average values that were used for the calibration

i [A/cm^2]	Vcell [V]	Top [^{o}C]
0.456	1.705	55.113
0.574	1.746	55.010
0.575	1.740	55.137
0.679	1.776	55.044
0.704	1.775	55.009
0.795	1.805	55.099
0.798	1.801	55.167
0.906	1.835	55.012
0.912	1.831	55.167
1.032	1.866	55.193
1.057	1.868	55.169
1.203	1.904	55.143
1.204	1.910	55.113
1.361	1.942	55.172
1.378	1.951	55.117
1.477	1.974	55.148
1.511	1.980	55.106
1.623	2.009	55.115
1.638	2.011	55.044
1.764	2.041	55.130
1.761	2.040	55.033
1.882	2.068	55.046
1.885	2.069	55.120
1.919	2.076	55.062

Table 4.1: The values of i, Vcell and Top that used for the calibration

Name	value	units
A_{cell}	213.68	cm^2
ε_{el}	0.3	-
$t_{el,a,c}$	0.0013	m
t_{mem}	Range: [1.25 e-4 : 2.5 e-4]	m
t_p	0,001	m
D_w	Eq. 20	m^2/s
D_λ	1.25e-10	m^2/s
λ	21	-
n_{eo}	5 or Eq.18	-
Kp_{O2}	1.62 e-16	mol/m s Pa
Kp_{H2}	3.0 e-16	mol/m s Pa
K_{darcy}	1.58e-18	m^2
P_{an}	2.5	bars
P_c	30	bars
ΔP_{an}	0.1	bars
n_e	2	
$i_{o,an}$	Range: [1 e-12: 1 e-6]	A/cm^2
$i_{o,c}$	Range: [1 e-6: e-3]	A/cm^2
iL	6.2	A/cm^2
α_{an}	Range: [0.5: 2]	-
α_c	Range: [0.25: 0.8]	-
ρ_{an} / ρ_c	0.0075	mΩ cm
σ_{mem}	Eq.24	S/cm
C_{th}	50.1	kJ/K

Table 4.2: The parameters of the model

The procedure that was chosen to perform the sensitivity analysis was the variation of the polarization curve (P-C). The current density was the input for the model's equation and the cell voltage the output. By changing the parameter that it wanted to be tested, it was possible to identify which of the parameters have a significal impact on the variation of the cell voltage. The width of membrane (t_{mem}) for the ranges that were introduced in Table 4.2, showed a variation almost null at low current density, but as the current density was increasing, the variation reached 8% difference on the Vcell when i equaled to 2.5 A/cm^2 and comparing the lowest and the highest value of the t_{mem}. The other parameters that were related with the geometrical characteristic of the cell, did not show any significant change on the Vcell and they are considered as fixed parameters. The electro-osmotic drag did not show any change at the P-C, in fact the difference was on the O.M of 10^{-10}, so practically zero. For the pressures a sensitivity analysis was held with respect to the cathode pressure which is the pressurized side of the cell. Two values were tested 10 bars and 50 bars. Both of them did not appear to have a significant change on the P-C, less than 1%, but the trend of the two pressures was the opposite since as pressure increases the losses are increasing due to the fact it penalizes the value of the ideal voltage. The most appreciable change in P-C was noticed when the exchange current and the transfer coefficient of anode and cathode were varied. These four terms affect the activation overpotential, so the P-C was moved vertically. The values that were tested, are depicted in Table 3.2. The results show that the P-C can change almost 30%. Figure 4.2 depicts the large variation on the Vcell. Lastly, all the curves are parallel with each other and only move up or down, the slope does not change, since there is no change in the ohmic losses. For the calibration the four parameters will be considered as fitting parameters to adjust the experimental data to the model. The last parameter which will be analyzed is the resistivity of the electrode. The resistivity will affect the slope of the curve meaning that if material with lower resistivity is used the slope will decrease. The problem with the ohmic losses is that there are too many parameters to be assumed, the resistivity and the width of the electrode, which both are used to calculate the Rohm. The ohmic losses also include the resistance of the separate plates which are made by the same material as the electrode. The values of the resistivity that were tested are 6.75 mΩ cm and 8.25 mΩ cm respect to the value of 7.5 mΩ cm that was assumed. The results showed that the resistivities do not affect the P-C. The P-C curves are almost equal and the relative change at its maximum value is 0.03%. In this case, even if it is observed that there is a small dependence, the resistivities will be used as fitting parameters in the model because there is only one parameter that counts for the ohmic losses and this is the width of the membrane.

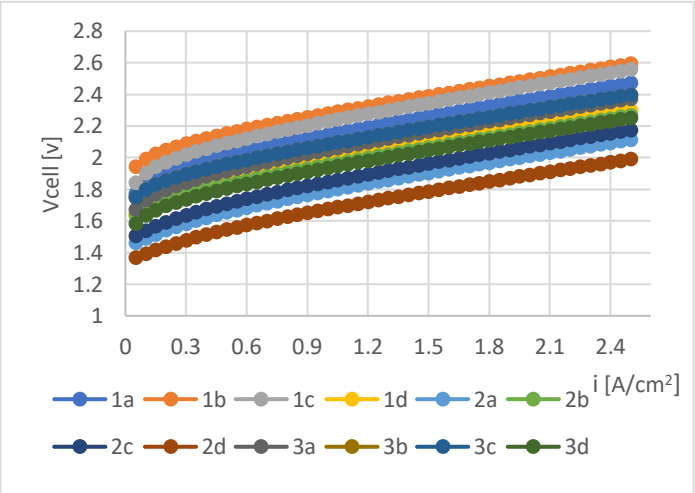

Figure 4.2: Different exchange currents and transfer coefficient were tested to obtain the dependence of Vcell

The calibration was performed in Aspen Custom Modeler. Aspen has a mathematical way to fit the parameters that were imposed on its software when the experimental data were introduced. Different cases for the estimation were performed, considering different procedures for each one of them. It has been noticed that the estimator of ACM is depending on the initial conditions that were set on the fitting parameters. So, the solutions obtained were not unique but were corresponding to the values that were set at the begging. Each case was evaluate respect to mean absolute relative deviation (MARD) from the experimental data (see Table 4.1). Twenty cases were examined and among them two were chosen with the lowest value (i.e. Est12 and Est18). Est12 has MARD equals to 0.104% and the Est18 has MARD 0.104%. The main difference of the two cases, is that the Est12 considers in the calibration the resistivities (ρ) of the electrodes and Est18 calculated a total Rel, which includes a lot of assumed parameters (i.e. the width of the electrodes, plates and the material). The ρel of the Est12 reached a value of 0.081 Ω cm, which according to the literature, no material, which was used to build the electrode of the PEMEC, fitted with this value, the value was high. So, during the fitting process the additional

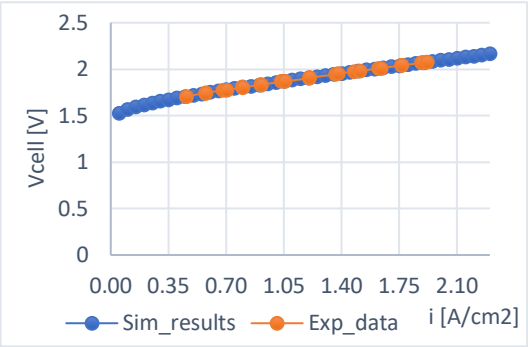

Figure 4.3: the result of the Est18 in terms of P-C comparing with the experimental data

resistivities of the plate and the width were included in the resistivities of the electrode. So physically, it would not be proper to show as a result, unrealistic values. Keep in mind that also the boundaries of the resistivities were imposed randomly. Between the two best fitted estimations the Est.18, was chosen because as it was explained the results need to have a physical correspondence. It should be noted also that the transfer coefficients have both almost symmetrical values for Est.18 which correspond with the literature's models. The exchange current for the anode is in the order of magnitude of 1e-7 which coincides with the papers of Z. Abdin et. al,[83] , Yigit et. al, [84] , Garcia-Valverde et. al,[74] and with Marangio et.al,[72], who said that this O.M. corresponds to the Pt catalyst. In Figure 4.3 is depicted the final P-C that was best fitted with the experimental data. The two lines are almost equal, which means that the calibration on the fitting parameters is representing the real stack; this also means that it can be used for further investigation in building a process that includes other parts of the real process, like the heat exchangers, pump, separators etc.

The model was validated by comparing the simulated results with experimental data that were obtained when the PEMEC system operated in full load. The results that were obtain in terms of MARD was 0.3%. Comparing the MARD of the Est18, 0.105% with the validating MARD, it is confirmed that the model almost perfectly predicts the voltage of the cell under various Top and i. in this point the stack can be used as a component to simulate a process that will represent a simplified process compared to the real one. Figure 4.4 visualizes the validation of the model. The first two dots represent the startup period of the system at partial load before the system reached the peak.

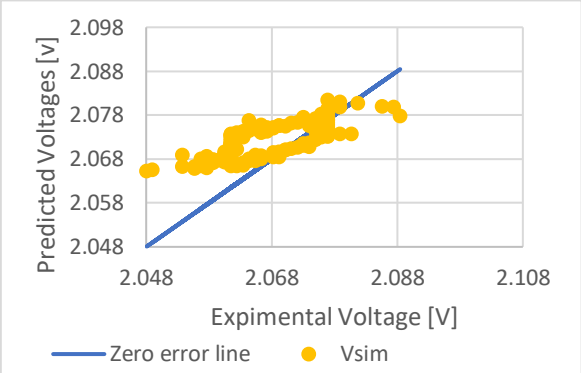

Figure 4.4: The validation results. The blue line is the zero-error line and the yellow dots are the results of the simulation against the experimental data.

5. Preliminary Dynamic Model of the System

It appears useful to integrate the dynamic model of the stack into a simulation of the entire system. Hence, a dynamic model of the electrolysis plant has been developed to investigate the performance. The system's components that were adopted for the analysis were: a) the stack, b) the separator of H_2O/H_2 and H_2O/O_2, c) the heat exchanger and d) two mixers. The simulation was set up in Aspen Plus dynamics. In addition, two PID controllers were added to the system related to temperature and power input because they are important to the system when the electrical input varies with time. The two PID controllers are introduced in the system for different reasons. The PIDel is connecting the stack with the electrical input. It reads the electrical input and generates a current density to the stack, which behaves as an input to the system to solve the equations of the stack's model. The variation of the electrical input has impact to the Top of the stack through the thermal sub-model. It is either increasing or decreasing the temperature of the system. The control of this behavior is done through the PIDtemp. The PIDtemp controls the Top by fixing the inlet temperature of water in the anode side. The set point of the controller is fixed to 56.6 ^oC, then the PIDtemp reads the temperature of the stack (Top) and as output signal gives signal to the HX1 to fix the temperature on the outlet stream S6, which is the inlet on the anode side of the stack. With these two controllers the simulated process tries to approach the real behavior of the system when the electrical input varies with time. The PIDel was tuned with very fast response since there were no data for the real controller's delay. While for the PIDtemp the strategy that was followed was to make reasonable assumptions for the three values that are responsible for the tuning (i.e. the proportional%, the integral time and the derivative time). The difficulty is that the temperature variation is not depending only on the PID controller but also on the C_{th}. The real system appears to have temperature perturbation even if it operates in almost constant power input. The results of The tuning of the PID controllers are depicted in Table 5.1

Table 5.1: The results of the tuned PID controllers of the simulated system

Controllers	Proportional [%]	Integraltime [h]	Derivative time [m]
PIDel	0.5	0.5	0
PIDtemp	0.06	2	10

The simulated configuration of the process does not include two components. The purification section, which would have required detailed information about the components and the control logics of that part of the process, which were not available, and the section where the hydrogen is compressed to be stored. From the two stages that were not considered in the system the most important is the purification column. It is affecting significantly the hydrogen production since part of the produced hydrogen is lost during this stage. The latter is depicted when the MARD is calculated between the theoretical and the experimental H_2 production (see. 4.1d). The theoretical H_2 is derived by simply applying eq. 7 for the H_2 and this is the maximum that it can be produced. From Figure 5.1 is derived that the loss of hydrogen from 0 to 300 mins declines from 80% to 13% that remain almost constant from 300 to 1400 mins and then it stars rising for the remaining time from 13% to 55%. It is clear that for every step in which the power is changed, also the current, the percentage is different when the cell is working in partial load. When it reaches the peak the penalty loss of hydrogen is less (around 15%) and it remains constant for the majority of the whole operation time. This indicate that its favourable for the stack to work in power input close to the peak since the electrical efficiency of the stack will be penalized less. It was chosen to run the simulation with the electrical power that corresponds to the peak load of the system. The same profile that was chosen to validate the steady state simulation. The time that the simulation was run was 990 s, where the first 90 s are characterized as start-up period. The simulation displayed the results every 15 s in order to be consistent with the real display time of the measurements. Between two time steps the simulation is running as in the steady state condition. Each perturbation of the electrical input is set to be a step wise variation and then the PIDel reads the signal and introduces the step wise variation with a delay of 2s. Figure 5.2 depicts the results that were obtained for the electrical input and current density, while Figure 5.3 shows the variation of the Tin, Top and the Texp with respect to time. Once again like the validation of the model in steady state condition, the measured current density is predicted well by the simulation with a MARD 4%. The difference on the current densities probably is mainly due to the purification stage and to the tuning of the PIDel. Nevertheless, they are almost equal, and it can be stated that the model of the whole system and not only the stack is able to have good approximation results on the current densities. The same will stand for the voltage, which is not depicted since it can be calculated by the power and the current density.

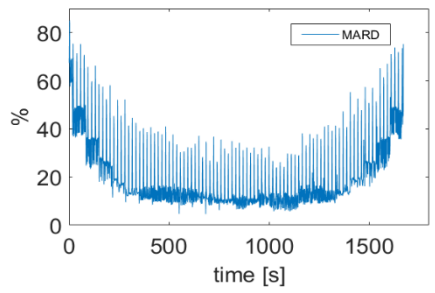

Figure 5.1: MARD between experimental and theoretical H_2 production.

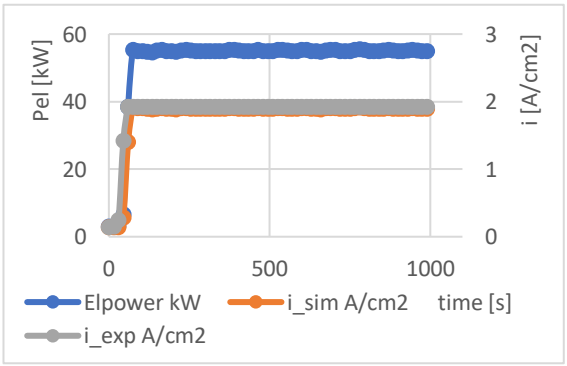

Figure 5.2: The variation over time of the electrical input and the simulated current density against the measured current density.

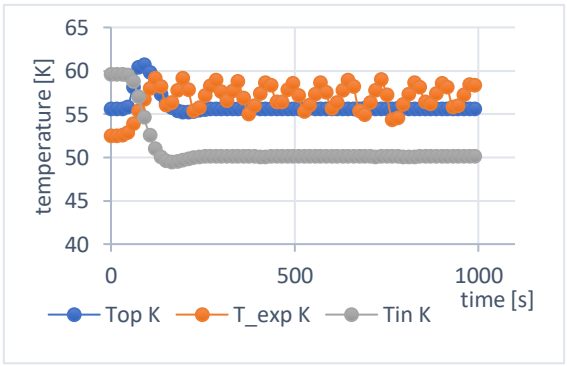

Figure 5.3: The temperature variation over time for the inlet, operation and measure temperatures

For the temperature profiles, in Figure 5.2, the simulation can predict up to a point the measured temperature, but it is constrained by the PIDtemp, even if the latter was not tuned with the best way to have some fluctuations. For small perturbation in the electrical input almost periodically there are some small peaks on the Texp which the Top from the simulation cannot predict. The cause of this, probably is related with the zero-dimensional model of the stack which is not calculating the change of the pressure in the anode and in the cathode side. Moreover, the simulated system is not built based on the real geometrical and material characteristics of the real process but from reasonable assumptions, which may lead to this temperature difference. As far as the Tin is concerned, at the beginning of the simulation it is higher than the Top meaning that the HX1 heats the water which enters the anode side of the stack. This behaviour was noticed generally when the system was working with a power input less than 20 kW, both in steady state and in the dynamic model. Generally, the heat exchanger on a PEMEC systems is designed to cool the stack. Probably, the latter was caused again on the implementation of a zero-dimension model in a simulated system. In the literature does not exist any zero-dimension model applicable to a simulated process, so no comparison was possible. Furthermore, at the begging of the operation, the experimental temperature is starting from around 52 °C, while the simulation temperature starts from 56 °C which is the set point of the PID. The simulation temperature follows this increase almost parallel but in higher temperature and it reaches the peak temperature (61 °C) in time equal to 80 s. The MARD again in this case is small 3%, but it cannot be a good indicator that the system will work perfectly for other applications for the reasons that were explained above. It was also tested the behaviour of the system when it was operated in partial load (36510 s to 37050 s) where its power input changed from 45 kW to 50 kW. The MARD once again was low around 2%. For the same partial load, it was also interesting to test the hydrogen production that the simulation predicts and to compare it with the theoretical and the experimental hydrogen production. Figure 5.4 shows the variation of hydrogen production among theoretical, simulated and experimental one. It also depicts the variation of the electrical input. Both the theoretical and simulated H_2 production follow the profile of the electrical input, since they have direct connections with it. The simulated production shows a small delay to adapt to the change in the electrical input, and this is a good indicator for the simulated system since it appears to have an inertial on the change which approaches better a real operation's behaviour. In the contrary the experimental H_2 cannot be predicted as it was expected since the purification stage is not implemented. The MARD between simulated and experimental is 11% and between the simulated and theoretical production is 19%. Generally, the simulated is predicting better the real production since in the model there is a small amount of H_2 that due to permeability of the Hydrogen through the membrane is lost in the anode side, also there are some parasitic losses in the current which are 1% (Faraday's efficiency) and lastly the delay of the system in the change of the electrical input. So, up to a point the simulation can be used to give some reasonable results on the production of hydrogen before the purification stage. Figure 5.1 depicts the difference between the theoretical and the experimental production of hydrogen for the step 10 and 11 (608 to 618 mins), MARD was almost 15%. For the simulation when it was running on this time step was 11%. According to the Company Proton On site the hydrogen that they lose in the purification stage in the peak load is almost 10%, very close with the result on the sample that the simulation was chosen to run.

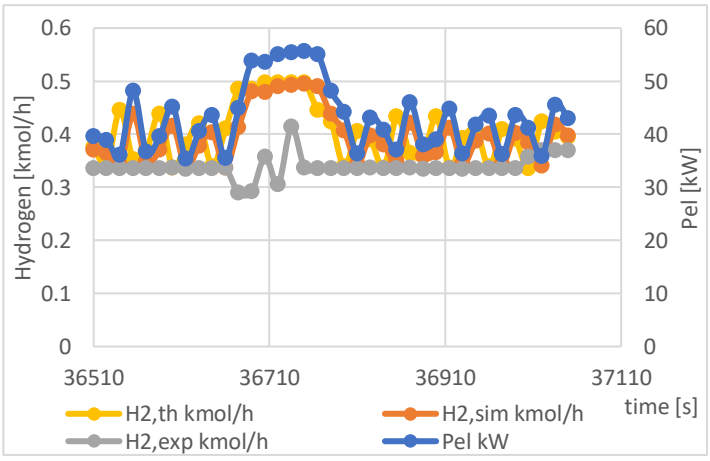

Figure 5.4: Comparison among the theoretical, simulated and experimental Hydrogen production.

6. Conclusions

The current thesis accomplishes to develop a stationary zero-dimension model for PEMEC which was implemented in a simulated system configuration based on a real process to analyze its behavior in a dynamic mode. The preliminary dynamic model that is suggested is able to predict with good approximation the temperature and the current variation when the power input varies. The hydrogen production is overestimated since the purification column is not included in the model. Further work will address a more detailed model in

higher dimension analysis than the current stationary model. Moreover, the stationary model can be validated with different experimental data sets which will be obtained from various PEMEC systems. For the dynamic simulated process, it is advisable to perform a complete validation of the model against a sufficient dataset of dynamic readings concerning reactant temperatures and flow rates. Finally, the modelling of the purification stage would be feasible to calibrate and validate the dynamic model in order to identified reasonable values for parameters that were assumed.

Acknowledgements

The work presented in this Master's thesis was carried out at the Politecnico Di Milano from May 2018 to April 2019 in the Department of Energy Engineering.

There are many people towards whom I am very grateful. First of all, I would like to direct huge thanks to my supervisors. First to *Professor Stefano Campanari* for giving me the chance to explore the exciting field of PEM water electrolysis and guided me safely through the difficulties of my thesis. Many thanks also to *Dr. Paolo Colbertaldo* for the hours, days and months that he spent to discuss all my problems by showing me the right path with his knowledge and all the material that he provided me during my thesis work.

I would like to give thanks to *Professor Andrea Casalegno* who did not participate in the current work but through his course, he initiated my passion about hydrogen technologies. Moreover, I am grateful that I had the chance to meet and discuss in academic and in personal manner with Professor *Luigi P. M. Colombo*, who always is present to help and guide all the students. I would like also to thank *Professor Gianluca Valenti*, whose dedication to his work induced students to become interested in energy, I hope that I passed him some knowledge about Greek letters.

To all my colleagues from the Master's degree, I wish you all the best for your future; if we manage to finish Politecnico Di Milano alive, we can accomplish whatever we aim for. The two years, I spent here were demanding and hard but there was also compensation: I met and became friends with people from all around the world. I would not have had the chance to share my joy, agony, problems and success with some persons that I met, if I had not made this big step in my life and I am glad that I did it. I give you thanks for all the support.

Last but not least, I would like to express my deep thanks, actually there are no words to describe it, to my father, my mother and the rest of my family whose support was astonishing. You make me a better person every day, thank you!

I hope that you find my work interesting and I hope that I was able to add a small piece of knowledge to the *"profound source of spirituality",* Science as *Carl Sagan* characterized it.

"*The more you know, the more you realize you know nothing.*", *Socrates said*, and this the reason why "*education is not something you can finish*", according to *Isaac Asimov.*

Abstract

Climate change and the accelerating depletion of fossil fuels have driven a tremendous surge in the development of clean and sustainable energy sources, *e.g.* wind, solar and hydro power. With an increasing market penetration of intermittent renewable energy generation, the need for energy storage is more apparent. Hydrogen has been identified as a suitable energy carrier and water electrolysis is the most promising way to produce it in a sustainable and environmentally friendly mode. PEM electrolysis is a rapidly evolving commercial technology which uses a solid polymer membrane as electrolyte in the device to split pure water into hydrogen and oxygen.

A layered zero-dimension model has been developed for this manner to simulate the performance of a PEMEC stack in Aspen Custom Modeler. In addition to the electrochemical equations that represent the water dissociation reaction, the model includes water, hydrogen and oxygen mass transport phenomena, electro-osmotic drag, diffusion and permeabilities through the membrane. A further feature of the model is that it considers a time-dependent lumped energy balance equation to analyze the dynamic inertia of the system when the electrical input fluctuates. Suitable values and assumptions were made to identify the model's parameters after an extended literature review.
To calibrate and validate the model, a set of experimental data was used which comes from experimental work performed by researchers of Politecnico di Milano. The experimental data were analyzed and evaluated in terms of the daily profiles when the electrical power input varies, using Matlab as software for the analysis, and these values were then used for the calibration of the model.

The model was calibrated and validated taking into consideration the most important parameters that affect the performance of the stack when it operates in steady state conditions. A sensitivity analysis was performed for each model's parameter and suitable ranges were identified to fit the experimental data. In particular, the parameters under investigation were the exchange currents and the transfer coefficients for both anode and cathode, the membrane thickness and the resistivities of the electrodes both at anode and at cathode. The results of the calibration were evaluated in term of mean absolute relative terms (MARD) and the best solution was obtained with MARD equals to 0.105%. The model was validated against different datasets, both with the stack operated at peak load for a day-long time horizon and for a variable input power. The results of the model validation showed an appropriate fitting, MARD equals 0.3%, with the stack behavior.

A preliminary dynamic system model was then implemented in Aspen Plus Dynamic to investigate the performance of the calibrated stack when the electrical input varies, considering the basic components that are present in an electrolyzer system: a heat exchanger, a water/oxygen and a water/hydrogen separator, a pump and two mixers. The data concerning the input-output flow rates, the variation of temperature and pressure of each component of the system were not available, so the assessment of the dynamic performance focused on the stack and the heat exchanger of the system that regulate the inlet anode temperature of the stack. The thermal capacity of the stack was obtained from the geometrical dimensions, with reasonable assumption on the materials of the stack. In this case, a calibration was not possible due to absence of suitable data. A comparison was performed in terms of current density and temperature between experimental and simulated results. The simulation predicted with good approximation both current density and temperature (4% and 3%)

into two different sample profiles of the experimental data. Lastly, a comparison was made between experimental and simulated hydrogen production. The simulated hydrogen production was overestimated and also appear to have fluctuating profile, whereas the experimental hydrogen production was more stable. This difference was mainly due to the hydrogen purification columns which were not included in this preliminary dynamic model of the system.

Sommario

Il cambiamento climatico e l'esaurimento dei combustibili fossili hanno avuto un ruolo importante nella ricerca e nello sviluppo di produzione energetica da fonti pulite e sostenibili, quali ad esempio eolico, solare e idroelettrico. Con la crescente penetrazione di fonti di energia rinnovabili intermittenti nel mercato elettrico, l'esigenza di immagazzinare energia prodotta diventa più rilevante. L'idrogeno è riconosciuto come un "energy carrier", ovvero un vettore energetico, generabile in modo pulito e sostenibile via idrolisi. L'elettrolisi via PEM è una tecnologia che si sta sviluppando rapidamente, già a maturità commerciale. Essa consiste nell'utilizzare un dispositivo basato su una membrana costituita da polimeri solidi per separare acqua pura in idrogeno ed ossigeno. Un modello zero-dimensionale *multi-layer* è stato sviluppato per rappresentare le prestazioni di uno stack PEMEC in Aspen Custom Modeler. Il modello considera il trasporto di massa di acqua, idrogeno e ossigeno, la resistenza elettro-osmotica, la diffusione e la permeabilità della membrana. Un'altra caratteristica del modello è l'inclusione di un bilancio energetico tempo-variante a parametri concentrati, allo scopo di considerare l'inerzia dinamica del sistema quando l'energia elettrica in ingresso varia o presenta oscillazioni. Dopo un'estesa revisione bibliografica, sono state identificate le principali assunzioni e i parametri del modello.

Il modello è stato calibrato e validato usando una serie di dati sperimentali ottenuti dal lavoro dei ricercatori del Politecnico di Milano. I dati sperimentali sono stati analizzati e processati in base alle variazioni giornaliere del profilo dell'energia elettrica in ingresso, usando Matlab come software di analisi, e questi valori sono poi stati usati per la calibrazione del modello. Il modello è stato calibrato e validato tenendo in considerazione i più importanti parametri che influenzano le prestazioni dello stack in condizioni di funzionamento stazionarie. Un'analisi di sensitività è stata sviluppata per ogni parametro del modello e sono stati ottenuti intervalli di valori appropriati da utilizzare nel *fitting* dei dati sperimentali. In particolare, i parametri analizzati sono la *exchange current* e i coefficienti di trasferimento sia per l'anodo che per il catodo, lo spessore della membrana e la resistività degli elettrodi all'anodo e al catodo. I risultati della calibrazione sono stati confrontati in termini di medie assolute relative (MARD), da cui è stata ottenuta la migliore soluzione. Il modello è stato validato tenendo in considerazione diversi set di dati, sia con lo stack che lavora a carico elettrico massimo, sia a carico variabile. Il risultato della validazione del modello mostra che il modello è in grado di rappresentare i dati sperimentali in maniera precisa.

Un modello dinamico preliminare dell'intero sistema di elettrolisi è stato sviluppato in Aspen Plus Dynamic per studiare le prestazioni dello stack al variare dell'energia elettrica in ingresso, tenendo in considerazione gli elementi base utilizzati nei sistemi di elettrolisi:: uno scambiatore di calore, un separatore acqua/ossigeno, un separatore acqua/idrogeno, una pompa e due miscelatori. I dati sui flussi in ingresso e in uscita e i dati sulle variazioni di temperatura e di pressione su tutti i componenti del sistema non erano disponibili, quindi l'analisi delle prestazioni dinamiche si è concentrata sullo stack e sullo scambiatore di calore che regola la temperatura del flusso in ingresso all'anodo. La capacità termica dello stack è stata stimata sulla base delle caratteristiche geometriche e di idonee ipotesi circa i materiali. Non sono state effettuate calibrazioni in tal senso in quanto non vi era

disponibile alcun dato utile. È stato effettuato un confronto tra i dati sperimentali e quelli simulati in termini di densità di corrente e temperatura. Il modello è stato in grado di predire con buona approssimazione entrambi i valori in due diversi profili campione di dati sperimentali. Infine, è stata confrontata la produzione di idrogeno tra i dati sperimentali e quelli simulati. La produzione di idrogeno risulta sovrastimata dal modello e risulta variabile nel tempo, mentre i dati sperimentali mostrano una produzione di idrogeno stazionaria. La differenza risiede principalmente nelle colonne di purificazione dell'idrogeno, che non sono state incluse in questo modello dinamico preliminare.

Table of Contents

List of Abbreviations

AEC	Alkaline Electrolysis Cell
ACM	Aspen Custom Modeler
APD	Aspen Plus Dynamics
B-V	Butler- Volmer
CL	Catalyst Layer
COP21	Paris Agreement
ESCA	Actual Electrocatalytic Surface Area
FC	Fuel Cell
GDL	Gas Diffusion Layer
GHG	Greenhouse Gases
HER	Hydrogen Evolution Reaction
HHV	Higher Heating Value
IEA	International Energy Agency
IHL	Inner Helmholtz Layer
LHV	Lower Heating Value
MARD	Mean Absolute Relative Difference
MEA	Membrane Electrode Assembly
OCV	Open Circuit Voltage
OER	Oxygen Evolution Reaction
OHL	Outer Helmholtz Layer
P-C	Polarization Curve
PEMEC	Proton Exchange Membrane Electrolysis Cell
PEMFC	Proton Exchange Membrane Fuel Cell
PFS	Perfluorinated Polymer
PFSA	Perfluorosulfonate Polymer Membrane
PV	Photovoltaic Panels
RDS	Rate Determining Step
SE4ALL	Sustainable Energy for All
SHE	Standard Hydrogen Electrode
SOEC	Solid Oxide Electrolysis Cell
TPES	Total Primary Energy Supply
UN	United Nations

Nomenclature

a Tafel slope [mV dec^{-1}]
a_i Activity of substance i [mol l^{-1}]
A Surface or area [m^2]
b Tafel constant [A m^{-2}]
c_i Molar concentration of substance [mol m^{-3}]
C_{th} Global thermal capacity [kJ K^{-}]
E_i Energy flow [kW]
D_{A-B} Binary diffusivity of the species [m s^{-1}]
Dw Diffusion Coefficient of water [m s^{-1}]
D_{eff} Effective diffusivity [m s^{-1}]
E_a Activation energy [kJ mol^{-1}]
E_{eq} Equilibrium potential [kJ mol^{-1}]
EW Equivalent weight
ΔG Molar Gibbs free energy [kJ mol^{-1}]
h_i Molar enthalpy of i [kJ mol^{-1}]
ΔH_i Enthalpy flow of substance i [kJ s^{-1}]
LHV Low heating value [kJ mol^{-1}]
i Current density [A cm^{-2}]
i_o Exchange current density [A cm^{-2}]
I Electrical current [A]
k Reaction rate constant [L mol^{-1} s^{-1}]
t_{mem} Membrane thickness [m]
m Mass [kg]
Mr Molecular mass [kg mol^{-1}]
N_i Amount of substance [mol]
n_{eo} Electro-osmotic drag coefficient
Fi Molar flow rate of i [mol s−1]
F Faraday's Constant [96,485 C mol^{-1}]
P Pressure [bar]
p_i Partial pressure of substance i [bar]
P_{el} Electrical power [kW]
Q_{loss} Heat flow to the environment [kW]
r Reaction rate per unit area [mol s^{-1} cm^{-2}]
R Universal gas constant [8.314 kJ $kmol^{-1}$ K^{-1}]
Ri Ohmic resistance of component i [Ω]
S Electrochemical active site [-]
ΔS Molar change in entropy [kJ K^{-1} mol^{-1}]
t Time interval [s]
T Temperature [K]
ΔT Temperature difference [K]
V Voltage [V]
z Charge number [-]

Greek letters

α transfer coefficient [-]
β Symmetry factor [-]
ε Porosity [-]
η Overpotential [V]
λ Water uptake [–]
ν Stoichiometric factor of i [–]
ρ_i Resistivity of i species [Ω cm]
ρ_{eff} Effective resistivity [Ω cm]
σ Conductivity [S cm−1]
σ_{boltz} Stefan- Boltzmann constant [$5.67 \cdot 10^{-8}$ W/m^2K^{-4}]
ω Water uptake

List of Figures

List of Tables

1. Introduction

1.1 The Climate Change Issue and the Role of Hydrogen

One of the main and most representative effects of climate change is global warming, which mostly depends upon the increased level of greenhouse gases (GHG) in the atmosphere. These gases include CO_2, CH_4 and other compounds that are released both naturally and from human activities. Their accumulation in the atmosphere enhances the greenhouse effect, which is beneficial for life up to certain levels, then determines dangerous effects. Greenhouse gas emissions from the energy sector represent roughly two-thirds of all anthropogenic greenhouse-gas emissions and CO_2 emissions from the sector have risen over the past century to even higher levels. The carbon dioxide released to the atmosphere is mainly produced during the combustion of fossil fuel (e.g., coal, oil, natural gas). Fossil fuels' combustion is the traditional way for humans to generate energy, and since energy is a driving force for technological and economic development, fossil fuels consumption and thus CO_2 concentration are increasing over time. The 20th century followed more or less the paradigm of the 19th century, during which development occurred by overexploiting the natural resources without taking into account the environmental impact. According to the international data provided by the International Energy Agency (IEA), the total primary energy supply (TPES) increased by almost 2.5 times between 1971 and 2016.[1]

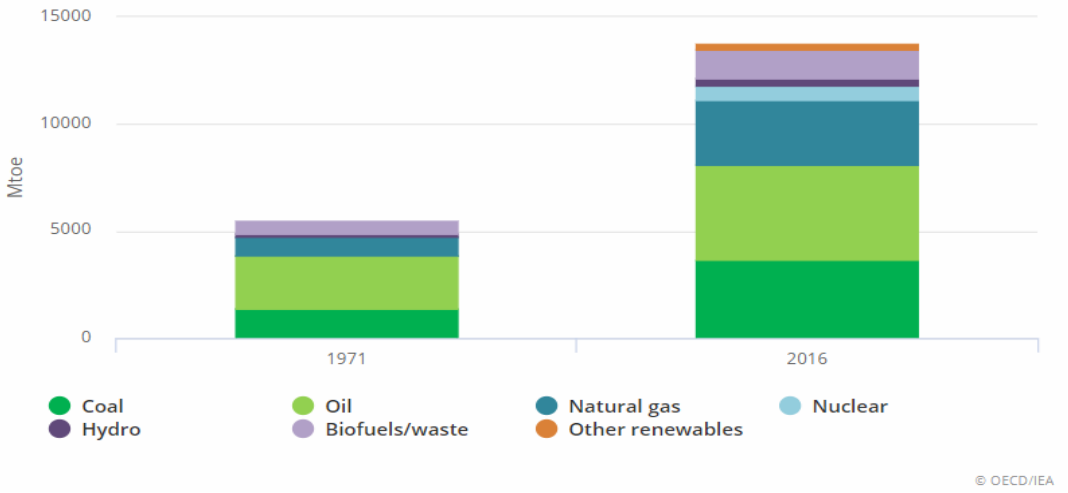

Figure 1.1: Total primary energy supply by fuel between for OECD countries in 1971 and in 2016 [2]

It can be seen from Figure 1.1 that oil was still the dominant fuel in 2016 but its share has decreased over the past decades. Moreover, Figure 1.2 indicates the increase on the annual emissions of CO_2 from 1971 to 2016. In 2016, global CO_2 emissions from fuel combustion were 32.31 $GtCO_2$, broadly the same as in 2015 (32.28 $GtCO_2$). They have more than doubled since the early seventies and increased by around 40% since 2000, generally linked to increased economic output.

These numbers indicate the urgent situation that causes global warning and the climate change. Several international conference have been held that gathered together countries to look for solution

to mitigate the problem of climate change, starting from the Kyoto's Protocol in 1990 which was put in effect in 1997 and is still in effect but is expected to cover only 10% of global GHG emissions (the target was to reduce the CO_2 emissions to a level 25% below the 1990 by 2020) by 2020. Furthermore, a major step to keep the global temperature rise below 2 ^oC has been introduced in the so-called Paris Agreement in 2015. The central aim of the Paris Agreement was to strengthen the global response to the threat of climate change [3]. Additionally, the agreement aimed to strengthen the ability of countries to deal with the impacts of climate change. To reach these ambitious goals, appropriate financial flows, a new technology framework and an enhanced capacity building framework will be put in place, thus supporting action by developing countries and the most vulnerable countries, in line with their own national objectives. The Agreement also provided for enhanced transparency of action and support through a more robust transparency framework. [1] [4]

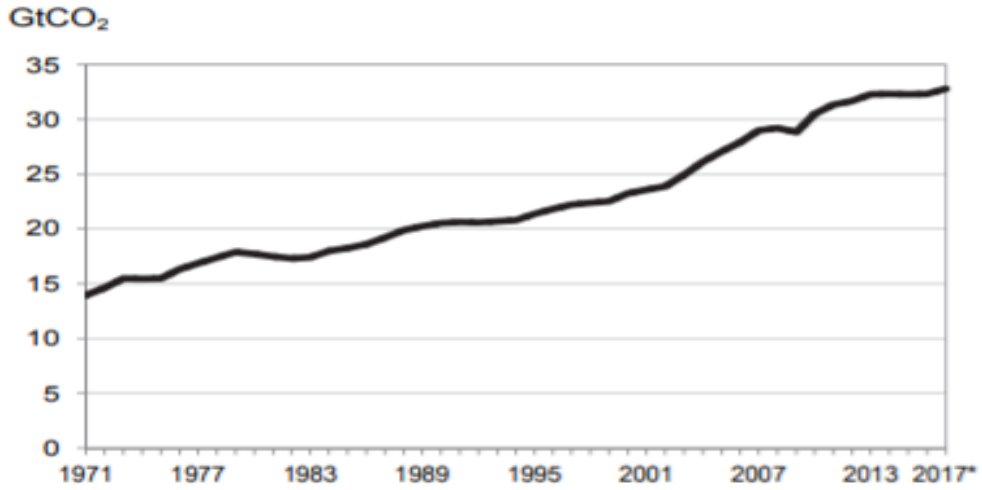

Figure 1.2: CO_2 emissions from fuel combustion; global trend

A robust solution to overcome the climate change effects was introduced with the use of clean sources of energy (e.g. solar, wind) to generate electricity. Specially, to cover the growing demand of energy with a sustainable way, as it was mentioned by the 2030 Agenda of the United Nations (UN), Paris Agreement (COP21) and Sustainable Energy for All (SE4ALL), the generation of electricity from environmentally friendly sources (e.g. hydro power, wind turbines and solar panels) is a good pathway. A more general path towards sustainability, that also includes the energy sectors, was introduced by the UN. They announced seventeen sustainable development goals and one-hundred-six targets in 2015 for the next 15 years in areas of critical importance for humanity and the planet. The seventh goal is to ensure access to affordable, reliable, sustainable and modern energy for all [5].

In the path towards the increase of the share of renewables in the energy map, new challenges are arising concerning storing and utilization of the surplus energy, system operation, distributed generation management, energy supply reliability, and future integration with an automotive sector based on the electric vehicle. The problem which rises with Renewables is that present significant challenges to grid operators, including intermittent output and a mismatch between peak output and peak demand, which can result in grid instability, negative pricing, and wasteful curtailment.

The traditional way to store electricity for non-residential application is pumped hydro storage but this way is not always available. Moreover, with the increasement of electricity generated by renewables technologies, the need of storage become more important. Batteries are the most used technology to store electricity generate by renewables in small scale power plants. Despite of the high electrical efficiency (90%), when batteries are couple with fluctuated electricity generation, such as the electricity profile of the renewables, they face degradation issues. The latter leads to more sophisticated and expensive plant configuration, which tends to do the investment on plant impractical. An alternative way of storage is through Hydrogen technologies meaning Fuel Cells (FC) and Electrolysis. Clean energy production devices such as fuel cells which use hydrogen and oxygen as reactants emphasize the role of hydrogen in future energy infrastructure. A major hurdle in the development of such technologies is the production of pure hydrogen gas. Electrolysis of water to break it into hydrogen and oxygen is a promising option for clean fuel production [6] .

1.2 Hydrogen and Technologies

Hydrogen is the simplest and lightest chemical element of the periodic table. Its density as a gas (0.0899 kg/Nm3) is 15 times lighter than that of air. Hydrogen is a fuel with a wide inflammability range both in air (from 4 to 75 % vol.), and in oxygen, from (4 to 95 %vol). It is also the fuel with the highest energy content per mass unit, with a higher heating value (HHV) equals to 3.54 kWh/Nm3 (39.42 kWh/kg), i.e. 2.5 and around three times larger than of methane and gasoline, respectively.[7, 8]. Hydrogen is the most abundant species in the Universe and thus on earth, but it cannot be found in pure state in nature. Today hydrogen is largely used in the chemical and petroleum industry and the biggest share of production is covered by fossil fuel transformation and only a small share of it comes from water electrolysis. Figure 1.3 shows the share of each fuel in the production of H_2.

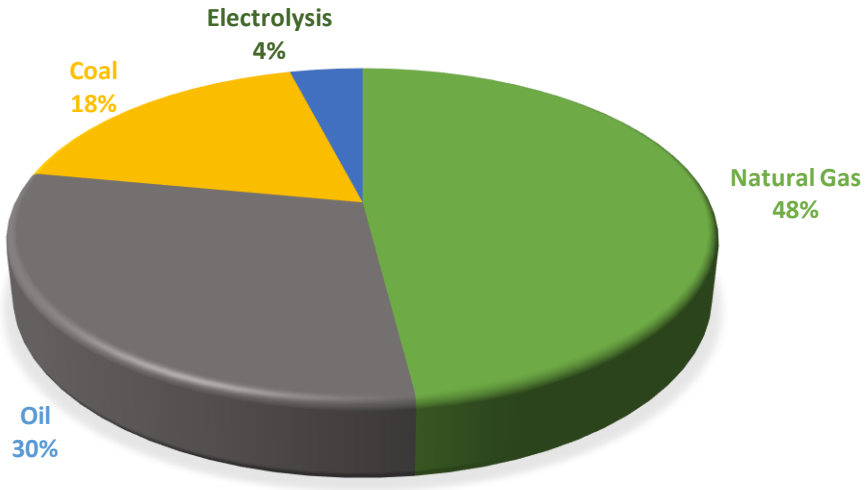

Figure 1.3: Current Processes for Producing Hydrogen [9]

Aiming at the decarbonization and the reduction of CO_2 setting as a goal the environmental sustainability, it can be easily understood that water electrolysis is widely agreed to be the most interesting source of sustainable hydrogen for the future, A particular advantaged is the integration with renewable energy sources [9]. At present, the drawback of hydrogen technologies is mainly focused at the economic competitiveness with respect to the traditional production ways. Indeed, steam methane reforming (SMR) is the most commonly process to produce hydrogen today, with a cost between 1 to 3 €/kgH_2. On the opposite, the most mature technologies for water electrolysis have a cost that varies between 3 to 15 €/kgH_2 depending on their size.

Beyond electrolysis, there are other technologies for hydrogen production from renewable sources that are currently under research and are being tested only in laboratory environment. In particular, bio-hydrogen technologies, use solar energy in the so-called bio-process photosynthesis. The main bioprocess technologies used for bio-hydrogen production include photolytic hydrogen production from water by green algae or cyanobacteria. It should be noted that only a small fraction of naturally occurring microorganisms have been discovered and functionally characterized. In addition, the known organisms are being modified to improve their characteristics. The feedstock for biological hydrogen is water for photolysis processes and biomass for fermentative processes. [9, 10]

A comprehensive summary of all technologies related with the hydrogen production was developed by Holladay and his colleagues and it is reported in Table 1.1 [10].

Table 1.1: Summary of technologies for hydrogen production

Technology	Feedstock	Efficiency	Maturity
Steam Methane Reforming	Hydrocarbons	70-85%[a]	Commercial
Partial Oxidation	Hydrocarbons	60-75%[a]	Commercial
Autothermal reforming	Hydrocarbons	60-75%[a]	Near term
Plasma reforming	Hydrocarbons	9-85%[b]	Long term
Aqueous phase reforming	Carbohydrates	35-55%[a]	Medium term
Ammonia reforming	Ammonia	n/a	Near term
Biomass gasification	Biomass	35-50%[a]	Commercial
Dark Fermentation	Biomass	60-80%[d]	Long term
Photo Fermentation	Biomass	0.1%[e]	Long term
Microbial electrolysis cells	Biomass	78%[f]	Long term
Photolysis	Sunlight + water	0.5%[c]	Long term
Alkaline Electrolysis Water	Water	50-60%[g]	Commercial
Solid Oxide Electrolysis	Water	40-70%[h]	Med. term
PEM electrolyzer	Water	55-70%[g]	Near term
Thermochemical water splitting	Water	n/a	Long term
Photoelectrochemical water splitting	Water	12.4%[i]	Long term

a Thermal efficiency based on the higher heating values.

b Solar to hydrogen via water splitting and does not include hydrogen purification.

c Percent of 4 mole H2 per mole glucose theoretical maximum.

d Solar to hydrogen via organic materials and does not include hydrogen purification
e Solar to hydrogen via water splitting and does not include hydrogen purification
f Lower heating value of hydrogen produced divided by the electrical energy to the electrolysis cell.
g High temperature electrolysis efficiency is dependent on the temperature the electrolyzer operates at and the efficiency of the thermal energy source. For example, SOEC operating from advanced high temperature nuclear reactors may be able to achieve up to 60% efficiency. If thermal energy input is ignored, efficiencies up to 90% have been reported

Table 1.1 includes the three main technologies which lead to the classification of electrolyzers into three major categories, referring to the electrolyte, the type of ionic agent (OH^-, H^+, O_2^-), the operation temperature. These categories are:

a) Alkaline electrolysis cell (AEC),
b) Proton exchange membrane electrolysis cell (PEMEC)
c) Solid oxide electrolysis (SOEC).

These are the most promising technologies that already are used commercially or are about to be introduced in the market in the near future. They are expected to play an important role in the hydrogen economy, i.e., an energy system that consider a significant presence of hydrogen as energy vector. In this future scenario hydrogen is produced through low-cost environmentally clean processes by means of renewable energy sources. Support policies and recent technological progress are contributing to cost reduction, knowledge improvement, and better social acceptance of these hydrogen technologies [11, 12].

The production of hydrogen via the electrolysis of water is, in principle, very simple. The basic electrolysis cell consists of a pair of electrodes immersed in a conducting electrolyte dissolved in water. When a direct current is passed through the cell from one electrode to the other, water is consumed so that hydrogen evolves at one electrode and, oxygen at the other. In an operating electrolysis cell, pure water is continuously supplied, and a stream of hydrogen and oxygen may be obtained from the electrodes. In practice, electrolysis cells are more complicated, containing various other components that allow them to work efficiently and economically. Since, the basic electrolysis cell has no moving parts, it is reliable and convenient; and electrolysis represents the least labor-intensive method of producing hydrogen. In addition to the convenient operation, electrolysis is the most efficient way of generating hydrogen under pressure. Electrolysis processes normally work more efficiently at a higher pressure due to the gain on the compression of H_2. The gain in efficiency is usually more than offsets the extra electrical energy required. An important characteristic of electrolysis is that hydrogen and oxygen are separated at the same time. This benefit is derived at the expense of having to use a high "energy form," namely electric power, as input to the cell [13][14]. Figure 1.4 illustrates the different technologies of water electrolysis.

	Low Temperature Electrolysis			High Temperature Electrolysis		
	Alkaline (OH^-) electrolysis		Proton Exchange (H^+) electrolysis	Oxygen ion(O^{2-}) electrolysis		
	Liquid	Polymer Electrolyte Membrane		Solid Oxide Electrolysis (SOE)		
	Conventional	Solid alkaline	H^+ - PEM	H^+ - SOE	O^{2-} - SOE	Co-electrolysis
Operation principles	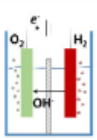	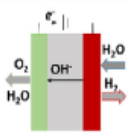	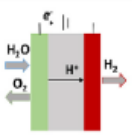	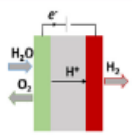	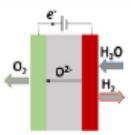	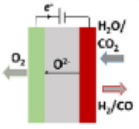
Charge carrier	OH^-	OH^-	H^+	H^+	O^{2-}	O^{2-}
Temperature	20-80°C	20-200°C	20-200°C	500-1000°C	500-1000°C	750-900°C
Electrolyte	liquid	solid (polymeric)	solid (polymeric)	solid (ceramic)	solid (ceramic)	solid (ceramic)
Anodic Reaction (OER)	$4OH^- \rightarrow 2H_2O + O_2 + 4e^-$	$4OH^- \rightarrow 2H_2O + O_2 + 4e^-$	$2H_2O \rightarrow 4H^+ + O_2 + 4e^-$	$2H_2O \rightarrow 4H^+ + 4e^- + O_2$	$O^{2-} \rightarrow {}^1/_2O_2 + 2e^-$	$O^{2-} \rightarrow {}^1/_2O_2 + 2e^-$
Anodes	Ni > Co > Fe (oxides) Perovskites: $Ba_{0.5}Sr_{0.5}Co_{0.8}Fe_{0.2}O_{3-\delta}$, $LaCoO_3$	Ni-based	IrO_2, RuO_2, $Ir_xRu_{1-x}O_2$ Supports: TiO_2, ITO, TiC	Perovskites with protonic-electronic conductivity	$La_xSr_{1-x}MnO_3$ + Y-Stabilized ZrO_2 (LSM-YSZ)	$La_xSr_{1-x}MnO_3$ + Y-Stabilized ZrO_2 (LSM-YSZ)
Cathodic Reaction (HER)	$2H_2O + 4e^- \rightarrow 4OH^- + 2H_2$	$2H_2O + 4e^- \rightarrow 4OH^- + 2H_2$	$4H^+ + 4e^- \rightarrow 2H_2$	$4H^+ + 4e^- \rightarrow 2H_2$	$H_2O + 2e^- \rightarrow H_2 + O^{2-}$	$H_2O + 2e^- \rightarrow H_2 + O^{2-}$ $CO_2 + 2e^- \rightarrow CO + O^{2-}$
Cathodes	Ni alloys	Ni, Ni-Fe, $NiFe_2O_4$	Pt/C MoS_2	Ni-cermets	Ni-YSZ Subst. $LaCrO_3$	Ni-YSZ perovskites
Efficiency	59-70%		65-82%	up to 100%	up to 100%	-

Figure 1.4: The main electrolysis technologies.

Each electrolysis technology has its own pros and cons (summarized in Table 1.1), but all three technologies are appealing and promising for sustainable energy application. Alkaline electrolysis is well established, and it is the most applied at commercial level technology, with many suppliers such De Nora SAP, Norsk Hydro, Electrolyzer Corp, Teledyne Energy Systems and General Electric [15]. The Main advantages of alkaline electrolysis are low cost owing to the use of non-noble electrodes and long-term stability. On the contrary, the acidic environment in PEM electrolyzers hinders the kinetics of the redox reactions and necessitates the use of expensive noble metal catalysts and materials for the bipolar plates. This, together with the high cost of polymeric membranes, is the main limitation for the commercialization of PEM electrolysis in the near term. Thermodynamic analysis by Todd et al [16] indicates that water electrolysis in elevated temperature and pressure has lower energy requirements. Alkaline electrolyzers can in principle operate at higher pressures, although at higher degradation rates. However, the use of a liquid electrolyte does not allow operation at differential pressures, in order to avoid gas and electrolyte permeation through the diaphragm. On the other hand, operation under different pressures at the two sides of the electrolyzer would facilitate hydrogen storage, since hydrogen will be produced at high pressure and the need for additional compressing systems will be eliminated, while on the other hand water could be supplied (and oxygen will be produced) at near atmospheric pressure. The solid form of the electrolyte in SOECs and PEMECs enables a more compact design and operation at differential pressures is feasible and favorable. Moreover, the solid nature of the electrolyte makes at least for PEMECs (SOECs need more tests due to high temperature) more dynamic systems with faster response upon application of a variable power load compared to liquid alkaline electrolyzers where diffusion rates can be slow.

Regarding ohmic losses, which account for the electrons and protons movement (see section 3.4), ionic conduction in the liquid electrolyte of alkaline electrolyzers is slow and the presence of the diaphragm can also further hinder OH^- transport, thus low current densities are generally observed in

this technology. Ohmic losses are smaller both in SOECs, due to better ion conduction at the high operating temperature, and in PEM electrolyzers, due to the wide availability of polymeric membranes with high protonic conductivity. The diaphragm in alkaline electrolysis largely prevents ionic conduction, but it can also be the source of reduced efficiency due to the unwanted permeation of gases. Apart from inhibiting the overall performance, it causes several safety issues. Gas crossover can occur also in the polymeric membrane in PEM electrolyzers, but to a lesser extent. In this case, the membrane thickness can minimize permeation of the gases. Even though ceramic electrolytes suppress gas permeation, safety issues also arise in the SOEC. Satisfactory sealing between the anodic and cathodic chambers is difficult to achieve for long term at high operation temperatures and the risk of a sudden cracking is not negligible [16, 17]. Instead, the high temperature makes SOEC advantageous compared to other technologies. The advantage and disadvantage of each technologies are presented at Table 1.2.

Table 1.2: Comparison between electrolysis technologies [10, 18]

TECHNOLOGY	ADVANTAGES	DISADVANTAGES
AEC	**Technology:** Oldest and Well established **Cost:** Cheapest and effective **Catalyst type:** Noble **Durability:** Long term **Stacks:** MW range **Efficiency:** 70% **Commercialized**	**Current Density:** Low **Degree of Purity:** Low (crossover of gases) **Electrolyte:** Liquid and Corrosive **Dynamics:** Low dynamic operation **Load range:** Low for partial load **Pressure:** Low operational pressure
PEMEC	**Current density:** High **Voltage efficiency:** High **Load range:** Good partial load range **System Design:** compact **Degree of Purity:** High gas purity **Dynamic:** high dynamic operation **Response:** rapid system response	**Technology:** New and partially established **Cost:** High cost of components **Catalyst type:** Noble catalyst **Corrosion:** acidic environment **Durability:** comparatively low **Stack:** Below MW range **Membrane:** limited and costly **Commercialization is in near term**
SOEC	**Efficiency:** 100% Thermal neutral efficiency> 100% w/hot steam **Catalyst:** Non-noble **Pressure:** High pressure operation	**Technology:** In laboratory phase **Durability:** low due to high heat, Ceramics **System Design:** Bulk system design

All the above indicate that a research effort is still required to characterize and improve PEMEC and SOEC; both in terms of numerical models and experimental analyses. As far as the PEMEC is concerned, it seems a more promising option since it offers efficient and flexible operation combined with practicality and high quality of the produced hydrogen. However, the development of PEMEC systems has been held back by the cost of components such as the polymeric membrane and the

precious metal electrocatalysts. Since there are still no non-noble metal electrocatalysts with satisfactory activities developed, it becomes vital to reduce production costs by improving the specific performance and durability of those noble metal electrocatalysts. On the hydrogen side of the cell, platinum provides the best performance and is commonly used for the PEMEC cathode. Most of the overpotential losses are related to the electrochemical processes at the anode, where the oxygen evolution reaction (OER) takes place. Therefore, the development and optimization of anode electrocatalysts is of great importance for PEMEC technology. Because of the acidic environment and high anode potential during water electrolysis, non-noble catalytic metals like Ni and Co cannot be used due to corrosion. In noble metal electrocatalysts, Pt forms a poorly conducting oxide film and shows a high overpotential for OER. However, electrocatalysts is consisting of Ir, Ru, or their oxides (which are reported to have the rutile structure and to be very good conductors) [18].

The study of PEM electrolyzers, both in term of stack and system, have been addressed by scientists only over the last 15 years. There have been numerous experimental studies investigating different aspects of PEMEC operation. Modelling of PEMEC systems have been developed, yet it is necessary to continue the investigation to be able to have better results in the future. Indeed, the development of PEMEC models provides powerful tools for the improvement of the PEMEC stacks and systems. These models can be used to establish fundamental characteristics that take place in the PEMEC to evaluate the behavior under different operating conditions and to optimize the design. The PEMEC system models quantitatively elaborate on the electrochemical phenomena that take place in the cells. The current status of the fundamental models of PEMEC engineering is backwards compared to PEMFC. The PEMEC process can be modelled at different levels depending on the needs of a researcher and the purpose of the simulation. In contrast, PEMFC models have recently become more advanced and complex, especially in multi dimensionality, multi-phase flow and non-isothermal properties.

The development of PEMEC models in engineering research can be divided into three groups based on their state and spatial dimensions. These groups are analytical, semi empirical and mechanistic. The state of modelling can be divided into steady state or dynamic conditions. The steady state model is where all state variables are constant and do not change over time. As the basis of design methods, the steady state model is widely used at the beginning of PEMEC cell modelling. This model is relatively simple to solve and is conceptually easier. However, the dynamic model is transient, which implies that it is time dependent and is used when analyzing step changes in operating conditions. The objective of dynamic modelling is to find the system response against load variations. This is especially useful when the PEMEC system is coupled with renewable energy sources such as wind or solar. The development of the model can be further divided into two parts: single phase isothermal/non-isothermal or multi-phase isothermal/ non-isothermal. The differences in these state-of-the-art modelling types is shown in Figure 1.5 [19].

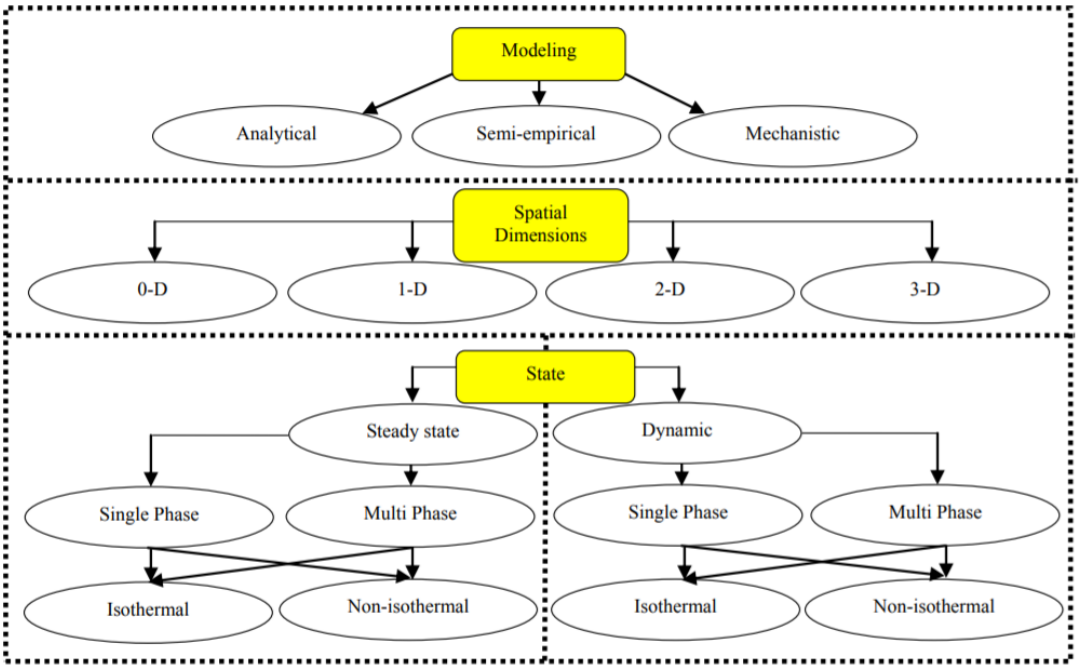

Figure 1.5: State of art of different models

1.3 Thesis Purpose

The current thesis presents a numerical model that describe a PEM electrolysis stack under a zero-dimension approach in both steady state and dynamic conditions. The aim is to simulate the operation of a commercial PEM electrolyzer that was experimentally tested, featuring a nominal power of 60 kW_{AC} manufactured by Proton On Site. First, the available literature on the topic will be reviewed to obtain suitable ranges of the model parameters. Second, a sensitivity analysis will be performed on steady state conditions to analyze the relevance of each parameter on the simulated voltage. Third, the most important parameters of the model will be calibrated based on with the experimental data. Last, a simplified dynamic model of the whole electrolysis system (stack and balance-of-plant) will be created to represent the real device in order to identify the interaction over time of the stack and the process components when the electric power input varies.

2. Water Electrolysis

2.1 Historical Background

Electrolysis is historically known as an electrochemical process for splitting water into hydrogen and oxygen. The overall chemical reaction involved can be written as:

$$2H_2O \rightarrow 2H_2 + O_2 \quad \textbf{Eq. 2.1}$$

The history of water electrolysis dates back to the 1800s and the discovery of electric water splitting by Nicholson and Carlisle using as DC current source the electric pile which Alessandro Volta had invited one year before [20].

It took more than a century from that stage to commercially develop the first electrolysis technology. During that time Faraday's law was developed [21] , the Nernst equation was derived, and the general science of electrochemistry was established. The early 20th century brought the first big scale applications of hydrogen production and definition of the classical methods of electrolysis.

In 1966 the first PEM electrolyzer was built by General Electric [22] as part of their development of PEM fuel cells e.g [23]], for the American space program. PEM electrolyzers were of great interest both for NASA and for military applications e.g. for situations where a production of oxygen was of the essence. It could be applications like space crafts or submarines [24] where the crew are reliant on a steady supply of oxygen to survive. Since the initial work by General Electric in the 1950s and 60s, Japan has put a large effort into the area with their Sunshine Project in the 1980s [25] followed in the 1990s with the WE-NET project [26] . In the European Union projects like GenHyPEM [27] (started in 2005) and WELTEMP (started in 2008) have been financed to improve the PEM electrolyzer technology. The research effort has since the development of PEM electrolyzers constantly been focused on improving the performance of PEM water electrolyzer and finding new suitable and cheaper materials in order to make the PEM technology more cost-competitive than alkaline electrolyzers and other hydrogen production technologies.

The first advanced alkaline systems started in 1978. The history ends up in our days with the development of proton exchange membranes, usable for water electrolysis units and fuel cells, by DuPont and other manufacturers, due to the developments in the field of high temperature solid oxide technology and by the optimization and reconstruction of alkaline water electrolyzers.

2.2 Thermodynamic Principles of Water Electrolysis

The chemical reaction in **Eq. *2.1*** thermodynamically speaking, is not expected to occur. This means that a form of energy must be provide in order to propagate it. So, a more corrective form of this equation can be seen in **Eq. *2.2***:

$$H_2O_{(l)} + 237.2\ kJ\ mol^{-1} + 48.6\ kJ\ mol^{-1} \rightarrow H_{2(g)} + 1/2O_{2(l)} \quad \textbf{Eq. 2.2}$$

The energy of 237.2 kJ/mol refers to the electricity that must be provided from an external source, while the 48.6 kJ/mol refers to the additional heat.[18]

The core of an electrolysis unit is an electrochemical cell, which is filled with pure water and has two electrodes connected with an external power supply. At a certain voltage, which is called ideal voltage, between both electrodes, the electrodes start to produce hydrogen gas at the negatively biased electrode and oxygen gas at the positively biased electrode.

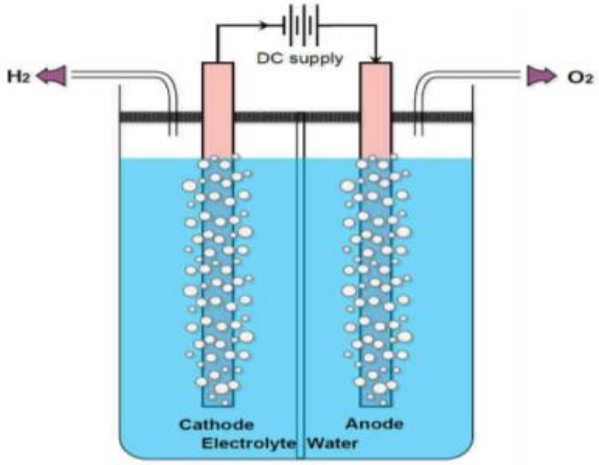

Figure 2.1: The fundamental cell of Water Electrolysis

In the electrochemical water electrolysis, the cell is separated into two different areas where two different electrochemical reactions occurred. Where oxidation of the species occurs, here water is split into O_2 and H^+ this is called anode (+) and for simplicity it is called oxygen evolution reaction (OER). Where reduction occurs, here where H_2 is formed, this is called cathode (-) and for simplicity it is called hydrogen evolution reaction (HER).

Thermodynamically all the equations for all the type of water electrolysis stand the same. Thermodynamics provides a framework for describing reaction equilibrium and thermal effects in electrochemical reactors. It also gives a basis for the definition of the driving forces for transport phenomena in electrolytes and leads to the description of the properties of the electrolyte solutions. In this section it will be introduced the general idea, while in the section of the description of PEM electrolyzers, it will be a more detailed analysis which will lead to the model of the PEMEC.

When an electrolytic cell operates at constant temperature and pressure, the required energy for the water electrolysis reaction is determined by the process enthalpy change ΔH. For this reaction to take place, part of the energy provided by electric power. This part corresponds to the Gibbs' free energy change ΔG. The rest is thermal energy Q and equals the product of the process temperature T and the entropy change ΔS. The following expression shows the relation among these thermodynamic magnitudes:

$$\Delta G = \Delta H - Q = \Delta H - T\Delta S \qquad \textbf{Eq. 2.3}$$

The electrolysis process is an endothermic ΔH >0 and nonspontaneous ΔG > 0 chemical reaction. The reverse process occurs in fuel cells and is exothermic ΔH <0 and spontaneous ΔG<0.

The ideal work consumed from a water electrolyzer can be extracted by **Eq. *2.3*** and it is called the reversible work W_{rev} or reversible potential difference E_{rev} (Open circuit voltage, OCV) when **Eq. *2.4*** is applied. The E_{rev} is the lowest required voltage for the electrolysis to take place. This voltage can be calculated as a function of Gibbs free energy as:

$$E_{rev} = \frac{\Delta G_R}{zF} \qquad \textbf{Eq. 2.4}$$

Where z is the numbers of electrons that participates in the reaction, in this case z=2 and F is the Faraday's constant which represents the charge on one mole of electrons (96,485 C/mol).

A better way to describe **Eq. *2.4*** is to refer E^{o}_{rev} which stands for the cell voltages under standard conditions (Pressure (P), Temperature (T): Constant). The latter can be explained because even if a system works under constant T, P if the operation conditions change, then the equilibrium potential also will be changed. At standard temperature and pressure (298.15 K and 1 atm), ΔG_R^{O} =237.21 kJ/mol, ΔS^{O}= 0.1631 kJ/mol K, and ΔH^{O}= 285.84 kJ/mol. By substituting ΔG_R^{O} and ΔH^{O} in **Eq. *2.3*** and **Eq. *2.4*** the E^{o}_{rev} = 1.229 V.[28] [29]

Without having an external heat source, the entire energy for the reaction to take place ΔH^{O}_{R} must be delivered by electrical energy. Hence, the voltage required is higher than E^{o}_{rev} and is called the thermoneutral voltage E^{o}_{th} at standard state.

$$E_{th} = \frac{\Delta H_R^O}{zF} = 1.481 \qquad \textbf{Eq. 2.5}$$

The equilibrium potential difference as it was mentioned previously, is a function of temperature at STP. Moreover, the E_{eq} is depending also on the activities (α_i) of the species. **Eq. *2.6*** shows this depends and it known as Nernst's equation[28] .

$$E_{rev} = E_{rev}^{O} - \frac{RT}{2F}\ln\left(\frac{\alpha_{H_2}\alpha_{O_2}^{0,5}}{\alpha_{H20}}\right) \qquad \textbf{Eq. 2.6}$$

With the reversible cell voltage at standard state E^{o}_{rev}, the universal gas constant R, the Faraday constant F, and the activities of the reactant α_{H2O} and products α_{H2} and α_{O2} with the respective stoichiometric factors. Replacing the activities by the partial pressures at standard temperature in reference to the operation pressure P_{op}, **Eq. *2.6*** can be written as [28]:

$$E = E_{rev}^{O} - \frac{RT}{2F}\ln\left(\frac{p_{H_2}p_{O_2}^{0,5}}{\alpha_{H20}}\right) \qquad \textbf{Eq. 2.7}$$

Where p_{H2} and p_{O2} are the partial pressure of hydrogen and oxygen, respectively. One other important relation for the electrochemical cells is Faraday's equation:

$$i = \frac{n_e F Q_i}{A_{cell}} \quad \textbf{Eq. 2.8}$$

Where n_e is the electrons moles per hydrogen moles for water the value is 2, i is the current density (A/cm^2), Qi (mol/s) is the molar mass flow of the species (in section 3.3 will be used letter F_i for molar flow rate) and Acell (cm^2) is the area of the cell. Faraday's equation is very important when the cell or stack is being modelled on the part of mass balance. This will be explained in the section 3**.** [28]

2.3 Alkaline Electrolysis Cells (AECs)

Alkaline electrolyzers (AEC) represent a very mature technology that is the current standard for large-scale electrolysis. The anode and cathode materials in these systems are typically made of nickel-plated steel and steel respectively. The electrolyte in these systems is a liquid one based on a highly caustic KOH solution. The ionic charge carrier is the hydroxyl ion, OH^- mostly caustic potash (KOH) solution, and a membrane porous to hydroxyl ions, but not to H_2 and O_2 provides gas separation. Key advantages of this technology include its maturity and its durability. Key disadvantages are its use of a highly caustic electrolyte and its inability to produce hydrogen at high pressures. This inability to produce high pressure hydrogen for storage results in the added need for an external compressor, which adds cost and complexity to the system. Moreover, the drawbacks of AEC are introduced mainly by the liquid phase on the anode and cathode plus the diaphragm, which does not completely prevent the gases to penetrate through it [18] ,[30]. Specifically, the corrosive environment, the low current density and the limited production rate of 25%-100% due to the diffusion of gases through the diaphragm at partial load.

The reactions that occur in AEC are:

a) Hydrogen evolution reaction (reduction)

$$2H_2O + 2e^- \rightarrow H_2 + 2OH^- \qquad E_{HER} = -0.83\,V \quad \textbf{Eq. 2.9}$$

b) Oxygen evolution reaction (oxidation)

$$2OH^- \rightarrow H_2O + 1/2O_2 + 2e^- \qquad E_{HER} = 0.4\,V \quad \textbf{Eq. 2.10}$$

where E is the equilibrium electrode potential calculated by Nernst's law versus the standard H_2 electrode (SHE) at pH= 14. The electrode reactions and the schematic structure of AEC can be seen in Figure 2.2.

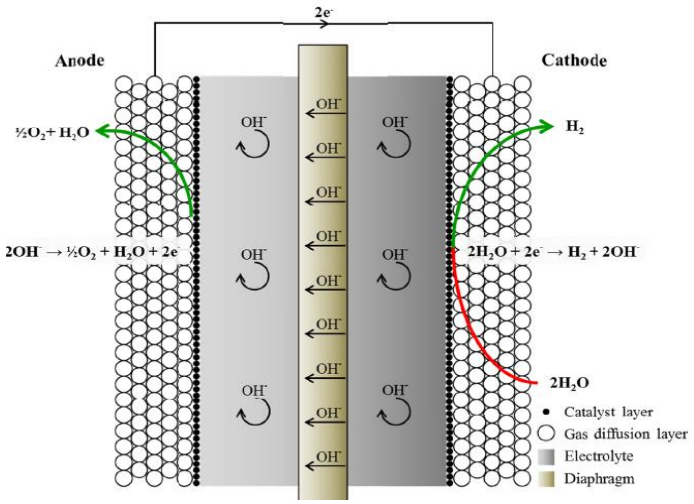

Figure 2.2: Schematic representation of an alkaline electrolysis cell

From Figure 2.2, it can be seen that the reactant water, is fed to the cathode side of the electrolysis cell. At the cathode the water is dissociated into protons and OH^- are transported across the electrolyte. On the anode side the OH^- are oxidized to oxygen under formation of water. On both sides of the diaphragm the electrolyte is recirculated to keep a constant OH^-. The gradient color of the electrolyte symbolizes how the OH^- are formed at the cathode and consumed at the anode. Hydrogen and oxygen gas bubbles, which are produced at cathode and anode, respectively, increase the cell resistance by reducing the contact between the electrodes and electrolyte. Consequently, efficiency is reduced. Particular attention should be given to cell design to maximize the contact between the electrode and the liquid electrolyte. Advanced alkaline cell uses a "zero gap configuration "to reduce the impact of gas bubbles and the ohmic losses by reducing the space between the electrodes [31]. There are two cell structures of alkaline electrolysis on market, unipolar and bipolar as reported in Figure 2.3. In the unipolar configuration, the cells are connected in parallel and the electrodes are connected to the corresponding DC power supply. The total voltage applied to the stack is the same as that applied to an individual cell, and the electrodes have a single polarity. Unipolar configuration is simpler from a fabrication point of view and permits an easier maintenance and reparation without shutting down of the whole stack.

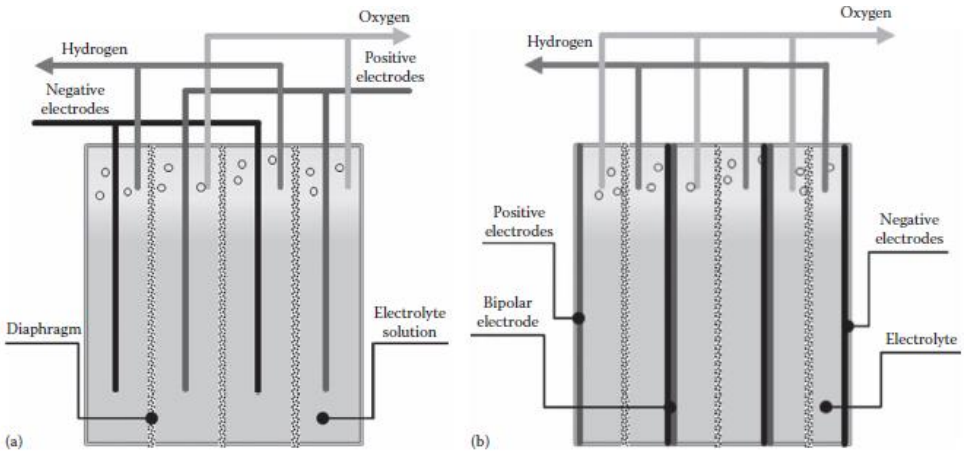

Figure 2.3: (a) Unipolar and (b) Bipolar stack design.

The disadvantage is that it usually operates at lower current densities and lower temperatures. In the bipolar configuration, each electrode has two polarities and the cells are connected in series. The voltage applied to the stack is the sum of single-cell voltage. The current that flows through the stack is the same for cells. The advantages of the bipolar design are higher current densities, which have capacity to produce higher pressure gas, and a more compact stack than unipolar design. The disadvantage is that it cannot be repaired without servicing the entire stack.[32]

2.4 Solid Oxide Electrolysis Cells (SOECs)

Where AEC systems have been commercial for decades, Solid Oxide Electrolysis cells (SOECs) are still only under development. The development of SOEC was slowed down around 1990 due to low fossil fuel prices but has become increasingly investigated in the recent years as a green energy technology. Beside steam electrolysis, SOECs are also capable of electrolyzing carbon dioxide to carbon monoxide and oxygen.

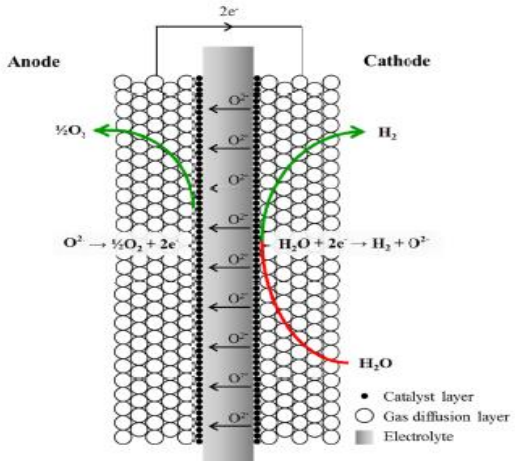

Figure 2.4: Schematic representation of a solid oxide electrolysis cell

In the Figure 2.4 the schematic structure of an SOEC can be seen and the electrode reactions are given for both anode and cathode. The color gradient in the electrolyte is used to symbolize the oxide ions are moving from the cathode to the anode. As in the AEC the reactant is fed to the cathode. Protons from the dissociated water are reduced to hydrogen, and oxide ions are transported across the oxide ions are oxidized to oxygen. SOEC's are operated at very high temperatures above 800 ^{o}C seems to be most common. In SOECs the most common electrolyte is (as in SO fuel cells) yttria (Y2O3) stabilized zirconia (ZrO2) (YSZ). Other stabilized zirconia electrolytes are also used, *e.g.* Scandia (Sc2O3) stabilized zirconia which has higher ionic conductivity than YSZ but suffers from higher cost and lower stability [32] [33] [34].

The net reactions for the SOEC depends largely on the reaction rates occurring at the triple phase boundary, operating temperature and pressure, supply of electricity, microstructure of the cell. Real reaction mechanisms are complex and still not well understood. The high temperature that SOEC

operate, give them a comparative advantage to the low temperature electrolyzers. From thermodynamic point of view the Gibbs free energy on higher temperature is lower than in lower temperatures [35] .The thermodynamic concept will be described in next chapters.

The simple structure for the net reactions at the cathode are:

$$H_2O(g) + 2e^- \rightarrow H_2(g) + O^= \quad \textbf{Eq. 2.11}$$

$$CO_2(g) + 2e^- \rightarrow CO(g) + O^= \quad \textbf{Eq. 2.12}$$

For the anode:

$$O^= \rightarrow 1/2O_2 + 2e^- \quad \textbf{Eq. 2.13}$$

The overall reaction becomes:

$$H_2O + CO_2 \rightarrow H_2 + CO + O_2 \quad \textbf{Eq. 2.14}$$

In the solid electrolyte the reactions can be approximate in the following manner. For the fuel electrode the cathode:

$$H_2O(g) + 2e^- + \ddot{V}_o \rightarrow H_2(g) + {O_o}^x \quad \textbf{Eq. 2.15}$$

$$CO_2(g) + 2e^- + \ddot{V}_o \rightarrow CO(g) + {O_o}^x \quad \textbf{Eq. 2.16}$$

For the air electrode (the anode):

$${O_o}^x + 2\dot{h} \rightarrow 1/2O_2(g) + {O_o}^x + \ddot{V}_o \quad \textbf{Eq. 2.17}$$

Small scale SO electrolysis cells have been produced, which have demonstrated hydrogen production electrical efficiency of 70-90% [36]. This is much higher than its low temperature (alkaline and PEM) electrolyzer equivalents.

A method of decreasing the electrical energy requirement for steam electrolysis even further is through the use of methane. In this process, the air on the anode side is replaced by methane, which reduces the open-circuit voltage and therefore the electrical energy consumption[37].

2.5 Proton Exchange Membrane Electrolysis Cells (PEMECs)

In this section, PEM electrolysers are extensively described more extensively than the previous two technologies, as this technology is the main focus of the current thesis work. Besides the

fundamentals of the technology, a description of the components that constitute a stack and the elements that are comprised in a full system are detailed.

2.5.1 Fundamentals of PEMEC

The reason why this technology was developed arises from the disadvantages that AEC shows during the operation. To deal with these issues General Electric in the 60s developed the first water electrolyzer based on a solid polymer electrolyte [38]. The idea was furthered utilized by Grubb where he used a solid sulfonated polystyrene membrane [39], [40]. Nowadays, most PEMECs use a PFSA (Nafion) type membrane in which the proton conductivity is strongly dependent on the water content in the membrane.

The working principle of PEM, reactions on each electrode and thermodynamics of the cell need to be known to better understand the PEM electrolyzers. Briefly, water electrolysis is a chemical reaction where water is the reactant whereas hydrogen and oxygen are the products. The electrolysis cell is a reaction medium composed of membrane electrode assembly (MEA), the electric current collectors, the gas distribution layers (GDL) and the gaskets. Unlike the alkaline electrolyzers, the electrolyte of a PEM electrolyzer is a solid perfluorinated membrane. A typically schematic representation of the parts of a single electrolysis cell is given in Figure 2.5. [41]

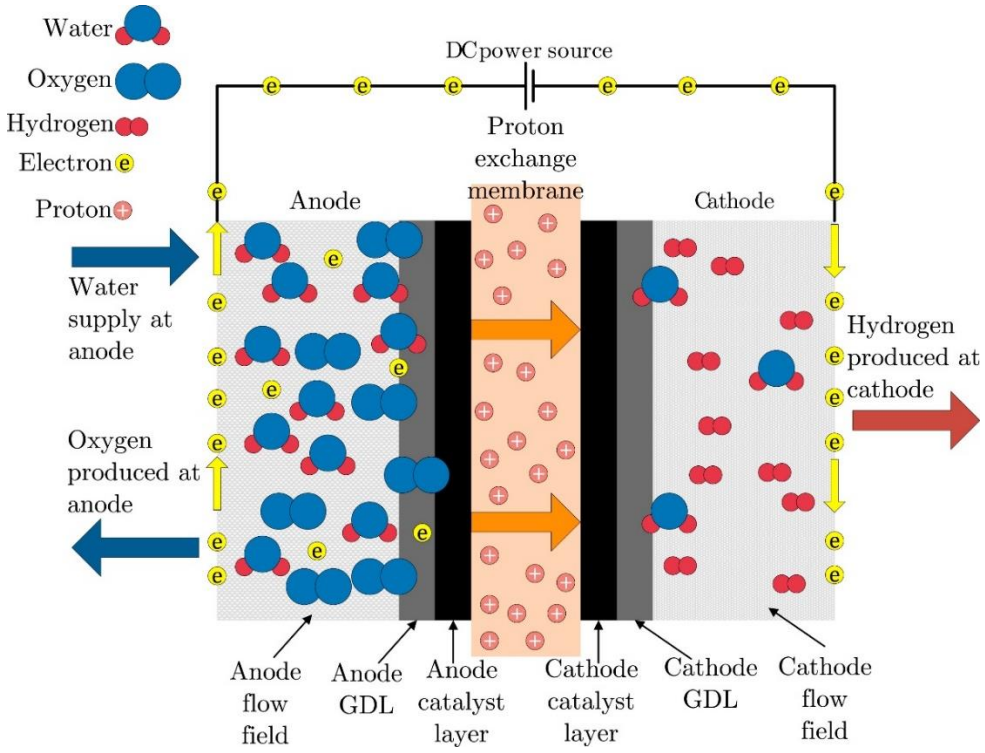

Figure 2.5: Schematic of a PEM electrolyzer

The chemical reactions that occur during hydrogen production are given by:

In the anode:

$$2H_2O \rightarrow 4e^- + O_2 \quad \text{Eq. 2.18}$$

In the cathode:

$$4H^+ + 4e^- \rightarrow 2H_2 \quad \text{Eq. 2.19}$$

Total:

$$2H_2O \rightarrow 2H_2 + O_2 \quad \text{Eq. 2.20}$$

One of the main drawbacks of PEMEC is the high cost of the membrane: electrocatalyst (doped with noble metal), the requirements of pure water and the high cost of constructional materials limit the wide usage of this type of electrolyzer. On the other hand, the PEM produce high purity of H_2 and can be operated in elevate pressures that compare to AEC, it does not need an addition pumping system, thus it reduces the operation and maintenance cost of the system. According to a technoeconomic study the elevated pressure makes more competitive the technology of PEMEC [42]. Table 2.1 summarizes the advantages and disadvantages of PEMEC [18]. Generally, the concept of the capital cost is important for energy technologies. The higher the capacity in terms of power (W) the better the economic feasibility of the plant, in terms of ROI (return of investment). Moreover, the price of H_2 and the tariff of electricity that are provided to the stack are critical and need be studied very carefully during the phase of economic strategy.

Table 2.1: Advantages and Disadvantages of PEMEC

Advantages	Disadvantages
High current densities	High cost of components
High voltage efficiency	Acidic corrosive environment
Good partial load range	Possibly low durability
Rapid system response	Commercialization
Compact system design	Stacks below MW range
High gas purity	
Dynamic operation	

Up until now, the most efficient electrolysis using PEM electrolyzers have been reported to operate at 1.556 cell voltage and 1 A/cm^2 at 80^{o}C (Yamaguchi et al. 2000) [43] , hence achieving 95.1% efficiency (based on high heating value of hydrogen). Moreover, PEM electrolyzers can operate over a wide range of temperature, pressure and current density as compared to alkaline-type water electrolyzers [44]. This unique feature makes PEM electrolyzers suitable for integrating with renewable energy sources which usually have variable electricity output due to their uncontrolled primary energy inputs. For example, the photovoltaic panels produce power proportional to solar intensity, which looks like a bell shape curve during the day or wind turbines produce power with the cubic function of the wind speed. Thus, hydrogen production based on PEM technology is a promising option for many renewable sources as it stores the uncontrolled production of electricity.

2.5.2 Components of PEM Electrolysis Cell

A PEMEC consists of seven essential elements: a solid electrolyte, two electrodes (anode and cathode), two gas diffusion layers (GDL), and two flow plates. The electrolyte and the electrodes (which often include the GDL) are also called the membrane electrode assembly (MEA). Other components that can be found in are the gaskets. When multiple cells are combined together to form a stack, the flow plates are substituted by bipolar plates and two end plates are needed at the first and last cell.

2.5.3 Membrane (MEA)

As mentioned in section 2.5 one the most important components of the cell electrolyzer is the membrane. This is similar to PEMFC and has two essential functions: it is a barrier that keeps hydrogen and oxygen gases separated, while it allows the motion of protons from anode to cathode. A critical advantage that it offers for electrochemistry is the capability to undergo high current densities.

Both sides of membrane are coated with noble metals which are usually Pt, Ir and Ru or some combinations of these metals. It is composed of a perfluorinated polymer (PFS) backbone having bonded pererflourinated side branches. The most common membrane is Nafion manufactured by Dupont. Figure 2.6 shows a schematic representation of the chemical structure of Nafion.[28]

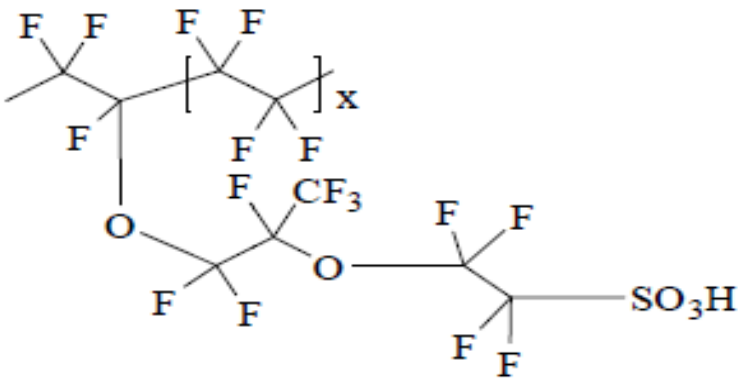

Figure 2.6: Schematic of the chemical structure of Nafion

Nafion® membranes are named with a three- or four- digit code after Nafion®, *e.g.* Nafion® 212 and Nafion® 1135. The two first numbers gives information about the degree of sulfonation of the membrane, commonly known as the equivalent weight (EW) [45], [46] . The EW is defined as the mass of the dry polymer per sulfonic acid group [47]. The 21 in Nafion® 212 means that the membrane has an EW of 2100 g per sulfonic acid group and the 11 in Nafion® 1135 means it has an EW of 1100 g per sulfonic acid group. The last (two) numbers in the three (or four) numbers code gives information about the thickness of the membrane. The number(s) tell(s) how many multiplies of a thousandth of an inch (approximately 25 microns) the membrane thickness is [32]. Hence a Nafion® 212 membrane

will have a thickness of 0.002 inch or approximately 50 microns and the Nafion® 1135 membrane has a thickness of 0.0035 inch or approximately 87.5 microns. As mentioned above the vast majority of PEM water electrolysis test has been conducted using Nafion® membranes as electrolyte. The most commonly used are: Nafion® 115 and Nafion® 117.

The properties of Nafion have been extensively studied to analyze PEMFC operation. However, the hydration state of the membrane differs between fuel cell operation and electrolysis operation. During PEMFC operation, the membrane is humidified by the humidified gases and equilibrated with water vapor, whereas during electrolysis operation, the electrolyte membrane is exposed to the liquid phase of water and fully hydrated during water electrolysis. Therefore, to analyze a PEM electrolyzer, the properties of a Nafion membrane need to be evaluated when the membrane is exposed to and equilibrated with liquid water.[32]

An important parameter for the Nafion® is the water uptake. Water uptake is important because is strongly related with the proton conductivity of the membrane. In other words, the membrane is effective, when it is well hydrated. This issue is more important for fuel cell, rather for electrolyzer since the anode side of the electrolyzer is fully flooded with water. The latter can rise different drawbacks related to the water cross-over from anode to cathode and affect the purity of H_2 in the outlet of the stack. This issue will be explained more in the next chapters. Water uptake can be represented as weight percent of water (ω) or water content (λ) In **Eq. *2.21*** and **Eq. *2.22*,** respectively, it can be seen how water uptake can be calculated.

Although, the mechanisms of how protons move through is out of the scope of the current thesis, it can be mentioned some very basic concepts can be mentioned. A very extensive work has been made by Krever, Paddison and Spohr in 2004 [48]. According to them, the proton conductivity of proton exchange membranes follows either or both of two major routes, these being the *vehicle mechanism* and the *Grotthuss mechanism*.

The vehicle mechanism operates as the name implies by transporting the proton on a carrier (vehicle) molecule in the case of most low temperature fuel cells and electrolyzers (most often PFSA electrolytes as Nafion®) these carrier molecules are water molecules. The proton is carried as different water complexes such as the hydronium ion (H_3O^+), the Zundel ion ($H_5O_2^+$) or the Eigen ion ($H_9O_4^+$). The transport of the positive proton on its water carrier complex ion is a typical example on an electro-osmotic flow, where the charged species is moving in the direction of the applied potential [48, 49].

Proton transport with the Grotthuss mechanism comes from a transport of a more or less common network of protons in the proton conducting media. In the case of electrolysis using PA doped membranes both of the PFSA type and PBI at elevated temperature and ambient pressure, the PA acts as the proton conducting media. When protons flow into the membrane at the anode side, it is not those specific protons that are transported through the membrane, but rather a rearrangement of the protons in the PA phase allowing for protons on the cathode side of the membrane to reach the cathode and be reduced to free hydrogen.

The water uptake as percentage depicted in ***Eq. 2.21***.

$$\omega = \frac{W_{wet} - W_{dry}}{W_{dry}} \ [\%] \qquad \textbf{Eq. 2.21}$$

Where W is based on the weight of the wet and dry sample.

The water uptake expressed as λ and represents the number of water molecules per sulfonic acid site (SO_3H^-). The relation between λ and ω depicted in **Eq. *2.22***.

$$\lambda = \frac{\omega * EW}{M_{H2O}} \qquad \textbf{Eq. 2.22}$$

2.5.4 Electrodes: Catalyst and Gas Diffusion Layer or Current Collectors

One of the most important aspect in electrochemist are the catalyst and the materials that used to obtain the products of the chemical reaction. There are some requirements for an electrocatalyst to well performing[18]:

- Low activation overpotential for the desired reaction (Hydrogen or Oxygen evolution),
- High active surface which facilitates good accessibility to the reactants and enough fast removal of products,
- High electrical conductivity,
- Chemical stability for the operation of the reaction,
- Electrochemical stability (Not being corroded for high overpotentials),
- Mechanical and Thermal stability,
- Availability and low cost,
- Health safety (preferably as low toxicity as possible).

An electrocatalyst is like an ordinary catalyst; a material which can accelerate a reaction without being consumed during the reaction, i.e. the catalyst lowers the activation energy for a reaction to take place. An electrocatalyst is a catalyst for a reaction where a net charge transfer takes place which means that electronic conductivity is essential for electrocatalysts. In a strict definition of an electrocatalyst the catalytic particles of the electrode should influence the rate of the electrode reaction *i.e.* the kinetic and mechanistic effect on the bonds formed by the reactants, product and/or intermediates with the electrode surface. Trasatti gives a broader meaning of the term electrocatalyst, which comes from a practical point of view. If a material gives a lower overpotential due to better conductivity it can still be consider a better electrocatalyst, although the kinetics and the electrode reaction are unchanged.[50, 51]

Moreover, the materials require to have stability and keep their properties for long term period, so the life time of the stack to be longer and the efficiency remain as high as possible. In other words, materials need to be stable and not degrade easily.

Unlike PEMFC, PEMEC use different materials in the anode and cathode side. The latter happens due to the fact, that in the anode side where oxygen evolution reaction occurs, it generates an acid

environment that become highly corroded for the materials of the anode. The PEMFC uses in both anode and cathode a carbon structure electrode with platinum as catalytic (C/Pt). While in the PEMEC the anode side is made by materials that can handle potentials greater than 2 V, where C will start to corrode.

In PEM electrolysers, the anode electrocatalyst is most often an oxide of a noble metal like iridium or ruthenium or mixtures. In 1984 Trasatti presented a paper giving an overview over some electrocatalysts used for oxygen and chlorine evolution [51]. He presented the data in a so-called volcano plot where the electrocatalytic overpotential towards oxygen evolution was plotted as a function of the transition enthalpy of going from the lower to the higher oxidation number. Figure 2.7 shows the volcano plot from reference. RuO_2 has the highest activity towards oxygen evolution since it has the lowest overpotential. However, RuO_2 is not stable in the oxygen evolution reaction, it is further oxidized to its highest oxidation number, $Ru^{(VIII)}$, RuO_4 is a liquid at room temperature. The melting point of RuO_4 is around 25 °C and the boiling point is approximately 130 °C. Hence under normal water electrolysis conditions of 80 °C RuO_2 will not be suitable for application since it will be corroded away.[52] [53] [51]

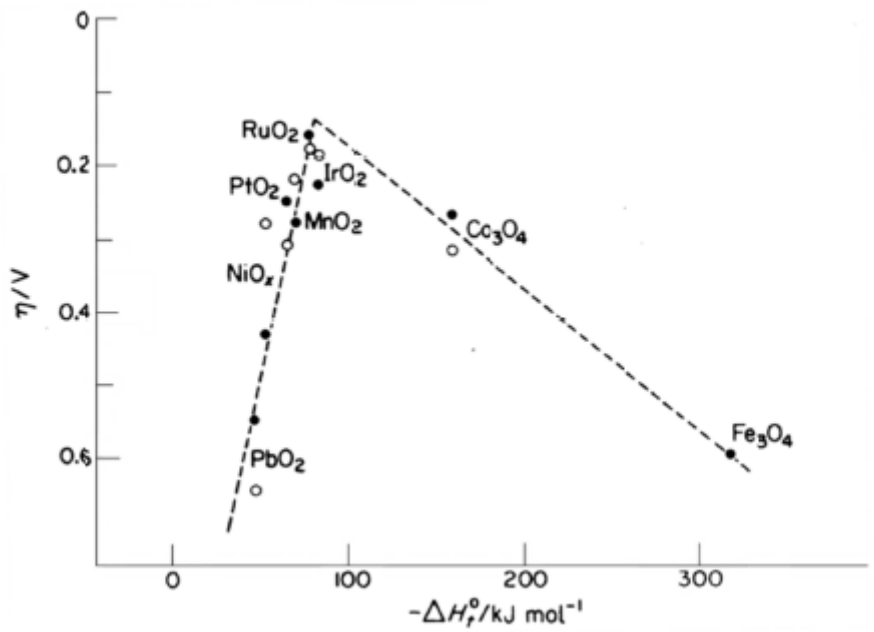

Figure 2.7: Vulvano plot for metal oxide in the OER. Overpotential(η) vs. transition enthalpy going from lower to higher oxidation state. The open circles are for reaction in alkaline media and the filled circles are for reaction in acid media.

IrO_2 is less active towards the OER but it is far more stable, so it has been extensively used on its one or in order to stabilize the RuO2 as a mixed oxide with IrxRu(1-x)O_2. Other commonly used electrocatalysts for the oxygen evolution reaction in PEM electrolyzers are Ir^{black} (powder $H_2IrCl_6x6H_2O$) and Pt [54]. More 'exotic electrocatalysts tested Pt-Ni, Pt-Co, Pt-Ir etc achieved reasonable cell voltages around 1.7-1.8 V at 1 A·cm-2 with Pt-Ni, Pt-Co, Pt-Ru-Ni, Pt-Ru-Co as anode catalysts and Pt as cathode. The anode consists not only of the electrocatalyst, but also an ionic

conducting component to facilitate the transport of ions. For this an ionomer of the same type as the polymeric membrane material is used.[18, 28]

On the cathode, the hydrogen evolution reaction is one of the most investigated and fundamentally important electrochemical reactions in heterogeneous catalysis, whereby hydrogen protons combine with electrons at an electrode surface to form hydrogen chemisorbed species and then desorb free hydrogen gas molecules. The electrocatalyst is very often Pt, either as Pt-black or as supported Pt on carbon (Pt/C). A commonly used catalyst support is Vulcan XC-72R carbon, which is carbon black with a very high surface area. Extensive research and development of HER catalysts has been performed. The great majority of these studies concentrated on further reductions of Pt loadings and potential Pt substitution (creating the so-called Pt-free catalysts). When using high Pt loadings, today lifetimes greater than 60,000 h can be achieved [55]. Studies on Pt loading reduction or Pt substitution now have to be pursued with major focus on the durability of these new HER catalyst systems [56]. If coupling PEM water electrolysis to renewable energy sources like wind energy and photovoltaics, the catalyst system must be able to withstand the seasonal characteristics of the power input (on/off, partial load operation, and overload operation) over thousands of hours. However, it is still questionable whether the intermittent power input condition will indeed affect the catalyst system durability [32]. Nowadays, the load of the Pt range between 0.5 to 1 mg cm^{-2} with the estimation that can be reach the value of 0.2 mg cm^{-2} to lower the cost. In section 3.4 it will be introduced that the losses for the activation over potential is mainly on the OER respect to the HER, and many times when a model is developed the HER over potential can be neglect it or can be simplified (from Butler-Volmer equation to Tafel see section 3.4).

Another important aspect for the cell to work properly besides the catalyst is the transportation of the H^+(protons) from the CL (Catalyst layer) to the membrane. In addition, the CL has a load of polymer solutions (ionomer) with ionic transport properties. In addition, two effects are achieved; one is the promotion of the protons from the bulk of CL to the membrane, enhancing the overall efficiency by decreasing the ohmic losses, and secondly, it decreases the electronic conductivity of CL since the polymer is electron resistant. Considering these controversial phenomena an optimization needs to be done in the so-called triple boundary (TPL). To better understand the mechanism of the triple boundary layer are depicted Figure 2.8 and Figure 2.9:

In Figure 2.9, one can notice that, the blue line stands for H_2O which arrives from bulk to the CL trough the porous media of the electrode, the black line represents the electrons that conduct through the solid structure and at the end the red lines represent the protons that produce at the surface of the solid where ionomer and catalyst are present. The figure depicts a fuel cells' cathode side in the catalyst layer where the protons (red arrows) are generated at the anode, then cross the membrane and react at the cathode side with O_2 (blue arrows) to produce water. The same mechanism stands for the electrolysis but with the inverse reaction. The black arrows are the electrons which move to the current collectors to be transport to the cathode (see Figure 2.5).

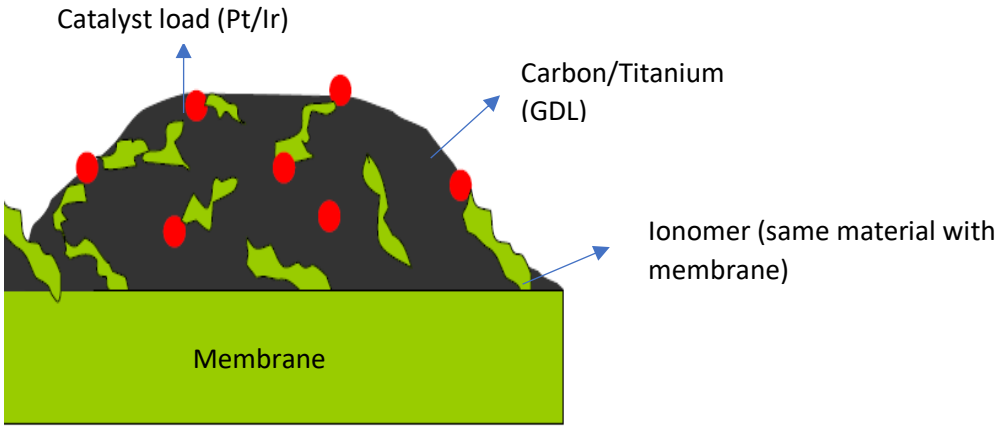

Figure 2.8: Rough approximation of the CL with catalyst load (Red) and Ionomer (Green) in the solid structure (Black).

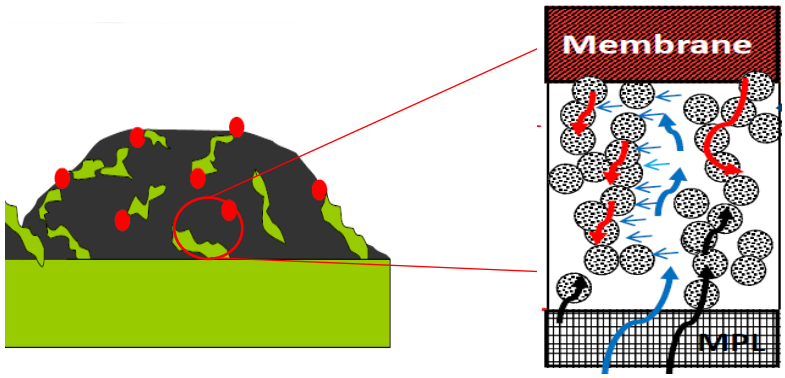

Figure 2.9: Representation of Triple boundary in the anode side. H_2O flows in the porous of the solid structure, while the grey particles represent the solid structure with ionomer and catalyst load.

The overall mechanism of the PEMEC from the bulk anode to the membrane and then to the bulk of cathode works generally; the water enters the cell in the anode sides, travels through the channels (optional: in the current study there are no channels) in the separator plates and diffuses thought the GDL of the anode (current collector). Then the water reaches the CL and the molecular are split into electrons, O2 and protons. The O2 gas flows back to the channels with the remaining water that did not react, while the electrons move from the CL through the current collectors, separator plates and then to the cathode side. The protons leave the anode catalytic layer through the ionomer, reaching the membrane and crossing to the cathode side, after reaching the catalytic layer they will combine with electrons to form H2. The hydrogen gas then has to flow across the cathode current collector, cathode separator plate and leave the cell.

This mechanism leaves some important issues to be studied for the development of GDL. Due to the high overpotential, the presence of oxygen, and the acidic environment provided by the solid acid electrolyte; the current collectors used must be corrosion resistant. (ii) They also have to have good electrical conductivities, and not passivate over time. (iii) The current collectors must also provide mechanical support to the membrane, especially under operational differential pressures. (iv)

The gases have to be effectively expelled and water must effectively reach the catalytic sites in counter flow. This is more important at high current densities where mass transport is the limiting factor. In this regard, current collectors with large porosity will promote facile gas removal but will decrease the electron transport and consequently decrease efficiency. Large porosity will also decrease the amount of water trapped into the catalytic layer. Conversely, small porosity will obstruct gas removal and increase mass transport resistances. Due to the need of an optimized pore size distribution, research methods have been developed for PEM fuel cells that could easily be applied to electrolysis to analyze the contact area as well as the mass transport aspects of the current collectors. Non-homogenous current distribution at the electrode current collector layer surface, due to bad contact, is also undesirable because it can result in the formation of hot spots which can eventually lead to melting of the membrane and producing defects on its surface.[18, 23, 57]

Therefore, an optimized current collector is required, and variables such as pore structure and design; pore size and distribution, electron conductivity, and corrosion resistance are key factors. As it was mentioned at the begging of this section, the high corrosive environment on the anode side end up using different solid structure for the anode's current collectors. This demands the use of scarce, expensive materials and components based on platinum group metals (e.g., Pt, Ir, and Ru), and Ti-based current collectors and separator plates. Grigoriev et al. performed an optimization of current collectors from both experimental and modelling approaches [58]. The results of this study conclude that the microstructure of porous titanium have a significant role on the overall cell efficiency. According to the results the most fictional geometry for the porous stands for spherical powder size in the range of 50-70 microns. In another study, Marshall et al. have shown that both perpendicular and lateral conductivity is required as the electrical contact to the layer is achieved through a porous support rather than a solid and flat electrode. Differences in the lateral and perpendicular conductivity will arise from the different particle vs. particle contact pressure in each direction. In this study, the porous titanium current collectors used had porosities around 50%, and therefore a loss of 50% in active surface area may be reasonable, if the lateral conductivity is very low. In other words, that is a reason for the addition of a micro porous layer (MPL, see Figure 2.9) to PEM fuel cell gas diffusion layers, to smooth the contact between the catalytic layer (nano-level) and current collectors (micro-level)[18, 58, 59]. Cheng et al. like Marshall investigate the performance of electrochemical properties of $Ir_xRu_{1-x}O_2$ oxides used as anodic electrocatalysts for a SPE water electrolyzer. They conclude that the increase of Ru content increases the average particles of catalysts and the $Ir_xRu_{1-x}O_2$ oxides is more active than IrO_2 and more stable than RuO_2 [60] .

2.5.5 Separator Plates

Separator plates either provide the electrolysis cell with structure or simply separating the cells of the stack or they can do both, which help maintain its stability in varying operating conditions. They also create a pathway for thermal and electron conduction and provide separation between the half-cell reactions. They are highly expensive and are responsible for 48% of the overall electrolysis stack cost as they are manufactured from expensive materials (titanium or graphite) and are not produced

on a large scale. At high current densities they are responsible for a large contribution to the Ohmic losses, resulting in higher required cell voltages.[18]

Titanium is one of the most commonly used materials for plates due to its low initial resistivity, high initial thermal conductivity and low permeability. However, over time titanium corrodes which causes the performance of the cell to decay [61-63]. Graphite is also frequently used due to its high conductivity. However, it is expensive, has high corrosion rates and has low strength[61] . To overcome the high costs of titanium and graphite stainless steel has been developed for use as a base material. It has low corrosion resistance so must be coated to resist the acid environment [62].

2.5.6 System Layout

The layout of the PEMEC system depends on the electrolyzer itself although the detailed plant configuration depends on manufacturer choices and components characteristics, and a general layout can be identified. Since the system has to operate on DC current input so the configuration of the plant needs to be changed according to the following: a) if you connect the electrolyzer directly to the electric source, that could be either the grid or wind turbines using AC-DC rectifier, b) not directly using DC-DC converter when it connects with photovoltaics panels (PV). In other worlds there is no general standard for the layout of PEMEC systems but Figure 2.10 demonstrates all the relevant components and subsystems of it. The PEM electrolyzer, the peripheral components for the operation condition of the stack (Temperature and Pressure) and last, the purification of the output product with storage. There are also components likes pumps that ensure the recirculation of water for the system. [32] In Figure 2.11 it can be seen an electrolyzer is represented in real application. All the components and the stacks are inside an ISO container. This configuration offers flexibility on the system and the footprint becomes small.

The system in Figure 2.11 was the first and the only rapid response PEMEC plant to be injecting hydrogen into the German gas network in 2013 with a capacity of 300 kW.

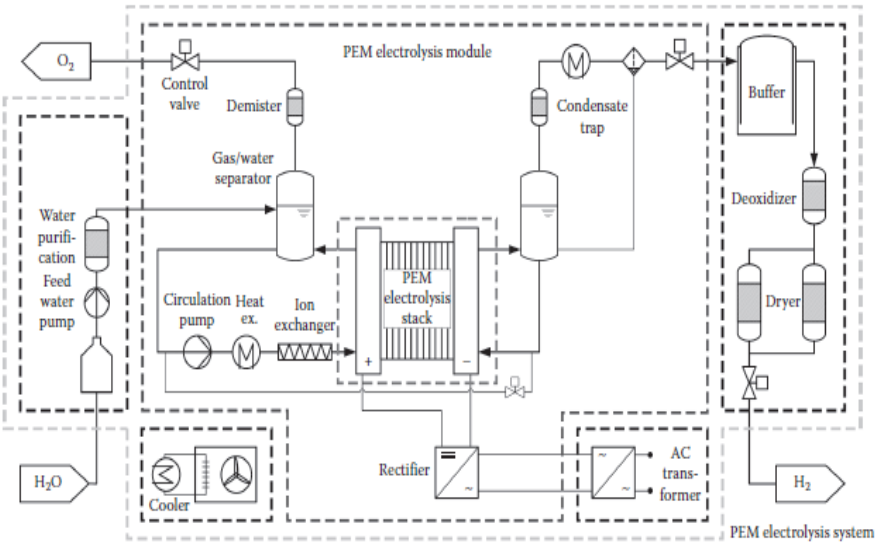

Figure 2.10: General layout of PEMEC

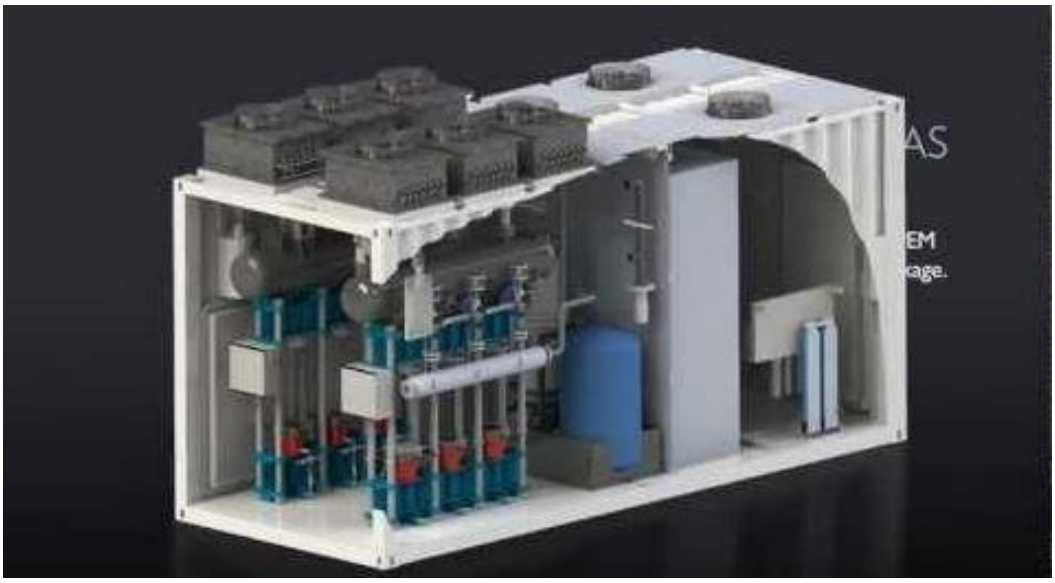

Figure 2.11: Thuga Group's electrolyzer for their energy storage project.

3. Modelling of PEM Electrolyzer

The current thesis developed a semi-empirical model in zero dimension, first for steady state and second for dynamic state. The PEM electrolyzer is based on the reactions that were described in the section 2.5.1. The developed model aims to determining the relationship between the current and voltage. This is done considering the interactions between various subgroups of the model on the anode, the cathode, voltage calculation, mass transport phenomena and thermal energy balance. The model is developed using Aspen Custom Modeler (ACM) for the steady state and for the dynamic model the Aspen Plus Dynamics (APD). The problem which arises in this model, is the selection of the values that each parameter or variable had to be assumed in order to set the steady state and then the dynamic model. The PEMEC that had been modelled is a close system where the geometrical and the physical parameters are not reported in the specifications sheets. In addition, it was needed to adapt a model and assumed some ranges for each values of every equation.

3.1 Literature Survey

In the last 10 to 15 years there has been an increase in the articles and studies released on the concept of PEMEC [18]. The availability of a model to reproduce the behavior of a real system is crucial to the study, as well as to verify how it can be incorporated with its power input fluctuation and the other parts of the plan. The models that have been developed, cover a wide range of aspects. Some models are focusing on specific performance of a component, others consider the balance of system in steady state or dynamic state. As a matter of fact, a PEMEC must be connected to a power converter to be properly supplied, and an equivalent model allows the whole system to be simulated and tested, avoiding the expensive damaging of the PEMEC. The same need occurs with fuel cell systems. The detailed dynamic behavior in which a transient of several seconds is noticeable in the current density is described in [64] for PEMFC where the dynamic response of current density is given by a three-dimensional transient model assessed in [65]. A detailed review of PEMFC models can be found elsewhere [66] . They share a lot of characteristics with electrolyzer systems. Yalcinoz et al. [67] have dynamically modelled an air breathing PEM fuel cell with a feedback control system. Gorgun et al. [68] presented a dynamic model of a PEM electrolyzer system. The model was based on mole balance equations at anode and cathode. The calculation of partial pressure of on anode side is done based on ideal gas equation. However, no comparison with experimental data has been made to validate the model. Dale et al. [69] developed a semi-empirical model of PEM electrolyzer system considering temperature dependent reversible cell voltage. Curve fitting methods are used to fit the experimental data to determine various model parameters. Biaku et al. [70] studied the temperature dependence of charge transfer coefficient at the anode using a semi-empirical model. Santarelli et al. [71] analyzed the effects of temperature, pressure and water feed rate on the electrolyzer operation with the help of a regression model. In another work, Marangio and Santarelli [72] present a detailed theoretical

model of electrolyzer system. The model presented includes activation, a complex model of the ohmic losses in electrodes and plates and in the membrane ohmic and diffusion overvoltage. It also considers the resistances of electrodes and plates along with resistance of membrane. The model is fitted to experimental data and a detailed analysis of operating parameters on electrolyzer performance is presented. Lebbal and Lecoeuche [73] also consider the concentration overpotential to model the kinetics of the reaction and they developed a steady-state electric model coupled with a dynamic thermal model of a PEM electrolyzer based on physical laws and electrochemical equations to select the control and monitoring parameters. Estimation of parameter values was achieved fitting the model to experimental data. The identification algorithm uses a non-linear least squares method for the estimation of the electrical model and the thermal model parameters estimated using first order response properties. Garcia-Valverde et al. [74] developed an electrochemical sub model which is based on electrochemical theory and depends only on the properties of the membrane and the electrocatalyst. Onda et al. [75] conduct an analysis of the electrical power needed to produce hydrogen at high pressure by water electrolysis. Both cases of atmospheric electrolysis with subsequent compression and high-pressure electrolysis are taken into consideration. Production power is estimated with the Nernst equation, considering that enthalpy and entropy change both with temperature and pressure. The results of the proposed model show that at 70 MPa power savings up to 6% can be achieved through high pressure electrolysis. However, just the ideal open-circuit voltage is taken into consideration: overvoltages are neglected since it is difficult to estimate real electrolysis power because of the lack of experimental data for high pressure water electrolysis Choi et al. [76] consider the cell voltage to be expressed as the sum of the open-circuit voltage and of the overvoltages; the losses taken into consideration are the activation ones (calculated using the Butler–Volmer equation both at the anode and at the cathode), the resistance of the membrane and the interfacial resistance between the electrodes and the membrane, but they only covered the electrochemical behavior. Diffusion overvoltages are neglected since it is assumed that no mass transport limitations exist. The overall consideration, the modelling of PEM water electrolysis has developed quickly, much due to the research efforts in PEM fuel cells. Although computational modelling of PEM electrolysis is still far behind the state of the PEM fuel cell, its progress is developing at a fast pace. More recently, Multiphysics approach has been utilized in CFD analysis including multiphase flow and heat effects. Thus, Agbli et al. (2011) used a graphical approach to visualize the interconnection among the various phenomena, namely, electrochemical, thermodynamic, thermal, and fluidic. Oliveira et al. (2013) have provided a multiscale model that includes a detailed molecular mechanism for the anode and cathode reactions, nanoscale catalyst electrolyte interface, and a continuum description of transport phenomena. They utilized it to investigate the effect of various design and operating parameters on PEMEC performance.[28]

The current thesis developed a lumped (zero dimension) analytical model considering a wide range of literature review; some of them was mentioned in the previous paragraph. It was based on the theoretical approached of the electrochemistry that covers the cell, but also takes into account all the possible irreversibilities that are generated by the system when it operates, meaning all the possible overpotential. In addition, the thesis investigated the mass transport phenomena that occur

in the gas diffusion layer, in terms of products and reactants. Lastly, it developed a simply thermal energy balance in order to calculate the thermal losses, but also the dynamic response of the system, in terms of operation temperature when it faces a change in the electrical output.

3.2 Main Features of the Considered Electrolysis System

Although the modelling work aims at generality, some features need to be specified to select the proper equations and assumptions. Moreover, the experimental data that will be used for validation (see Section 5) comes from experimental work performed by researchers of the Department of Energy of Politecnico di Milano that inevitably involves a specific device. Hence, it is relevant to detail some characteristics of the tested device.

The electrolyzer under consideration is a commercial product manufactured by Proton On Site, a USA-based company that designs and manufactures gas equipment, mostly focused on PEM electrolyzers and air separators. For the former, the company offers products that range from very small scale (200 cc/min) to large applications (over 400 Nm3/h). It was recently acquired by the Norwegian company NEL which is active in the alkaline electrolysis technology, showing how complementarity exists and market expansion requires large investments. The main technical characteristics of the electrolyzer are listed in Table 3.1

Table 3.1: List of main technical characteristics of the considered device by Proton On Site

	Parameter	***Value***
System	Nominal power	60 kW
	Number of stacks	1
	Outlet H_2 flow rate	10 Nm^3/h
	Nominal H_2 delivery pressure	30 barg
	H_2 delivery purity	99.9998 %
	Expected specific consumption	68.9 kWh/kg_{H2}
Stack	Number of cells	65
	Active area per cell	213,67 cm^2
	Nominal voltage	137 V
	Nominal current density	1.9 A cm^{-2}

In Figure 3.1 and Figure 3.2, it is depicted the outside and the inside parts of the PEM electrolyzer, respectively. The Figure 3.2, will be analyzed further when the simulation of the system's configuration it will be introduced in the Section 6.

Figure 3.1: The PEMEC's box cover with the control panel upfront and the flows inlet/outlet of the products/reacts at the right side

Figure 3.2: The inside parts of PEMEC's system. The blue at the right left is modelled the stack

3.3 Mass Balance

The mass balance of each species that participate in the reaction is defined on the control volume that are produced or reacted. To do the analysis It was decided to examine what happens on each cell and not for the whole stack.

- **Anode side**

In the anode side of the cell the mass balance is needed to calculate the properties that are important for the electrochemistry of the system. Partial pressure of oxygen, vapor pressure, molar composition and from the operation temperature and pressure all the thermodynamics properties can be calculated that be used in the overvoltages equations.

For Oxygen that is produced in the anode side of the cell, where water is oxidized (releases e^-), the equation is:

$$\frac{dN_{O_2}}{dt} = F_{O_2}^{in} - F_{O_2}^{out} + F_{O_2}^{gen} - F_{O_2}^{perm} \quad \textbf{Eq. 3.1}$$

Where N is the amount of mole of O_2 in the anode side, F^{in} is the oxygen that flows in the inlet of the anode, the value is zero since pure water enters in the anode.

F^{gen} is the flow of that produce from the reaction. This quantity is calculated **Eq. *2.8***:

$$F_{O_2}^{gen} = \frac{0.5\ i\ A_{cell}}{2\ F} = \frac{I}{4F} \quad \textbf{Eq. 3.2}$$

Where A_{cell} is the area of the cell in cm^2.

The term F^{perm} stands for the cross penetration O_2 that potentially can travel through the membrane. According to the bibliography a small portion of the produced hydrogen permeates the membrane and migrates to the anode in the gas state, where some molecules undergo decomposition into protons and electrons at the electrode while the rest are brought into the anode flow channel. The protons move back to the cathode through the membrane. This phenomenon was reviewed by Ito et al. [8]. According to their study, due to the pressure difference between the anode and the cathode, in the model the anode pressure is 2.5 bar and the cathode pressure is 30 bar, the water which floods all the anode is cross over the membrane as will be described for the mass balance of the water, probably some O_2 has been dissolved in the water. The latter is very important for safety reasons of the cell since the mixtures of H_2-O_2 have broad flammability limits [32]. Ito derived an equation that takes account of the difference in pressures between anode and cathode, introducing a constant (not really a constant because in depends on the properties of Nafion, temperature and pressure) to fit the experimental data. The equation is:

$$F_{O_2}^{perm} = \frac{K_{p,O_2}\ A_{cell}\ (\ y_{O_2}^{mean_{an}} P_{mean}^{an} - y_{O_2}^{out_c} P_c)}{(t_{mem} + t_{el}^{an} + \ t_{el}^{c})} \quad \textbf{Eq. 3.3}$$

Where $K_{P,O2}$ [mol/(m s Pa)] is the permeability coefficient for O_2. The values that are reported in the literature are very small comparing to the other flows so many times they do not consider in their analysis the flow of O_2 that crosses the membrane. Kim et al.[77] , suggest that this flow is significantly lower than the H_2 due to the size of the molecules, so they neglect it. Nevertheless, in the current study for the validity of the model it is included it and it is handled as a fixed parameter; its value is obtained from the literature ($1.62 \cdot 10^{-16}$ mol/m s Pa) [78].

F^{out} of oxygen is the outlet flow from the anode side it is calculated by the mass balance of Water, Oxygen and Hydrogen (that cross-over the membrane from the cathode). To calculate the F^{out} of O_2, the mass balance of H_2O is needed:

$$\frac{dN_{H_2O}}{dt} = F_{H_2O}^{in} \ - \ F_{H_2O}^{out} - \ F_{H_2O}^{cons} - F_{H_2O}^{mem} \quad \textbf{Eq. 3.4}$$

Where F^{in} is the water flow inlet in the anode side. This value was obtained from the data of the experiment and for this model it is a fixed parameter, $F^{in}(H_2O) = 100 \cdot 10^3$ mol / 3600s = 2.78 mol/s.

F^{cons} is the flow of that consume from the reaction. This quantity is calculated from ***Eq. 2.8***:

$$F_{H_2O}^{cons} = \ \frac{i\ A_{cell}}{2\ F} = \frac{I}{2F} \quad \textbf{Eq. 3.5}$$

For the F^{mem} it will be introduced an explanation of how this value was obtained and which properties were considered in the membrane's water mass balance. Assuming that this value is known additional information is needed to calculate the outlet flow for both species. Note that there is small portion of H_2 that which is considered in the model with a similar form as F^{perm} of oxygen.

$$F_{H_2}^{perm} = \frac{K_{p,H_2}\ A_{cell}(\ y_{H_2}^{out_c} P_C - y_{H_2}^{mean_{an}} P_{mean}^{an})}{(t_{mem} + t_{el}^{an} + \ t_{el}^{c})} \quad \textbf{Eq. 3.6}$$

The $K_{P,H2}$ [mol/(m s Pa)] is again a small value but according to [78], [77] , [32] this value is twice than the value of the oxygen permeability, so the assumption is $3 \cdot 10^{-16}$ mol/m s Pa. Nevertheless, flows are very small compared to the others flows, and they do not have a significant role in the performance of the model.

For the anode side H_2 balance can been written:

$$\frac{dN_{H_2}}{dt} = \ F_{H_2}^{perm} - \ F_{H_2}^{out} \quad \textbf{Eq. 3.7}$$

If the difference of pressure in the anode and cathode remain constant during the operation of the cell, these values remain constant in steady state. If there is a dynamic simulation, the values might change due to the fluctuation of temperature of the stack, but since it is assumed that the cell must work with constant temperature, it can be set these parameters as fixed even in the dynamic simulation.

Knowing the flows on the anode, it is easy to calculate the fraction for gas (yi) and liquid (xi). From that it is easy to calculate the partial pressures of each species which later will be used in the voltage calculations. The procedure that followed in the model to calculate the pressures is describe below. The partial pressures of the oxygen and hydrogen are calculated by:

For H_2:

$$P_{H_2} = P_{mean}^{an} * y_{H_2} \quad \textbf{Eq. 3.8}$$

and for O_2:

$$P_{O_2} = P_{mean}^{an} * y_{O_2}^{mean_{an}} \quad \textbf{Eq. 3.9}$$

P^{an}_{mean} is the mean pressure of the anode side. For the zero-dimension model that was followed in the current study it has been assumed that the Pin, inlet pressure on the anode side, is decreasing linearly with a slope 0.1 (10% pressure drop). So, the mean value of the pressure in the anode side is given by:

$$P_{mean}^{an} = \frac{(P_{in} + P_{out}^{an})}{2} \quad \textbf{Eq. 3.10}$$

Where $P_{out\,an}$ is the pressure on the outlet in the anode side and is calculated by:

$$P_{out}^{an} = P_{in} * (1 - \Delta p) \quad \textbf{Eq. 3.11}$$

Moreover, for the composition of the inlet Z_{in} (composition at the anode) which for electrolyzer is only water, while for the anode outlet composition it was assumed the equality:

$$z_{out}^{an} = z_{meam}^{an} \quad \textbf{Eq. 3.12}$$

The $z_{out,an}$ is the overall composition in the anode for O_2 and H_2O. $z_{mean,an}$ is the bulk anode molar composition. Both were calculated by a function of ACM which when given the temperature, pressure and composition of a fluid, it performs a vapor-liquid flash and calculates:

- Vapor molar fraction (yi)
- Liquid molar fraction (xi)
- Phase compositions
- Phase and overall molar enthalpy (h) [J/mol]
- Phase and overall molar entropy (s) [J/mol]
- Phase molar weights (v_f) [m^3/mol]
- Phase molar densities ρ_f [mol/m^3]

If the overall molar enthalpy, molar entropy or vapor molar fraction is known, these can be specified, and temperature or pressure is calculated.
It was computed also the volume of the anode side, assuming for the gas phase ideal gas behavior.

$$P_{mean}^{an}\ V_{vap}^{an} = RT\ (N_{H2}^{an} + N_{O2}^{an}) \quad \textbf{Eq. 3.13}$$

And for the liquid (only water):

$$V_{liq}^{an} = \frac{N_{H2O}^{an}}{\rho_{H2O}^{an}} \quad \textbf{Eq. 3.14}$$

So, the total volume is the summation of ***Eq. 3.13*** and **Eq. *3.14***. Note all the values was obtain in the mean condition and not at the outlet condition.

- **Cathode side**

The cathode side calculates hydrogen and water partial pressures and their flows at the cathode, where protons are reduced according to **Eq. *2.19***. The material balance equations for the cathode side are:
For H_2:

$$\frac{dN_{H_2}}{dt} = F_{H_2}^{in} - F_{H_2}^{out} + F_{H_2}^{gen} - F_{H_2}^{perm} \quad \textbf{Eq. 3.15}$$

For H_2O:

$$\frac{dN_{H_2O}}{dt} = F_{H_2O}^{in} - F_{H_2O}^{out} + F_{H_2O}^{mem} \quad \textbf{Eq. 3.16}$$

For O_2:

$$\frac{dN_{O_2}}{dt} = F_{O_2}^{perm} - F_{O_2}^{out} \quad \textbf{Eq. 3.17}$$

F^{perm} of oxygen is calculated by ***Eq. 3.3***, while the values F^{in} for both the water and the hydrogen are equal to zero. And this is a main difference between PEMFC and PEMEC, where PEMFC have inlet for both sides to supply oxygen and hydrogen, while in PEMEC the anode side is flooded with water, and hydrogen is produced at the cathode. In steady state conditions where the cumulative term is zero for water and oxygen, the outlets are equal to the F^{mem} for water and F^{perm} for oxygen.

Hydrogen is generated in the cathode and the flow is calculated:

$$F_{H_2}^{gen} = \frac{I}{2F} \qquad \textbf{Eq. 3.18}$$

- **Membrane's water mass balance F^{mem}**

The bulk of the water fed to the anode undergoes the oxygen evolution reaction (OER) to generate protons and oxygen. The net water flow through the membrane can be expressed in terms of three processes: (1) electro-osmotic drag, (2) diffusion and (3) hydraulic pressure effect. Thus:

$$F_{H_2O}^{mem} = F_{H_2O}^{diff} + F_{H_2O}^{eo} - F_{H_2O}^{pe} \qquad \textbf{Eq. 3.19}$$

Where F^{diff} is the molar flow rate of water due to diffusion from anode to cathode, F^{eo} is the molar flow rate of water from anode to cathode due to electro-osmotic drag and F^{pe} is the molar flow rate of water from the cathode to the anode due to the pressure effect.
In practice, electro-osmotic drag is the dominant mechanism, in which water molecules are coordinated around the migrating H_3O^+ species and dragged to the cathode.

(1) electro-osmotic drag

This phenomenon was known from the studies made by Springer et al. 1991, Zawodzinski et al. 1993 [32] . The electro-osmotic drag is directly related to the flux of hydrated protons migrating from the anode to the cathode through the membrane and so the molar flow rate can be expressed as:

$$F_{H_2O}^{eo} = \frac{n_{eo} I}{F} \qquad \textbf{Eq. 3.20}$$

Where the n_{eo} is the electro-osmotic drag coefficient [mol_{H2O} /mol $_{H3O+}$]. The electro-osmotic drag coefficient n_{eo} is defined as the number of water molecules "dragged along" per H^+. n_{eo} depends on the water content in the membrane as the same as the proton conductivity.

For this value there are two choices to investigate. Either it is expressed it as a fixed parameter, or a correlation is obtained from the literature where other fixed parameters are defined. Both choices were examined to identify the performance of the cell.

There are several correlations in the bibliography that indicate the value of n_{eo}. Most of them are referring to fuel cell where the membrane humidification is a crucial phenomenon for the cell to work property. In the electrolyzers this phenomenon is irrelevant since the anode is fully flooded where the water split to O_2 and protons. According to Santarelli and Medina [79] the coefficient depends on the current density, pressure and temperature of the cell. They performed experiments measuring the water produced in the cathode side. Although, in their paper they do not demonstrate any correlation, they perform a linear regression model assigning four different constants for each feature (Pc, Tm, i, bias (=1)). On the other hand, Kim, Park and Lee [77] indicate a function of n_{eo} as:

$$n_{eo} = 0.025P_C - 1.9073i + 0.0189T_m - 27892 \quad \textbf{Eq. 3.21}$$

Where Pc is the cathode pressure, i the current density and Tm is the operation temperature of the cell (Top for this model). The equation to which they refer is the one of Santarelli and Medina. Santarelli and Medina demonstrate some results according to their analysis as can be seen on Table 3.2:

Table 3.2: Values obtained for the neo coefficient from the designed algorithm

T (°C)	P (bars)	i (A/cm^2)	neo (mol_{H2O}/mol_{H+})
40	7	0,25	2,39
40	7	1	1,94
40	70	0,25	4,7
40	70	1	2,55
40	7	0,25	2,59
55	7	1	2,05
55	70	0,25	5,33
55	70	1	2,74

Applying **3.20** to test the validity, it was observed that it does not agree with last results that Santarelli and Medina found. So, this correlation was not used in this model. Moreover, one other correlation for the n_{eo} is suggested by Gorgun [80]. He used a correlation, based on Dutta S, Shimpalaee S, Zee JWV (2001) paper, which depending on the arithmetic mean of water content in the membrane between cathode and anode.

$$n_{eo} = 0.0029\lambda_m^2 + 0.05\lambda_m - 3.4e^{-19} \quad \textbf{Eq. 3.22}$$

Where λ_m is the degree of hydration [mol_{H2O}/mol_{so-3}] (or water uptake see eq. **Eq. *2.21***) of the membrane and it depends on the water activity α_w on the interfaces of the membrane. The degree of hydration is a parameter that either is taken as fixed or is calculated with a function. For fuel cells it is quite important to evaluate λ since the membrane hydration can vary in a large interval, in the case of this PEM electrolyzer the whole membrane can be considered fully hydrated, since water is present in huge quantities in the anodic chambers. Measuring the water content, λ, of membrane in contact with liquid water, Zawodzinski et al. [81] reported λ values of 17 and 22 of Nafion membrane in

contact with liquid water at 30 and 80 °C, respectively. However, Ise et al. [82] reported the λ value of 20 for the fully hydrated Nafion membrane at 79 °C. The specific PEMEC is working at a temperature around 55 °C and with a Pc at 30 bars. So, it was chosen to fix the parameter of λ in the highest value that found in the literature, thus λ = 21. For the n_{eo} as reported in [83], the values that were obtained from the literature are quite scattered. For example, the value of Marangio and Santarelli [72] n_{eo}=0.27 that they found from the literature (Dutta S, Shimpalaee S, Zee JWV) is low, that is why they suggest calculating n_{eo} as a fitting parameter in their model and at the end they obtain the value of 7. While in [83] the value of their model is 5. Figure 3.3 demonstrates the values of n_{eo}=f (λ).

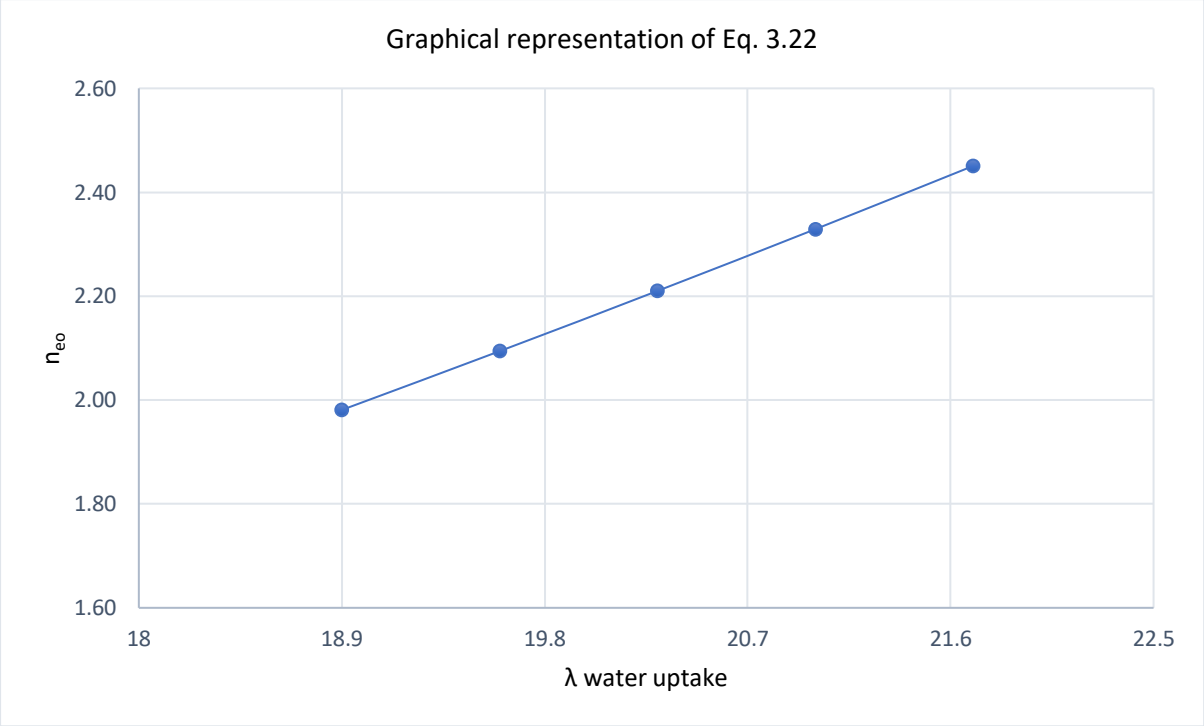

Figure 3.3: The graph shows the dependence of n_{eo} respect to λ.

Figure 3.3 shows a linear dependence of n_{eo} as a function of λ. For the value of λ = 21 that assumed, the result is that n_{eo} = 2.33. This value is compared with the data shown in Table 3.2, it corresponds for T=55 °C, Pc= 70 bars and i= 1 A/cm^2. So, one chooses to test the value of n_{eo} = 5 and the value n_{eo}= 2.33.

(2) Diffusion of water

The flow through the membrane due to diffusion is expressed by a Fick's law relation between the two membrane interfaces (anode and cathode):

$$F_{H_2O}^{diff} = \frac{AD_w}{t_{mem}}\left(C_{H2O,mem}^{an} - C_{H2O,mem}^{c} \right) \qquad \textbf{Eq. 3.23}$$

For this term again, it is needed to evaluate three terms, the D_w [m^2 /s] which is the diffusion coefficient of water in the membrane and the two concentration of water in the anode and the cathode interface (the "mem" subscription) respectively.

First for the D_W the choice is either a relation to calculate or a fixed value taken from the bibliography. For fixed value some papers suggest the value of $1.25 \cdot 10^{-10}$ m^2/s [6, 80]. Other papers suggest the value $1.28 \cdot 10^{-10}$ m^2/s [77, 83] It should be noted that there is almost negligible difference between the two values.

In the [68, 84, 85] they introduce D_w as a function of temperature and λ:

$$D_w = D_\lambda \exp\left[2416\left(\frac{1}{T_{amb}} - \frac{1}{T_{op}}\right)\right] \quad \textbf{Eq. 3.24}$$

Where D_λ is the value $1.25 \cdot 10^{-10}$ m^2/s for λ > 4.5.

Lastly, in [79] they report a different function of the water diffusion coefficient:

$$D_w = 0.256 * 10^{-4}\left(\frac{T_{cell}}{273.15}\right)^{1.823} \quad \textbf{Eq. 3.25}$$

It has applied a sensitivity analysis on the last expression, and compared it with the values suggested by other papers when temperature is varied and assuming λ=21:

Table 3.3: Comparison of the two-equations reported in the literature

Tcell (°C)	Dw Eq. 3.25 (m^2/s)	Dw Eq. 3.24 (m^2/s)
15	2,9E-09	8E-11
20	3,02E-09	1E-10
25	3,14E-09	1E-10
30	3,26E-09	1E-10
35	3,39E-09	1E-10
40	3,52E-09	2E-10
45	3,65E-09	2E-10
50	3,79E-09	2E-10
55	3,93E-09	2E-10
60	4,07E-09	3E-10
65	4,21E-09	3E-10
70	4,36E-09	3E-10
75	4,51E-09	4E-10
80	4,66E-09	4E-10

It is noticed that ***Eq. 3.25*** is over estimating the value of D_w by ten times more with respect to the ***Eq. 3.24,*** which varies very little and corresponds very well with the other references. When the validity of the ***Eq. 3.25*** was checked it was found out that the reference paper is that the reference paper is G.Lin et al.[86] which use this correlation to account the diffusivity of vapor water in the PEMFC. But also, they also suggest the ***Eq. 3.24*** for liquid water where the pre-exponential term is a function of λ. Which for λ=21 it is obtained the same value as it was shown in ***Eq. 3.24***. So, for the model was used the ***Eq. 3.24*** and not a single value in order to include the dependence of the temperature.

To calculate the concentration of water in the membrane it is necessary to study the diffusion mechanism on the GDL. The diffusion process within a porous medium depends mainly on two mechanisms, molecular diffusion and Knudsen diffusion. If the pore size is much larger than the mean free path of the molecular species, then molecular diffusion is the dominant mechanism. In this case, the molecule-molecule interaction governs the diffusion process. On the other hand, if the pore size is much smaller than the mean free path of the species, the molecule-pore wall interaction dominates over the molecule-molecule interaction, leading to Knudsen diffusion [83]. For this analysis the Knudsen diffusion was not accounted for since the knowledge of the GDL structure was unknow and also was out of the scope of the current thesis. Assuming Fick's diffusion all over the GDL and being aware that there are no- channels in the anode and in the cathode side of the cell, an analysis was adopted which counts the difference of water concentration from bulk to the membrane only for water. For oxygen and Hydrogen, the mean values are considered between inlet and outlet [6], [72].
For the difference between concertation of water from bulk to membrane in the anode:

$$C_{H2O,mem}^{an} = C_{H2O,bulk}^{an} - t_{el,an} * \frac{n_{H2O}^{an}}{D_{eff,an}} \quad \textbf{Eq. 3.26}$$

For the difference between concertation of water from bulk to membrane in the cathode:

$$C_{H2O,mem}^{c} = C_{H2O,bulk}^{c} - t_{el,c} * \frac{n_{H2O}^{c}}{D_{eff,c}} \quad \textbf{Eq. 3.27}$$

Where $t_{el,a}$ and $t_{el,c}$ are the thickness of the anode and cathode GDL (=0.0013 m). D_{eff} [m^2/s] is the effective diffusivity of the porous media and depends on the porosity and the binary diffusivity of water/oxygen and water/hydrogen. n_l [mol/m^2s] is the molar flux of water in the anode and in the cathode side.
According to [87] the correlation for D_{eff} is given by:

$$D_{eff,A-B} = D_{A-B}\ \varepsilon \left(\frac{\varepsilon - \varepsilon_p}{1-\varepsilon}\right)^{\alpha} \quad \textbf{Eq. 3.28}$$

Where ε is the porosity of the GDL (ε_e) and typically in models are used the value of 0.3. Grigoriev *et al.* [58] reported that the optimal porosity for a liquid electrolyzer should be between 30 % and 50 %, though their experiment and calculations were done on sintered spherical titanium particles which pack in a more ordered way. ε_p is the percolation threshold and is equal to 0.11 and α is an empirical coefficient equal to 0.785 [72], [88].

The binary diffusion coefficient D_{A-B} [m^2/s] for any given mixture of the two substances A and B can be estimated as follows:

$$P_i D_{A-B} = a * \left(\frac{T}{sqr(T_{C,A} * T_{C,B})}\right)^b * (P_{C,A} * P_{C,B})^{\frac{1}{3}} (T_{C,A} * T_{C,B})^{\frac{5}{12}} \left(\frac{1}{M_{C,A}} + \frac{1}{M_{C,B}}\right)^{\frac{1}{2}} \quad \textbf{Eq. 3.29}$$

Where P_i is the pressure, to be measured in [atm]. T is the temperature [K]. a and b are dimensionless empirical coefficients. Tc, Pc and Mr are the critical temperature, critical pressure and molar mass, respectively, which are calculated from the libraries of ACM. a and b are depending on the mixture components. Since there are pairs of water and nonpolar gases (H_2/O_2), $\alpha = 3.640 \cdot 10^{-4}$ and b= 2.334. [72]

Solving the **Eq. 3.26** to **Eq. 3.29** the value of the F^{diff} is calculated. For the current it is necessary to adopt two different sub-models: the one that was mentioned before and the other one assuming the concentration of water in the average value in the anode and in the cathode.

(3) Hydraulic pressure effect

The cell works at different pressures between anode and cathode. This pressure opposes the motion of water that is essentially pulled across the membrane by the electro-osmotic drag. The mechanism to calculate this effect derives from Darcy's law.

$$F_{H_2O}^{pe} = K_{Darcy} A_{cell} \frac{\rho_{H2O,C} \left(P_c - P_{mean,an}\right)}{\mu_{H2O} * t_{mem}} \quad \textbf{Eq. 3.30}$$

Where K_{Darcy} is the membrane permeability (m^2) to water, μ_{H2O} is the viscosity of water and ρ_{H2O} is the density of water in the cathode side. The value of K_{Darcy} is obtained by the literature $1.58 \cdot 10^{-18}$ m^2.[6, 72, 77, 79]

3.4 Electrochemical Relations

The developed theoretical model aims at expressing the relationship between the electrolytic cell voltage and cell current. As is widely known the real cell voltage in an electrolytic cell is higher than the ideal open-circuit voltage and can be expressed as:

$$Vcell = E_{rev} + \eta_{ohmic} + \eta_{act} + \eta_{diff} \quad \textbf{Eq. 3.31}$$

- **Ideal voltages E_{rev}**

Where the E_{rev} is the ideal voltage of the cell which is calculated by Nernst's equation (**Eq. *2.7***). The E^o_{rev} (standard reversible voltage) of the **Eq. *2.7*** calculated with ACM library tables by giving the temperature, pressure and composition in the Gibbs free energy function. Then the Ideal potential is calculated by **Eq. *2.4*** ($E_{rev}=V_{id}$) the partial pressures and the corresponding vapor fraction are calculated by the mass balances, as it was described in the previous chapter.

For the temperature on the Nernst's equation, the operation temperature (T_{op}) of the system in Kelvin was used. The value of the temperature is strongly related to the electrical input on the stack and the inlet temperature of the water at the anode side that controls the Top of the stack. Since the overall reaction is exothermal in each recirculation the temperature of the stack will rise, so the Tin at the anode needs to be regulated in order for the Top to remain constant. The regulation is achieved by the water inlet temperature. So, the overall system needs a heat exchanger to control the Tin according to the load of which the stack operates.

- **Activation overpotential (η_{act})**

The next term that needs to be identified is the activation overpotential (η_{act}). This term is one of the most important loss of the cell and a lot of investigations have been performed by scientist to introduce new materials and sophisticated geometrical schemes to utilize the load of the catalysis and the ionomer. For more details on the issues see.0. The η_{act} depends on the kinetics of the reactions that occur in a thin layer called catalyst layer (CL) in the anode and in the cathode side. In this thin layer near to the electrode (CL-GDL) and electrolyte (Membrane) interface, it has been proven that an electrical double layer (DL) was formed. When the system is under operation, the ions that are produced adjacent to the electrode undergo migration in the solution to form the DL. In Figure 3.4 is depicted the DL theoretical scheme:

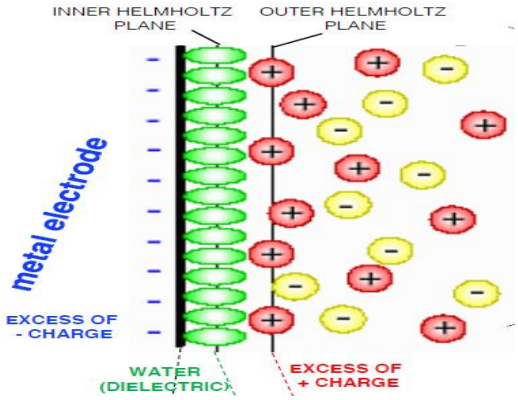

Figure 3.4: Schematic representation of the electric double layer (EDL). The surface due to the presence of charge has a potential E0. The outer Helmholtz plane (OHP) marks the closest distance that counter ions can come to the surface

When a current is forced to flow between two electrodes through an electrolyte, charge separation is created at each solid/liquid interface and two electrochemical capacitors are formed. In these capacitors at the electrode/electrolyte interface, dissolved ions in the bulk electrolyte are attracted to the electrode surface by an equal and opposite charge. It is considered that the behavior at the interface is described in terms of a capacitor. It is a consequence of the "free charge" approach that when a continuous current flow is applied through the interface a strict distinction should be made between Faraday and non-Faraday currents. Faraday currents are responsible for charging of the double-layer capacitor, while non-Faraday currents are the charge flow connected with the charge

transfer processes occurring at the interface. An interface at constant pressure and temperature can be changed by varying the concentration of the components in the bulk phases.

The accumulation of ions near the electrode forms two mobile layers. The layer closest to the electrode is called the inner Helmholtz layer (IHL), where the ions are well ordered and aligned with one another. The other layer is termed the outer Helmholtz layer (OHL), which consists of non-uniform ions adjacent to the IHL. The ionic charges of the ions adjacent to the electrode surface are balanced by oppositely charged ions in the electrode itself. The potential between the electrode and ions can be plotted against the distance from the electrode surface [28] . This is shown in Figure 3.5.

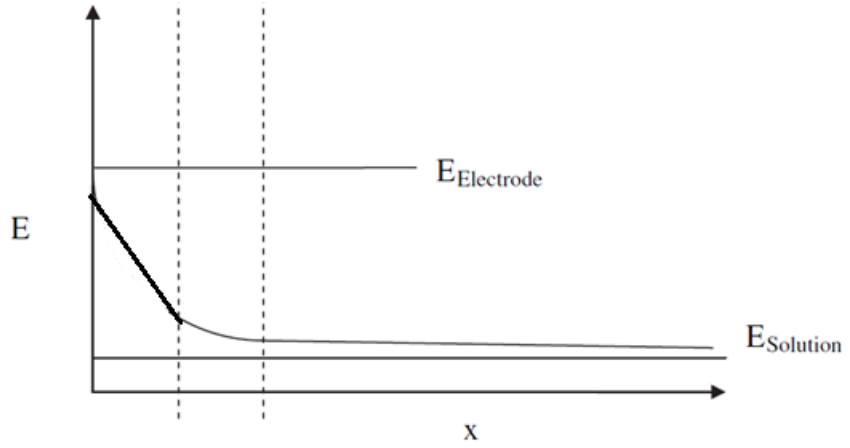

Figure 3.5: Effect of Distance on the Potential Between the Electrode and Ions

Figure 3.5 shows that voltage exists between the electrode and electrolyte solution. This is a direct result of the double layer. The addition of inert electrolyte to the electrolysis process compresses (reduces the thickness of) the double layer and consequently the distance that the potential decays to zero is much shorter. The electrical double layer phenomenon leads to capacitive behavior of the electrode reaction. This principle of the electrical double layer acting as capacitor needs to be considered for the electrode kinetics.

Although the electrode kinetics have been modelled with quite accuracy in terms of equations and parameters that are depending on, since they are related with the activation losses they need to be carefully described when a model is being developed. Modelling these phenomena accurately can be challenging as material processing, temperature, active catalyst areas, utilization, distribution, age, pressure, morphology and many other parameters some very difficult to quantify, all play a role [18, 74]

In PEMEC the kinetics that occur in the two electrodes are different since as it was described at 0 , they are made of different materials. Nevertheless, the equation that described both anode and cathode is the same and is called Butler-Volmer (B-V) expression which is valid for an elementary electrode reaction step. The equation is:

$$i_{el} = i_{el,0}\ \{\exp\left[\frac{\beta_{el} z F \eta_{el}}{RT}\right] - \exp\left[\frac{(\beta_{el}-1) z F \eta_{el}}{RT}\right]\} \quad [A/cm^2\ ESCA] \qquad \textbf{Eq. 3.32}$$

Where:
βel is the symmetry factor, F is Faraday's constant, z is the electrons that participate in the reaction, ESCA is the actual electrocatalytic surface area, i is the current density and η_{el} is the overpotential voltage and is expressed as the difference between the actual voltage with respect to the voltages at equilibrium of the system, see eq. **Eq. *3.33*** . The notation 'el' stands for the elementary reaction.[28]

$$\eta_{el} = \Phi_{el} - \Phi_s \qquad \textbf{Eq. 3.33}$$

Where Φ_{el} is the electrode potential and Φ_s is the solution potential. Practically these properties cannot be measured and therefore it was used the difference of them.

The ***Eq. 3.32*** derived by the rate of the reaction that occurs in an electrode translated in terms of current using Faraday's relation (see ***Eq. 2.8***). The concept is when a reaction occurs in an electrode both reduction and oxidization happened but only one is the most dominant.

The rate of electrolysis can be expressed as:

$$F_i = \frac{I}{nF} \qquad \textbf{Eq. 3.34}$$

Both i^{ox} and i^{red} current densities are expressed with kinetics rate constants K^{ox} and K^{red} for oxidation and reduction respectively. The Ki is calculated by Arrhenius relation:

$$k_i = A \exp\left[\frac{E_a}{RT}\right] \qquad \textbf{Eq. 3.35}$$

Where A is the pre-exponential factor, and E_a is the activation energy [kJ/cm^2]. E_a is equal of the ΔG of the reaction for both oxidation and reduction since the driving force for the reaction stands from the Gibbs free energy, thus the correspond thermodynamic property is the chemical potential μi. Keep in mind that:

$$\Delta G = \sum_i (v_i \mu_i) \qquad \textbf{Eq. 3.36}$$

When Temperature and Pressure are constant. The total current of the reaction calculated by:

$$i = i_{ox} - i_{red} \qquad \textbf{Eq. 3.37}$$

Combining the equations from ***Eq. 3.32*** to **Eq. *3.37*** and the Nernst's equation the B-V's equation ***Eq. 3.32*** is formulated.

Two important aspects arise from this analysis: First, what is the value of the βi and second what is the value of i_o which is called exchanged current density. More often βi is seen as 1-αi where αi is

called transfer coefficient and takes values between zero and one. To understand the nature of i_o, it is better to depict the transition-state theory, illustrated in Figure 3.6, which shows the reaction path for the electrochemical reactions in terms of the Gibbs free energy of the reactions, and the position of coordinates in the reaction path.

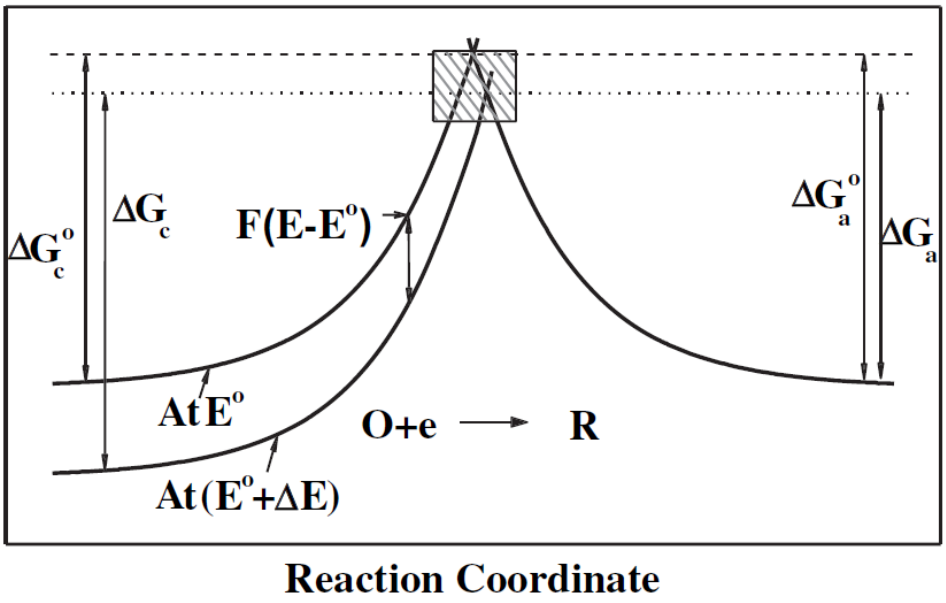

Figure 3.6: Transition-state theory for HER example

When the potential is increased by ΔE, as shown in Figure 3.6: Transition-state theory for HER example the decrease in Gibbs free energy is $F(E-E^o)$. As a result there is a reduction in Gibbs free energy of hydrogen ions in the HER by $(1-\alpha)(E-E^o)$, and the increase in Gibbs free energy of hydrogen gas by $\alpha(E-E^o)$. So, the i_o stands when equilibrium exists and can be calculated by:

$$i_o = n_E A (K_{ox} C_O)^{1-\alpha} (K_{red} C_{red})^{\alpha} \qquad \textbf{Eq. 3.38}$$

The concentration C_o and Cr_{ed} it can been found in B-V' equation as activities but since the model is based on dealing with constant pressure and assuming Ideal Gas, they can be written them with this form. Both concentrations can be derived solving Nernst's equation when E equals to 0 V. The standard exchange current density is akin to the electrochemical equivalent of the rate constant at standard electrode potential, and consequently, varies strongly as a function of temperature as given by its Arrhenius form. These relations show the powerful effect of electrode overpotential (η) and that of temperature on reaction thermodynamics and kinetics. In other words, temperature and potential are complementary tools for accomplishing favorable kinetics and thermodynamics. Thus, performance can be substantially enhanced by operating the electrolyzer at a higher temperature, the latter being usually limited by the performance and stability of the electrolyte used. Thus, the PEMEC is usually limited to an operating temperature less than 100°C.

Moreover, the transfer coefficient is the second parameter that needs to be identified, and it is strongly correlated with the nature of the chemical reaction in the electrode/catalyst interphase. Since the reaction is heterogenous the model that is used to describe this phenomenon is called rate determining stem (RDS). According to the latter, the reaction progress with different steps each time where one of them is the slowest step in terms of reaction rate. Thus, it will be that one which is determining the evolution of the whole reaction. But the number of elementary steps in a given sequence, are not known and often with more than one parallel pathway. If a single rate-determining step (RDS) exists in a sequence of steps, however, one can still often use the Butler–Volmer equation as being applicable for the electrodes, at least over a limited range, since the OR rate is then controlled by that of the elementary RDS. However, the OER and HER rates vary over such a large range by virtue of the strong effect of potential that a single Butler–Volmer equation cannot in general describe the electrode or kinetics over the complete range of potentials which are of interest [32].

The graphical representation of current and activation over potential is depicted in Figure 3.7

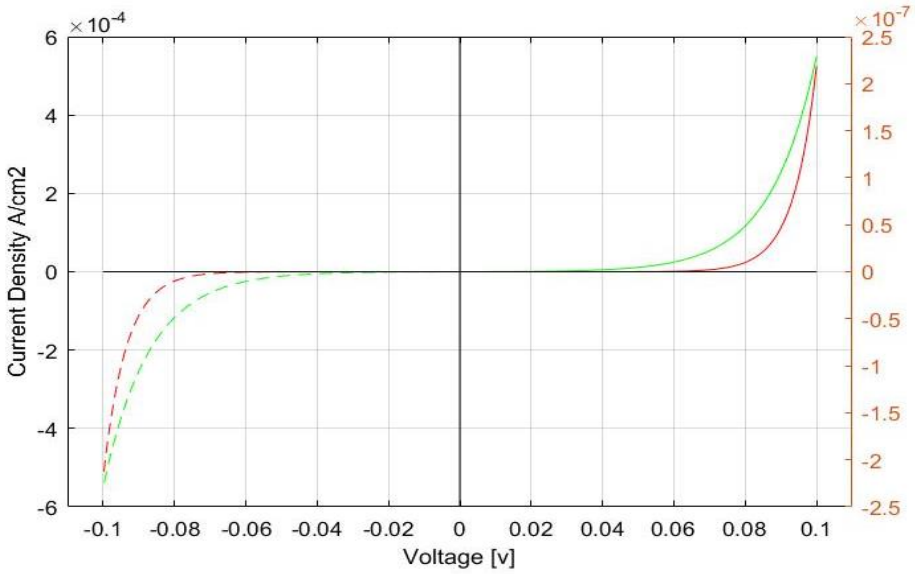

Figure 3.7: Butler-Volmer graphical representation between i and V with two different α

In Figure 3.7 one can see that the green line represents a transfer coefficient with lower value than the red line ($\alpha_{green} = 0.5$ and $\alpha_{red} = 1$). Meaning that the losses are higher in terms of overpotential for the green line. Notice that the order of magnitude of y right axis and y left axis is almost 10000 different so for the same voltage the green line gets lower value of i than the red line. So, the intuition is that it is needed to have electro-kinetics that favor as much as higher the transfer coefficient. The same behavior follows for the exchange current. The higher the better the performance of the PEMEC.

If the system of PEM electrolyzer does not vary a lot from equilibrium in terms of over voltage (η_{el}) then the term zFη << RT in BV's equation. One can use in this situation the exponent term as series ($e^x = 1 + x + x^2/2! + \ldots$) and keep the two first terms, the expression can be written as:

$$i = i_o \left[1 + \frac{azF\eta_{el}}{RT} - 1 + \frac{(1-a)zF\eta_{el}}{RT}\right] \quad \textbf{Eq. 3.39}$$

Eq. *3.39* shows that in this region of small over potential there is a linear correlation between i and η with an error of 1% [89]. When one works now, in high over potential where the current density is very high, one of the terms of B-V equation becomes relatively too small with respect to the other. For example, if the η takes negative values then the reaction which is dominant is the reduction. The equation becomes:

$$i = i_o \exp\left[\frac{(1-a)zF\eta}{RT}\right] \quad \textbf{Eq. 3.40}$$

Taking the log of the latter equation, it can be derived:

$$\eta = \mathrm{a} + b\ log\ i \quad \textbf{Eq. 3.41}$$

Where a = (2.3RT)/(aF) log i_o and b = (-2.3RT)/(aF). The **Eq. *3.41*** is called Tafel's equation.

The proportional relationship between the overpotential and the logarithm of current density is determined by exchange current density, i_o, and the slope b; known as the Tafel slope. Both parameters are used to measure the reaction kinetics of electrodes for electrochemistry [89]. For the current thesis both cases are adopted, of B-V and Tafel, and the results between these two are compared. For the parameters of α and i_o, there is a variety of values in the literature. For this reason, for this model suitable ranges must be found for both cathode and anode, in order to use them as fitting parameters for the model calibration since the chemistry of the tested electrolyzer is not known.

Table 3.4: Exchange currents and Transfer coefficient from literature

Paper	Exchange current (an/c) [A/cm^2]	α (an/c) [-]
[83]	an: 10^{-7}, c: 10^{-1}	αan = 0.8, αc = 0.25
[67]	an: $2{\cdot}10^{-7}$, c: $2{\cdot}10^{-3}$	αan = 2, αc = 0.5
[3]	an/c: range [10^{-13} -10^{-6}]	αan = range [0.18- 0.42]
[63]	an: 10^{-7}, c: 10^{-3}	αan = 0.5, αc = 0.5
[69]	an: 10^{-6}, c: (-)	αan = (-), αc = (-)
[61]	an: 10^{-7}, c: 10^{-3}	αan = 0.5, αc = 0.5
[58]	an: range [10^{-9}- 10^{-12}], c: 10^{-3}	αan = range [0.1- 0.6], αc = 0.5

Table 3.4 shows that also in the literature there is a scarcity of data about the mentioned parameters. Sometimes even if a paper indicates a performance of PEMEC that is constructed by the authors, they let these parameters to be calculated by fitting them with the experimental data that they get. One does not know a priory their values but only if one constructs MEA as component. Generally, when one constructs his own stack, MEA is bought by related companies that deal with the optimization of the CL and the membrane. In many of the existence models of PEMEC these four values are chosen to be calibrated parameters of the model. All the papers that are mentioned in Table 3.4: Exchange currents and Transfer coefficient from literature follow this strategy, as done with for this model.

- **Ohmic overpotential (η_{ohm})**

The ohmic overpotential is related to two mechanisms. First, the electrons which are moving in the different components of the cell and second with the proton's movement through the membrane. Activation losses are dominant at low current densities, while the ohmic overpotential becomes dominant at mid current densities. So, it is very important to investigate the ohmic losses due to the fact that PEMEC preferably will operate at high current densities (1-2 A/cm^2). If the resistance of the cell is not well optimized, the efficiency of the cell is penalized, and as a result the operation of the whole system. In fact, the easier approach to understand the importance of ohmic losses is to understand that the anticipated heat related to the current and the protons movement depends on I in the power of 2 (Q= I^2R). So, R needs to be carefully obtained.

Generally, the ohmic losses can be seen in different components of the cell. It has been already mentioned the membrane which is related to the protons. The GDL, bipolar plates and channel are related with electrons. There is also the resistance of the cables which transfer the electricity to the system, but this is out of the system's control volume and it is not considered in this study.

The ohmic overpotential is (by definition assumed) linearly proportional to the current:

$$\eta_{ohm} = IR_{tot} \quad \textbf{Eq. 3.42}$$

The I is the current that flows in the cell, while the R_{tot} is the total resistance [Ω]. The R_{tot} is calculated by two terms:

$$R_{tot} = R_{mem} + R_{el} \quad \textbf{Eq. 3.43}$$

Where R_{mem} is the ohmic resistance of the membrane and R_{el} is the total resistance in the GDL and the separate plate.

For the current thesis, the electrolyzer that is used as a model does not have channels so the porous media of the GDL or the so-called electrode of the cell plays two roles: 1) brings the water to the CL, 2) removes the products of the reaction plus the water that did not react. This particular case makes the problem of the electrode resistance a bit easier since for the zero-dimension model no

account is taken of the two dimensions (width z, height y) of the cell; the electrode is considered homogeneous on each layer of these two axes. Only the x-axis (t_{el}) is studied. The assumption in a zero-dimension model of polarization is that the current density per unit of area is uniform at the interface between each electrode and the membrane. The latter procedure was also adopted since as already mentioned the structure of the stack is almost unknown by the manufacturer. Moreover, the resistance of the electrodes, following the movement of the electrons that are produced in the CL, is: GDL, channels, separate plates and current collectors. In this model there are no channels and thus it is assumed also that the separate plates, current collectors and the GDL are made of the same material. The last thing that was considered, was the porous media of the GDL, which lowers the conductivity of the material since the path that electrons move has become smaller.

In the bibliography there are several studies that apply a resistance network to account for the possible resistances that the electrode has [18, 72, 83, 90] . Since, the geometrical values are not known it was chosen to assume only one parameter, the t_{el} and account the electrode resistivity as one parameter.

The ohmic resistance of the electrode can be expressed by the ohmic law for a media:

$$R_{el} = \rho_{eff} \frac{t_{el}}{A_{cell}} \qquad \textbf{Eq. 3.44}$$

Where t_{el} is the length of the electrode, A_{cell} the area of the cell and ρ_{eff} is the effective resistivity of the material of the electrode. The latter is considered since there is a porous structure involved, so the resistivity is increasing.

The effective resistivity was calculated using the percolation theory suggested by [91]

$$\rho_{eff} = \frac{\rho}{(1-\varepsilon)^{1.5}} \qquad \textbf{Eq. 3.45}$$

Where ρ (Ω cm) is the resistivity of the material and ε is the porosity of the media. There is a similarity between the **Eq. *3.45*** and **Eq. *3.28*.** , which also accounts for the porosity. The difference is that on **Eq. *3.28*** a void is assumed where the solid material does not exist, while for the resistivity a material is assumed through which where the electrons are passing. The problem that arises for the latter expression is the value of the resistivity. After a lot of research, no representatives' values were found. The issue is that every paper investigates or uses as models' different cases, where porous geometry, materials and operation conditions are varying. In [83], they mention 10.6 μΩ cm, while in [58] they calculate the resistivity of Ti powder structure for the anode side with a range between 6.7 to 9.2 mΩ cm, which is quite high; it must be noted that in [28] they reported that carbon resistivity is 7.8 μΩ cm. For this study the 7.5 μΩ cm (carbon) is used, although it is known that the Protons On Site company has done a lot of research of sophisticated material and loads of the catalyst to reduce cost [92].

Lastly, it is needed to identify which is the resistance of the membrane when protons move through it. Since this measure the protons conductivity, in most cases is referred as ionic resistance

and it is the dominant contribution for ohmic over potential. The formation of the equation expresses with ohm's law:

$$i = \sigma_{mem}\eta_{ohm} \quad \textbf{Eq. 3.46}$$

Where σ_{mem} is the membrane conductivity [s/cm] (the inverse of the resistance). A small description behind the conductivity is described in the 2.5.3. The majority of the papers are using a correlation that was first introduced by [93]. They suggested that the proton's conductivity is depending on the water content and temperature. They measure the conductivity of Nafion 117 at 30 ^{o}C and they notice a linear dependence on λ. The equation is described as:

$$\sigma_{mem} = (0.005139\lambda - 0.00326)\exp\left[1268\left(\frac{1}{303} - \frac{1}{T}\right)\right] \quad \textbf{Eq. 3.47}$$

The latter equation is used by several papers and they find one of the most valid one for the PEME[6, 18, 77, 78, 80, 83, 84]. Where for λ, it was assigned the value of 21 as it was described in **Eq. *3.23*** which counts that the anode side is fully flooded with water, so it is fully hydrated. The relation to calculate the R_{mem} is given by:

$$R_{mem} = \frac{t_{mem}}{A_{cell}\,\sigma_{mem}} \quad \textbf{Eq. 3.48}$$

- **Diffusion overpotential (η_{diff})**

The concentration/diffusion overpotential occurs due to the change in concentration of the reactants at the electrode surface when electrolysis is in progress. A concentration overpotential develops when the current is high enough to change the reaction rate in the CL surface with oxygen gas bubbles and hence slowing down the reaction rate. In general, the diffusion overpotential is characterized by the limiting current density i_L. In principle, this could be due to the mass transport limitations of any of the reactant or product species at either electrode. In PEMFC, the dominant mass transfer resistance that determines the limiting current, i_L, is the resistance to diffusion of O_2 through the GDL that is loaded with water produced at the cathode. However, the PEMEC would not suffer from this diffusion limitation, although at high current densities, bubbling of exiting oxygen could limit the permeation of water to the anode.[28]

The general analytical expression shows a Nernst-like dependence on the temperature and on the concentration in the bulk phase and in the reaction phase [18] . However, the overpotential can be modelled by setting a upper value of limited current density and considering only the anode side, whose contribution is the dominant one [74] :

$$\eta_{diff} = \frac{RT}{\alpha_{an}\,neF}\ln\left(\frac{i_L}{i_L - i}\right) \quad \textbf{Eq. 3.49}$$

The limited current in the PEMEC is hardly to be observed in the usually operating conditions of the cell. In our case, the maximum current density is around 2 A/cm^2, while the i_L is taking from the literature around 6.2 A/cm^2. In addition, this loss has very low contribution in the performance of the cell, so a lot of researchers neglect it.

3.5 Energy Balance

For the energy balance the model adopts a zero-dimension thermal capacitance model which represents a simplified approximation of the thermal models. Generally, the thermal models are considering the temperature variation along the different axis and they account also the heat transfer mechanism that can be observed in the porous media of the GDL or in the membrane by applying local analysis, for mass and heat transfer. Moreover, working the cell in elevated temperature can have a beneficial impact on the value of the reversible potential, but still needs to be keep steady and almost uniform to account a homogeneous operation of the stack. In this point the evaporation of water in the working condition is negligible in Top 55 ^{o}C. The Balance can be written as:

$$c_{th}\frac{d(T)}{d(t)} = \dot{E}_{in} - \dot{E}_{out} + P_{el} + \dot{Q}_{loss} \qquad \textbf{Eq. 3.50}$$

Where C_{th} [kJ/K] $_{is}$ the global thermal capacity of the stack, if the whole system is considered. A small analysis to calculate the global thermal capacity will be presented in section 6.3. The P_{el} is the electrical input of the external source that generates the whole process of the electrolysis. The Q_{loss} is the heat flow from the stack to the environment due to free convection (if there is no external ventilation of the system) and radiation. The latter can be neglected since the temperature of the stack is low, around 55 ^{o}C but since this can be calculated, it will be considered. The equation that is adopted for the thermal losses is obtained from the global energy balance of basic heat transfer:

$$\dot{Q}_{loss} = U_{th}\, S_{ext}\left(T_{w_{ext}} - T_{amb}\right) \qquad \textbf{Eq. 3.51}$$

Where U_{th} is the global thermal heat transfer coefficient [kW/K] and it is calculated by the summation of the free convection and radiative heat transfer coefficient:

$$U_{th} = U_r + U_c \qquad \textbf{Eq. 3.52}$$

U_r is calculated by:

$$U_r = \sigma_{boltz}\, F_{ext}\, S_{ext}\left(T_{w_{ext}} + T_{amb}\right)\left(T_{w_{ext}}^2 + T_{amb}^2\right) \qquad \textbf{Eq. 3.53}$$

Where σ_{boltz} is the Stefan- Boltzmann constant ($5.67 \cdot 10^{-8}$ W/m^{2}K^{-4}), F_{ext} an external factor that counts for increase of the outside surface for 50% (i.e. insulation), Sext is the external surface of the

cell, Tw_{ext} is the temperature of the external surface that is assumed as 10 ^{o}C degrees of temperature variation from the T_{op} of the cell to the Tw_{ext} to count for the conduction heat transfer, T_{amb} is the ambient temperature. U_c is calculated by assuming free convection, Ra (Rayleigh number) is calculated, the Nusselt number is also calculated and from that the h_{ext} is derived which is the heat transfer coefficient, which multiplied with the S_{ext} gives the global heat transfer for free convection.

The last to account for the energy balance is the inlet and outlet flows. Since the values are known for the flows and the fraction in vapor and liquid phases, in T and P the enthalpy of the mixture in the inlet and at the outlet can be calculated. The enthalpies are obtained from the ACM' libraries.

. The importance of the energy balance stands for the fact that the stack is generating heat because electrolysis is an exothermal reaction. Also, each overpotential, is a source of heat generation for the cell. Hotspots and nonuniform temperature distributions need to be avoided by having enough measures for heat spreading and dissipation. Temperature control of the PEMEC stack is important, because it directly impacts the cell-to-cell voltage distribution on more than one level. Firstly, the membrane proton conductivity, secondly the water management inlet temperature, which in the current work it is imposed as control parameter, introducing a heat exchanger in the inlet of the anode, thirdly the Nernst compression voltage, and lastly the back diffusion which is influenced by temperature as well.

4. Analysis of Experimental Data

Before examining the validity of the model and calibrate the parameters or change some procedures, it is advisable to perform an analysis on the experimental data that have been obtained. As already mentioned, the experimental data were collected from an experiment that was implemented on a commercial electrolyzer (Proton On Site) and have been collected to justify its performance.

4.1 Operation at Nominal and Partial Load

The experimental data represent all the parameters when the electrolyzer is in operation. These include current, voltage, pressures (anode and cathode), temperatures, flows for all the species, time and various other parameters that account for the control system of the whole process. For the present analysis in order to perform the calibration one needs to act on the current, the voltage and the temperature. The Pel is not accounted for since in the steady state conditions it is the product of the voltage and current. The H_2 production was not used on the outlet of the cathode, since the data of it, are after the purification of H_2, where hydrogen is lost on the production to clean the purification columns from water. Lastly, the pressure in both the anode and cathode remain almost constant.

The importance of the analysis is that in the simulation in order to perform the calibration, it is needed to run a sufficient amount of cases, meaning different input and output parameters in steady state condition. The data, that were used, represent the operation of the system in a whole day. Each, data was recorded every 15s, meaning that each day there were more than 16,167 data per variable. Each day, the experiment was performed in different conditions, either it was operated in full load (60 kW) or in variable load. A variable profile was chosen, whereby at the morning it was operated in partial load, during noon it reached the peak load and then again partial load. In Figure 4.1, Figure 4.2 and Figure 4.3 is depicted the profile of the current density, cell voltage and temperature over time respectively, to visualize the real profile of each one. It is clear from the profiles, that all of them face a lot of fluctuations over time. This is normal for real application because the system changes its own properties to adjust with the demand that the output required. First, when analysing the current density (Figure 4.1), it is noticed that it varies between the values of 0.4 to 1.9 A/cm^2 approximately. The profile corresponds to a typical profile of current density if the power was generated by Photovoltaic panels. During the morning (0 s - $4.5 \cdot 10^4$ s) the current density starts to operate with a small value and then gradually it is increasing with a time step every hour (real t= 4000s). It is mentioned here that the first 990s were excluded, where during this time a start-up period was noticed that cannot be considered in the analysis. Then, from $4.5 \cdot 10^4$ s to $5.8 \cdot 10^4$ s the work was carried out at the Peak load and for less than an hour the fluctuation disappears. After the peak the profile follows almost a symmetrical trend until it ends up at the value of 0.4 A/cm^2. The fluctuations of the system are strongly related to the production of the H_2 and the power Input. PEMEC, needs to work as much as it can in steady properties due to the fact, that variation penalizes the efficiency and the life time not only of the stack but also of the other components of the system. The system of a

PEMEC includes heat exchangers, pumps, separators, purification columns, valves, storage tanks etc. All of these have a delay of time when the system demands more H_2; Keep in mind also that the control system adds an additional delay to the system. Generally, the system acts quickly to each variation, which is also the main advantage of it when couples with renewables electrical input. Nevertheless, a test is needed to understand how these fluctuations affect the overall process.

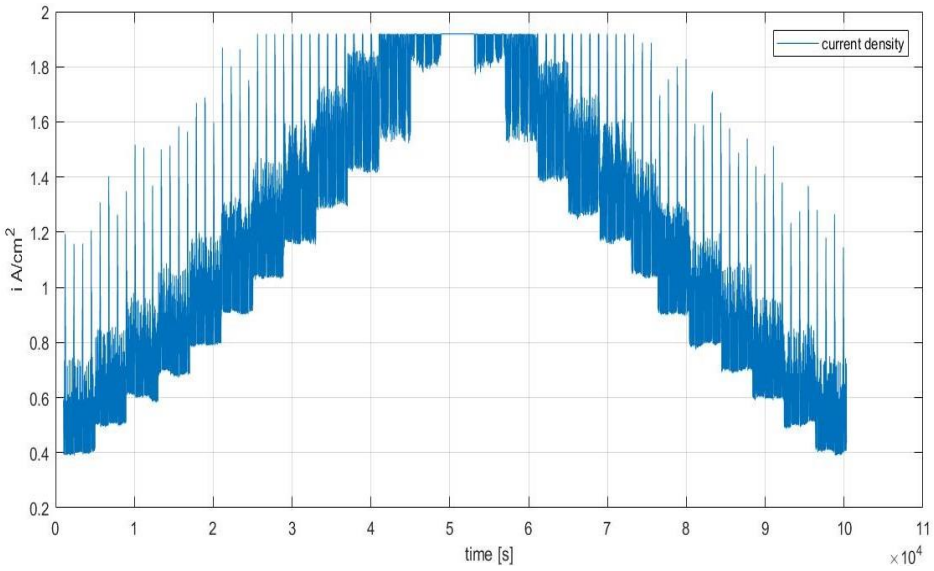

Figure 4.1: Current density variation over time

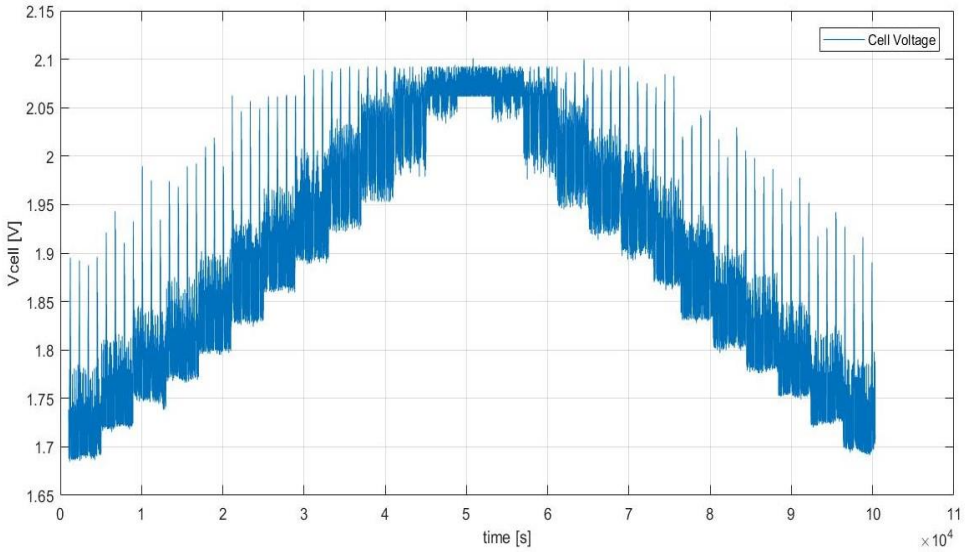

Figure 4.2: Cell voltage's variation over time

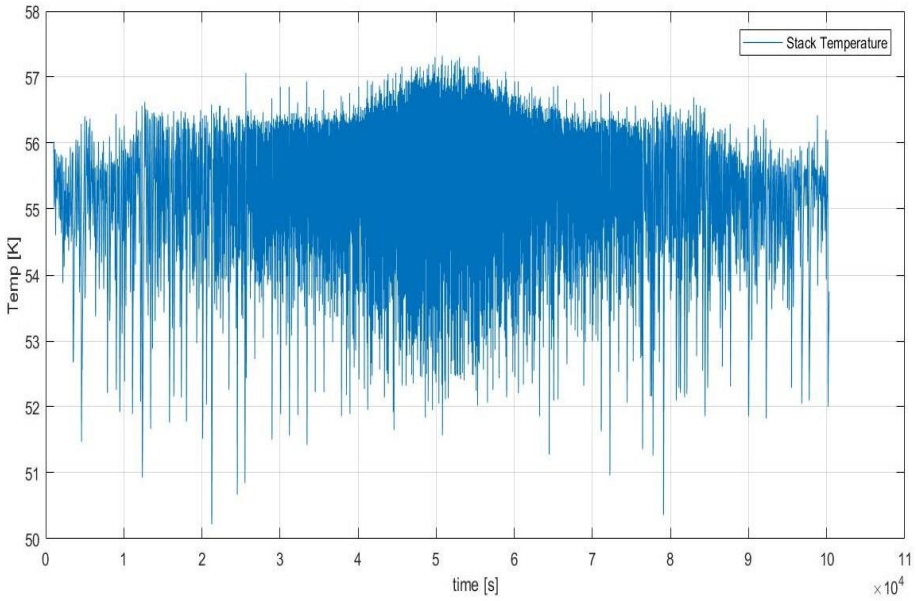

Figure 4.3: Temperature of the stack over time

The high peaks that are noticed, mainly appeared from the H_2 production that the system demands in partial load to clean the purification columns from H_2O. When the system reaches the peak, it loses H_2 from the real production without consuming more energy, since the system cannot operate in higher power. This is the reason why, as the peak power is reached, the range of variations tends to become smaller and smaller. Second, in Figure 4.2 it is shown that the stack voltage varies almost with the same trend as the current density. The minimum value is around 1.7 Volts (corresponds to i = 0.4 A/cm^2) and the maximum value is around 2.08 Volts (correspond for i = 1.9 A/cm^2). The main difference between the two profiles is that on the peak load the voltage keeps fluctuating. The main reason is that the voltage depends on the losses that the system has. Since the system is in high current density, the losses are mainly due to ohmic losses. The latter can be explained also with the temperature profile, that will be examined in the next paragraph

The temperature of the system is a very important aspect for the system to operate with high efficiency and without stretching the components. The temperature profile is different than the other two, since the cell must work in a constant value. The set point of the control system is 55.6 ^oC. The regulation of the system's temperature is performed with the input water which enters at the anode side. Before the stack, as has already been explained, there is a heat exchanger to heat or cool the water according to the current density or the power input. If the system is left without cooling for example, the temperature will keep rising which at the end will lead to damage to the stack. The variation of the temperature is lying between 50 to 58 ^oC. This variation is not so large and seems to work fine for the current process, although one can see that the mean value that the variations occur is the set point. As anticipated from the previous paragraph, it was observed that the fluctuations tend to become more often and have strong variations as the peak load is reached. The latter is related with the ohmic losses which are increasing even more if the exothermic reaction is considered that increases also the Top of the stack.

As mentioned at the begging of this chapter the scope is to apply a methodology which will help to run the calibration of the model according to the experimental data. It should be noted that it was not considered for the production of H_2 to fit the experimental data. It is useful to depict the profile of the real production that is characterized as "Dry Hydrogen production" since the measures obtained after the purification stage where there is a loss of an amount of H_2. Also, it is useful to show the pressure in the cathode side which the regulation is made by a valve in order to keep it constant.

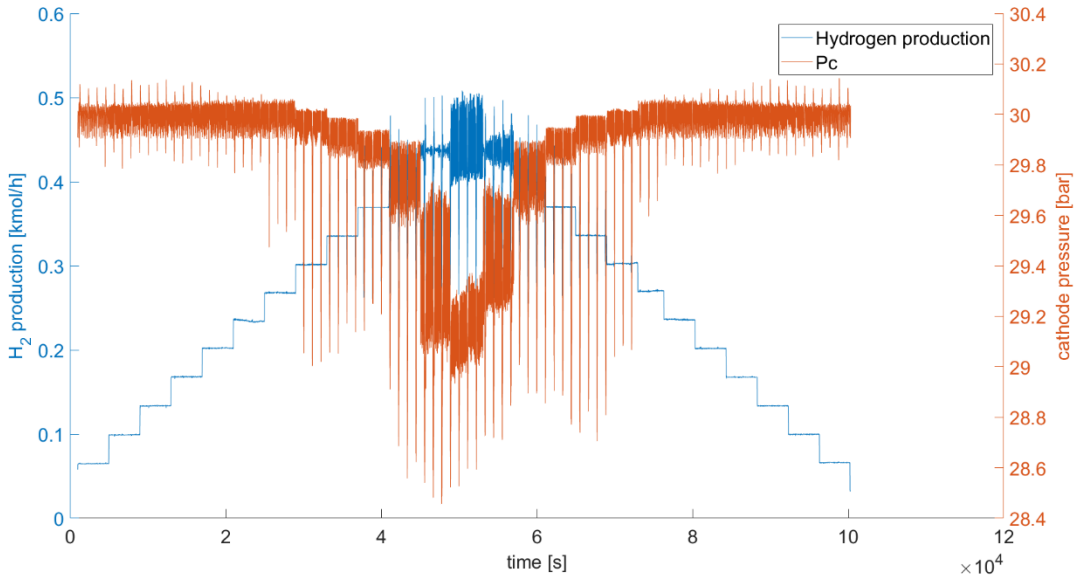

Figure 4.4: Hydrogen production and Pressure in the cathode side versus time

Figure 4.4 shows the variations of the Pc and the H_2 production. One can notice that practically the pressure remains constant even if it has some variations. The fluctuations are very small, and they vary between 28,8 to 30.1 bars. This response, for a real application, can be characterized almost as ideal, since the valve which regulates the pressure works as expected. Going back to the model, the variation of pressure during the operation strictly corresponds with the mass balances. If one had developed a model that also takes into account the accumulation of the mass d()/dt, one would have included the pressure variation, but since the dynamic model is thermally oriented, and also the pressure is almost constant, the cumulative term in the mass balances can be neglected from the model (see. **Eq. *3.1***,**Eq. *3.4***, **Eq. *3.7***, **Eq. *3.15***, **Eq. *3.16*** and **Eq. *3.17***). On the other hand, the production of H_2 follows the trend of current and voltage. This is normal since the current and H_2 are related with Faraday's law. It is worth mentioning a characteristic of this curve; this is that the fluctuations are very small during the partial load. This corresponds to the strategy of the production that must be followed when the electric power input is almost constant. When one moves to the peak load, the fluctuations are increasing, and this is mainly linked to the purification stage of the process. The dry H_2 as mentioned in the Figure 4.4 is indicating that no humidity exists on the outlet. The water is collected and recirculated back to the system.

4.2 Management of the Experimental Data

The management of the experimental data is crucial to find the best values that will help to determine the validity and the calibration of the fitting parameters that chosen. Moreover, a lot of the data that obtained do not correspond to the stack only but also to other parameters that are not considered at the moment. For example, the peaks on the profiles due to the purification of H_2 in the partial loads need to be excluded from the analysis. The latter action may lead to loss of some information of the real performance of the system, but on the other hand it gives a better representation of how the stack behaves when it works alone.

For the current analysis, the choice is to act on average values on the current density, voltage and temperature. The procedure is to analyse the profile and set a time step where the power input is increasing and to consider that during this time, the cell works as if in steady state. The average value alone is over estimating the single values that are to be obtained, so a different procedure is needed to exclude the unnecessary points that do not correspond to the steady state condition of the time that the testing was taking place. Table 4.1 depicts the time and the number of points where the power input was assumed to operate in steady state conditions.

Table 4.1: Number of steps vs time that it was considered that the stack is worked in steady state condition.

NUMBER	*RANGE OF TIME WHERE IT WAS ASSUMED STEADY STATE [S]*
1	1005 - 4995
2	4995 - 8985
3	8985 - 12975
4	12975 - 16965
6	16965 - 20955
7	20955 - 24945
8	24945 - 28935
9	28935 - 32925
10	32925 - 36915
11	36915 - 40905
12	40905 - 44895
13	44895 - 48885
14	48885 - 52875
15	52875 - 56865
16	56865 - 60855
17	60855 - 64845
18	64845 - 68835
19	68835 - 72825
20	72825 - 76815
21	76815 - 80805
22	80805 - 84795
23	84795 - 88758
24	88758 - 92775

The next step was to determine a suitable value for the average quantities in the time steps that were introduced in Table 4.1. It was decided to use Matlab software, to perform the analysis. Matlab has a variety of functions that visualize the distribution of the data around a mean value. One can mention that the data follow a normal distribution (or Gaussian distribution) around the mean value. The only problem was the fluctuations of the data around the time steps which in typical mean values calculations, the deviation of the data is considered and thus tends to increase the value. Accordingly, the data presented excludes the 25% of low values and the 75% of the higher ones. Figure 4.5 depicts the visualized results:

a)

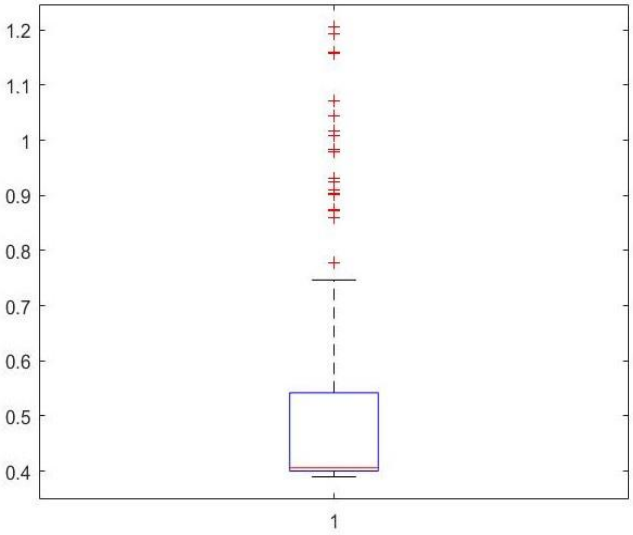

b)

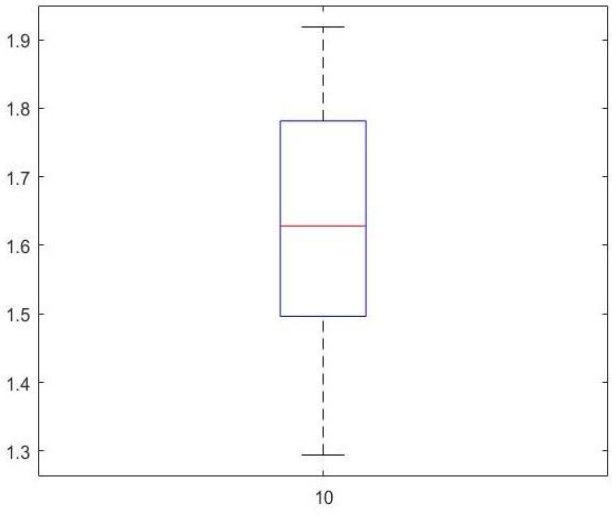

Figure 4.5: The two figures represent two different current density a) step(1) and b) step(10) which are related with the steps of Table 4.1

Figure 4.5, shows that in step (1) where partial load applies, the data that fall out of the range of 75% are more than the data of the step (10). The red line in the two boxes represents the average

values considering only the data which fall- within the range [25% - 75%] of the normal distribution. The calculations of the average values were obtained with different functions of Matlab software: a) mean, b) trimmean and c) quartiles. Below one can see the results for the three different average values for: i, V_{cell} and T_{op}.

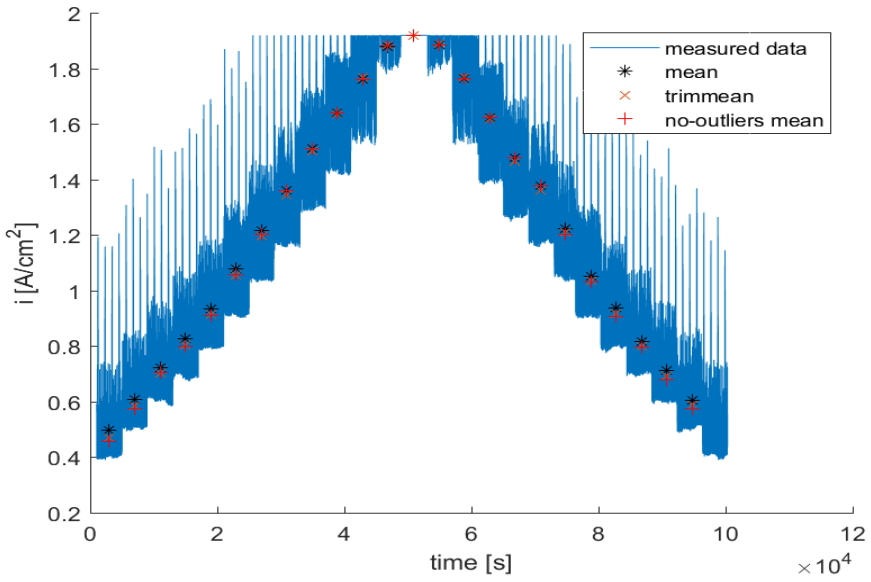

Figure 4.6: Graphical representation of the mean, trimmean and quartiles values of current density

Figure 4.6 presents the three different types of average values. It is observed that as the peak is reached, the three values tend to coincide each other, because the fluctuations are minimized. Between trimmean and quartiles, the latter is chosen since in the partial load it tends towards lower values for each step where there is more dense data. The problem which arises at the profile is that in some steps (9 and 10) the averages values tend to the right, while the other steps are more centralized. The step that was introduced is 3990 s and it was the one that predicts better for all the steps the average values. The error is small since in higher current densities the fluctuations are fewer than in partial load, so the average is calculated taking into account more values, as depicted in Figure 4.5 of the second graph.

Figure 4.7 shows again the different types of average values. Again, for this profile, the quartiles were chosen which predict better the cell voltage. For both, current density and V_{cell}, the maximum difference (step (1) and step (24)) between the average values lies around 8% to 10%. Therefore, taking the mean, the error is not significant. On the other hand, the result is to have as much as possible reliable data to perform the calibration.

Figure 4.8 illustrates the temperature variation vs time and the mean values of it. In most of the cases the T_{op} remain constant and the values are almost the same. Step (3) and step (20) seem to have the bigger variance. It is noted that deep changes in the temperature affect the average mean value. Hence, for these points the quartiles seem to work better. The values obtained from this analysis are depicted in the next table:

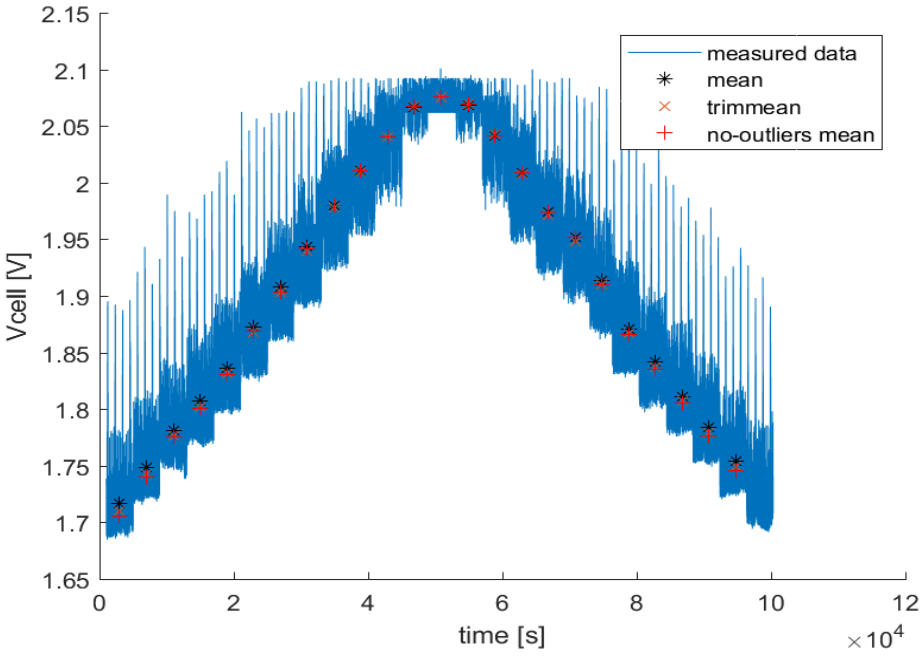

Figure 4.7: Graphical representation of the mean, trimmean and quartiles values of cell voltage

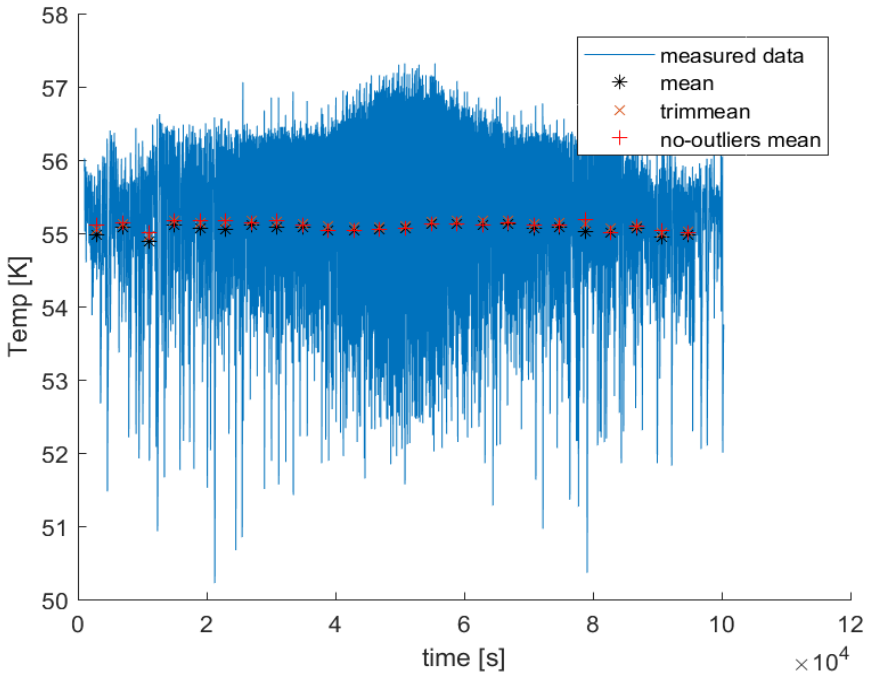

Figure 4.8: Graphical representation of the mean, trimmean and quartiles values of Cell voltage

Table 4.2: The final values of i, Vcell and Top that obtain from the data analysis with respect of the correspond time step

Step	i [A/cm^2]	Vcell [V]	Top [^{o}C]
1	0.456	1.705	55.113
24	0.574	1.746	55.010
2	0.575	1.740	55.137
23	0.679	1.776	55.044
3	0.704	1.775	55.009
22	0.795	1.805	55.099
4	0.798	1.801	55.167
21	0.906	1.835	55.012
5	0.912	1.831	55.167
20	1.032	1.866	55.193
6	1.057	1.868	55.169
7	1.203	1.904	55.143
19	1.204	1.910	55.113
8	1.361	1.942	55.172
18	1.378	1.951	55.117
17	1.477	1.974	55.148
9	1.511	1.980	55.106
16	1.623	2.009	55.115
10	1.638	2.011	55.044
15	1.764	2.041	55.130
11	1.761	2.040	55.033
12	1.882	2.068	55.046
14	1.885	2.069	55.120
13	1.919	2.076	55.062

Table 4.2, shows the results that will be used to calibrate the model. These values represent the real behaviour of the stack when it operates in real conditions. Notice that they were arranged from the lowest current density to the highest one and the corresponding time step that was introduced in Table 4.1

4.3 Outlet Hydrogen Flow

In the first stage of the system where only the stack is calibrated in steady state conditions, one cannot consider the H_2 production to be a reliable indicator. The theoretical production should be higher than the real one and the amount that lost, will be calculated from the results of the whole process. It is useful to depict the comparison between the theoretical hydrogen production and the one which was obtained from the experimental data (the profile is showed in Figure 4.4). This analysis will be useful when the process is set up for the dynamic analysis of the PEM electrolyzer system. The theoretical H_2 production can be calculate according to the equation **Eq. *2.8*** (Nernst's equation) where i is the current density that was obtained from the experimental data and depicted in Figure 4.1.

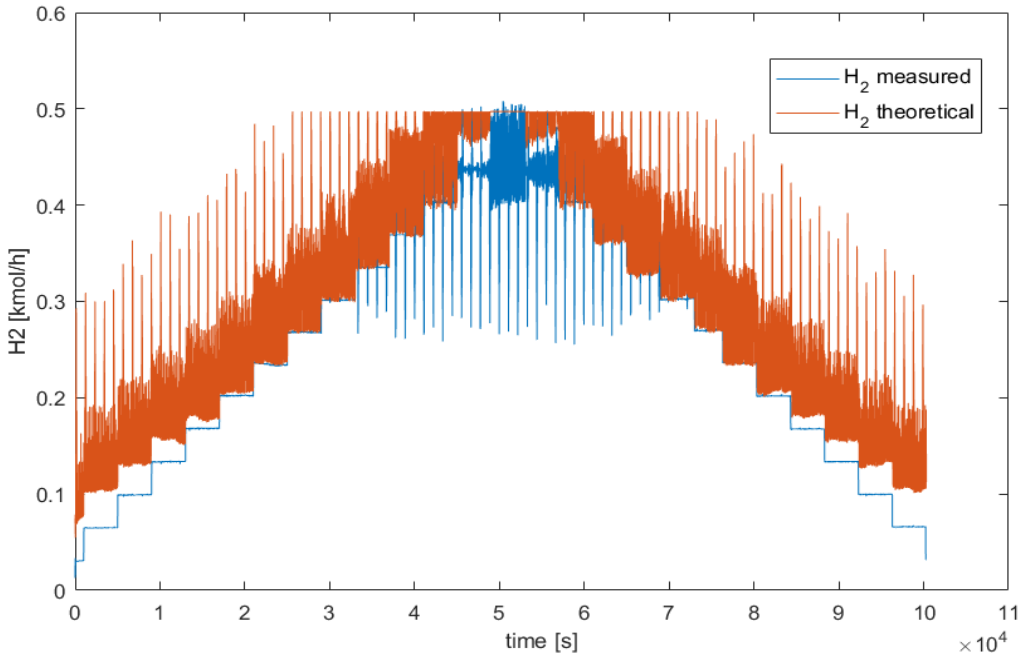

Figure 4.9: Comparison of the theoretical and measured hydrogen production in kmol/h

Figure 4.9 depicts the proportionality between the theoretical hydrogen production and Nernst' equation, this is the reason, both the current density and the theoretical hydrogen have the same profile. Comparing now, the two curves, it can be seen that the hydrogen loss during the real process mainly due to purification is different in partial load and in the peak load. It is noticed that at the partial load and around 20,000s the two profiles are almost coincided. Even if the theoretical hydrogen production has fluctuations, the blue curve joins the blue one. The latter indicates that the partial load is penalized in terms of hydrogen loss and probably efficiency more than in the peak load. Figure 4.9, shows the molar mass flow rate respect to time. In order to understand better how much hydrogen is lost during the real process, it useful to calculate the amount of mols that are produce each minute and make the comparison in terms of absolute difference (see. **Eq. *5.1***)

Figure 4.10 shows the same trend for both curves as in Figure 4.9. The profiles especially for the theoretical hydrogen production is much smoother than the previous. The latter can be explained due to the integration of the values over one minute. Since, there were four measurements every one minute some of the picks are accumulated. The main difference that it can be noticed, is that there is an almost constant difference between the profiles. Meaning that the purification stage demands a specific amount of H_2 to clean the column from the humidity. There are different phenomenon that can explain the behaviour of peaks on the theoretical and on the measured H_2. The peaks on the theoretical is mainly depend on when the purification column is saturated with water, in this case the system demands more H_2 than normally. Also, it can be notice that there is almost a periodic time when the peaks appear. It can be note here that when the current density increases the electro-osmotic flow rate of water increases (see. Eq. ***3.20***), meaning that either it needs to adjust the separator conditions to extract more water from the cathode flow or this extra water will be separated in the purification stage. According to the current data, it cannot be said with certainty which of the

two cases is performed, but it seems that the there is no difference on the purification stage, so probably the water is extracted in the separation stage. Furthermore, the nadir points at the peak load of the measure curve (600-1100 mins) indicates that some of the produce H_2 is bunted to the purification since the stack cannot demand more power as it did when it works in partial load to clean it.

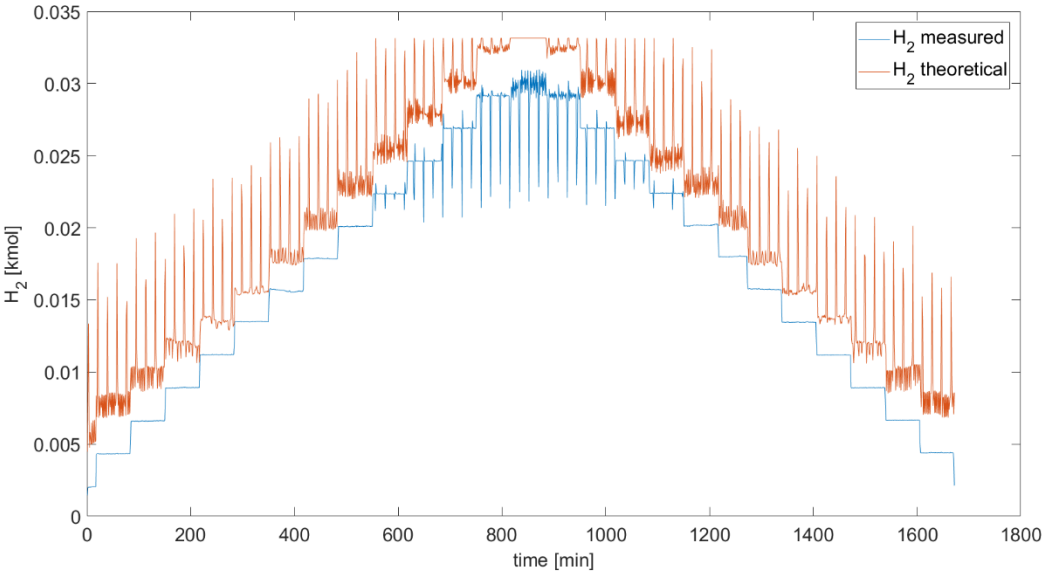

Figure 4.10: Comparison of measured and theoretical hydrogen in kmol respect to time in minutes

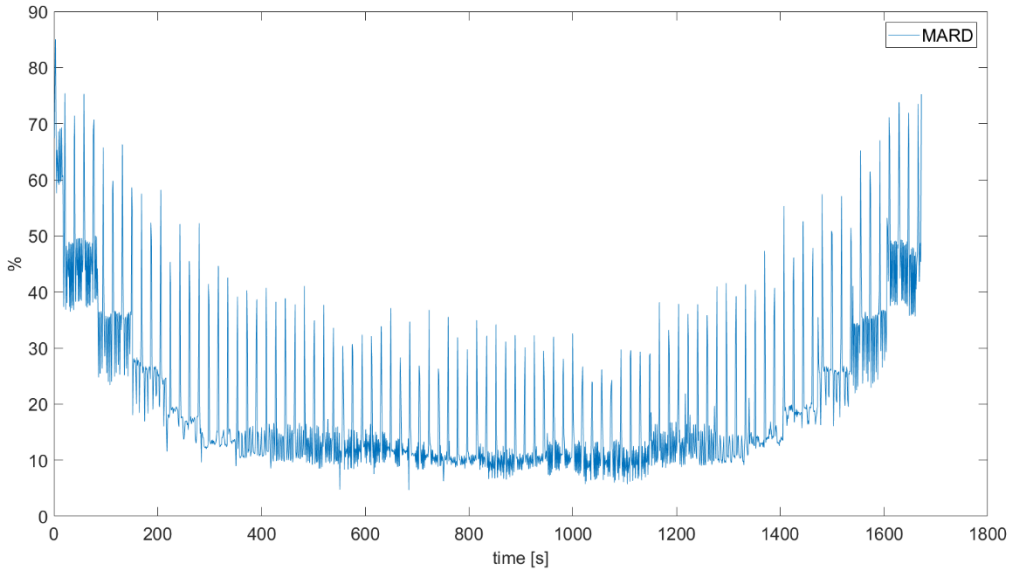

Figure 4.11: Mean absolute relative difference (MARD) between theoretical and measure data

The percentage difference shows ,Figure 4.11, that the loss of hydrogen from 0 to 300 mins declines from 80% to 13% that remain almost constant from 300 to 1400 mins and then it is stars rising

for the remaining time from 13% to 55%. It is clear that for every step in which the power is changed, thus the current, the percentage is different when the cell is working in partial load. When it reaches the peak the penalize of the hydrogen loss is less (around 15%) and it remains constant for the majority of the whole operation time. This indicate that its favour for the stack to work in power input close to the peak since the electrical efficiency of the stack will penalize less. This profile it will need to be take considered when the simulate dynamic process is set up since in the current thesis the purification stage is not include in the dynamic simulation.

5. Model Calibration & Validation

5.1 Sensitivity Analysis

In order to perform the calibration, it is necessary first to identify which variables or parameters affect more the model. Moreover, there is a need to account also for the parameters that one cannot be certain about their value even if one looks in the literature. Some parameters are not mentioned by the manufacturers and so one can only assume some typical order of magnitude to perform the calibration. One other strategy in the calibration is to group some parameters that are correlating with each other and using this to calculate other variables. An example is the width of the anode and cathode; their values are not known to calculate the ohmic resistance of the electrode, so one must either to assume a typical value or perform the strategy that was mentioned.

Before proceeding deeper in the calibration, it is useful to show the parameters and the variables that are studied in the model:

Table 5.1: The parameters of the model

	NAME	VALUE	UNITS
GEOMETRIC PARAMETERS	A_{cell}	213.678	cm^2
	ε_{el}	0.3	-
	S_{ext}	0.31	m^2
	$t_{el,a}$	0.0013	m
	$t_{el,c}$	0.0013	m
	t_{mem}	Range: [1.25 e-4 : 2.5 e-4]	m
	t_p	0,001	m
MASS BALANCE PARAMETERS	$D_{H2O/O2}$	Eq. 3.29	m^2/s
	$D_{H2O/H2}$	Eq. 3.29	m^2/s
	D_w	Eq. 3.24	m^2/s
	D_{eff}	Eq.3.28	m^2/s
	D_λ	1.25e-10	m^2/s
	λ	21	-
	n_{eo}	5 or Eq.3.21	-
	Kp_{O2}	1.62 e-16	mol/m s Pa
	Kp_{H2}	3.0 e-16	mol/m s Pa
	K_{darcy}	1.58e-18	m^2
	P_{an}	2.5	bars
	P_c	30	bars
	ΔP_{anode}	0.1	bars
ELECTROCHEMISTRY PARAMETERS	n_e	2	
	$i_{o,an}$	Range: [1 e-12: 1 e-6]	A/cm^2
	$i_{o,c}$	Range: [1 e-6: e-3]	A/cm^2
	iL	6.2	A/cm^2
	α_{an}	Range: [0.5: 2]	-
	α_c	Range: [0.25: 0.8]	-
	ρ_{an} / ρ_c	0.0075	mΩ cm
	ρ_{eff}	Eq. 3.45	Ω cm
	σ_{mem}	Eq. 3.47	S/cm
THERMAL BALANCE PARAMETERS	C_{th}	50.1	kJ/K
	T_{amb}	25	°C
	Ur	Eq 3.53	kW/K
	F_{ext}	1.5	-

The first step is to assign a basic polarization curve (P-C) which will be used as an indicator to depict how the parameters change the Vcell when different current densities are applied. The parameters, that chosen, are presented in Table 5.1 and the values of the basic P-C are:

- t_{mem} = 2.5e-4 [m]
- $i_{o,an}$ = 1e-10 [A/cm^2]
- $i_{o,c}$ = 1e-3 [A/cm^2]
- $\alpha_{an} = \alpha_c = 0.5$ [-]
- T_{op} = 55.6 [°C]
- Pc = 30 [bars]
- Pan = 2.5 [bars]
- Numbers of cells = 65
- $n_{eo} = 5$
- The activation losses are calculated with B-V' equation (see. **Eq. *3.32***)
- The ohmic losses are calculated with **Eq. *3.42*** - **Eq. *3.45*** assuming the resistivities equal for both anode and cathode with the value of 0.0075 Ω cm
- For water diffusion through the membrane was used **Eq. *3.22***, **Eq. *3.24***, **Eq. *3.26*** - **Eq. *3.29***
- Inlet flow rate of water in the anode 100 kmol/h

The simulation's results are depicted in the next Figure:

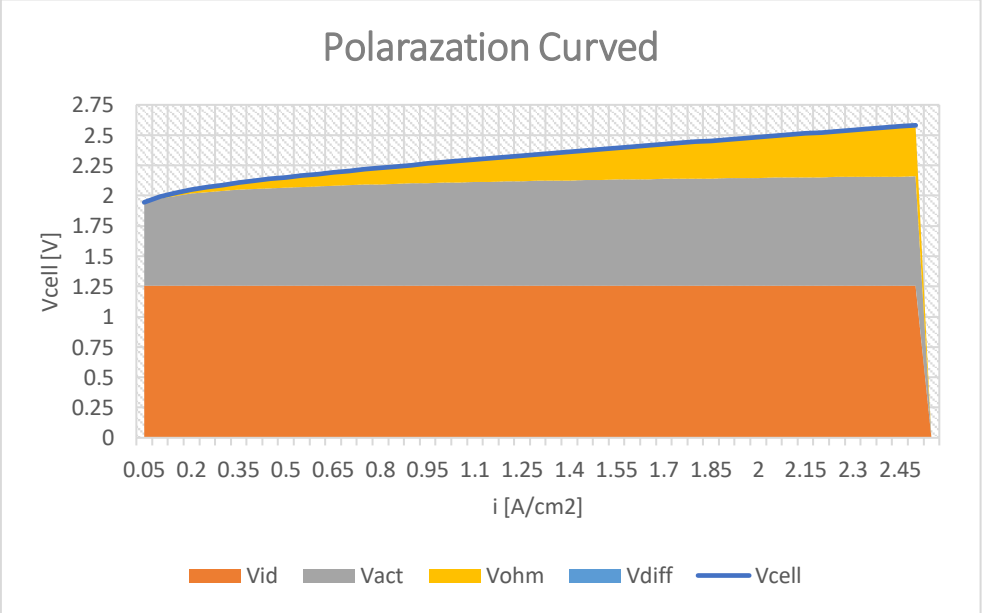

Figure 5.1: Basic polarization curve

Figure 5.1 depicts a typical P-C. At low current density the main loss is due to the activation over potential; it should be noted here that it was reported that Vact the activation over potential but in

section 3.4 it was denoted with the Greek letter η. Then, as the current density increases the activation loss remains almost constant and the increase of the voltage is due to the ohmic losses (Vohm or η_{ohm}) which increase linearly following Ohm's law. The Vdiff has almost null contribution since as mentioned in section 3.4, the limited current is too high with respect to the typical current densities that PEMEC is operating. This P-C will be the basic curve on which the variables or parameters that have a significant impact on its shape will be specified. It is now time to analyse the four different packs of parameters as depicted Table 5.1.

5.1.1 Geometrical Parameters

Geometrical parameters generally are an important issue when one tries to build the cell from the beginning. Also, it is important when models are developed that are more than one dimension, it is necessary to apply CFD models for the pressure gradient or the flow along the channels etc. In this model the specific geometrical parameters are unknown, thus one cannot be constrained to calibrate the zero-dimension model with these parameters. Although their impact on the P-C curve can be observed when some of them are changed. One parameter that according to the literature has a significant role is the conductivity of the membrane. But since it was stated in section 3.3 that this depends on the water content λ and the temperature, both of which for the steady state are characterized as fixed parameters, as a result σ_{mem} will be also fixed. The only parameter that can be used and to be sure about its physical meaning and which is close to reality is the width of the membrane t_{mem}. The width of the electrodes both in the anode, cathode (t_{el}) and the width of the plate (t_p) can be varied a lot from manufacturer to manufacturer according to what they want to achieve. Meaning, companies try either to minimize the cost of their components so they are using sophisticated materials to make thinner the widths or other companies focus on the efficiency which may lead to penalize the width of the plates or the electrodes to use different catalysis or change the membrane width with a Nafion with better conductivity, which at the end are more important ohmic losses. Figure 5.2, shows the dependence of the Vcell when a sensitivity analysis is performed on the width of the membrane. It is obvious that as the width becomes lower, when t= 1.25e-4 m, the losses tend to decrease, and it reaches 8% lower voltage with respect to the basic P-C when the current density is at 2.5 A/cm^2. When the width is 1.75e-4 m the at 2.5 A/cm^2 the difference is about 5%. For both widths the dependence on lower current densities is very small and until 0.6 A/cm^2 the difference is less than 3%. The results point that the width of the membrane needs to be consider in the calibration of the stack since it is the only parameter for which the range of it is known with certainty. Moreover, the experimental data starts from current densities higher than 0.4 A/cm^2 and mainly concentrate to a range of 1.8-2.1 4 A/cm^2 (see Table 4.2). The last point to discuss about the t_{mem} is that ohmic losses are calculated with Ohm's law equation, accordingly it changes the slope of the curve without changing the intercept on the voltage. The latter effect is illustrated also in Figure 5.1.

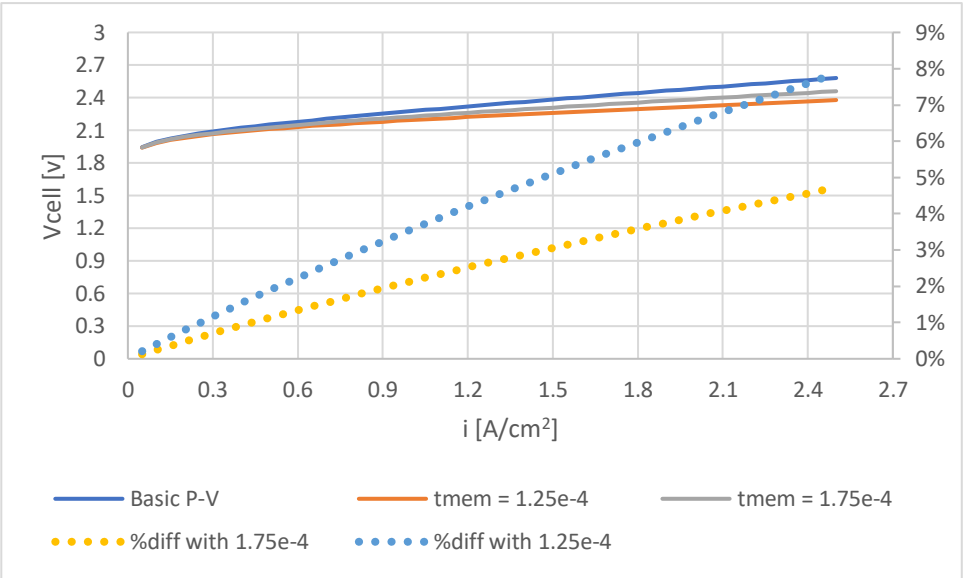

Figure 5.2: The figure illustrates the dependence of the Vcell change the width of the membrane. Also, it shows the % difference on the voltage output when the current density increases

The other parameters that are characterized as geometrical are the width of the anode and the cathode. For the porosity of the electrode, the Acell and the volume of the anode and cathode their values are fixed. For the porosity as explained in section 3.3, the value 0.3 is generally used for modelling of PEMEC. The Acell and the volume of the anode and cathode their values were mentioned by the manufacturer.

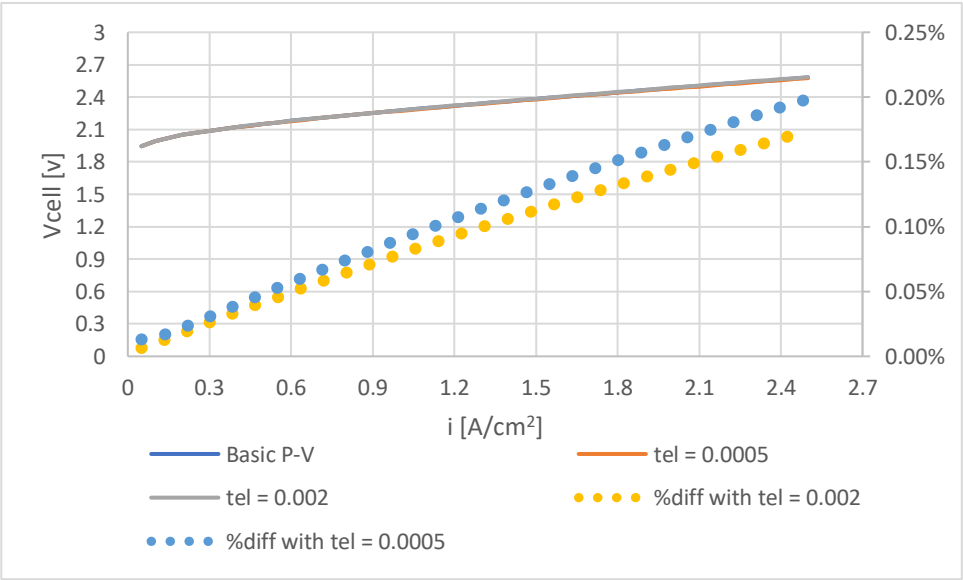

Figure 5.3: The figure depicts the dependence of Vcell on the width of anode and cathode

The results that are presented in Figure 5.3, demonstrate that Vcell does not depend on the width of anode and cathode. This may be misleading due to the fact that the model is zero dimensions, so one cannot generalize any conclusion. In fact, the width of the cell contributes both in the mass balance and the ohmic resistance of the cell, so a more detailed model can show higher dependence

on these values. Similarly, the structure of the electrode, meaning the porosity and the type of the material that is included for building the electrodes affect the geometry. It must be repeated that electrodes and bipolar plates are important for the compact of the cell and also the cost of the cell, since they include the MPL (micro porous layer) where the noble catalyst is introduced. In Figure 5.3, the yellow dot line was calculated in absolute terms because the Vcell is higher than the basic P-C. The highest difference is only 0.2%, so for the calibration these values are considered as fixed.

5.1.2 Mass Balance Parameters

According to Table 5.1, the only mass balance parameter that one can act on is the electro-osmotic drag coefficient n_{eo}. The other parameters are either fixed from a formula like the binary diffusivities or reported as fixed value from the literature. As already mentioned in the analysis of the model, the most important water transport mechanism from anode to cathode is the electroosmotic. Water transport from anode to cathode cannot affect directly the performance of the stack. The anode side is fully flooded with water and as a result the membrane is fully hydrate. The performance of the cell is related by the production of H_2 for the power that is provided to the stack. In terms of steady state, the water content of the membrane does not change and also the membrane prefers to transport protons for which the concentration is lower than the concentration of water. Accordingly, the efficiency of the stack itself will not affect the production of the H_2. In [83], it is mentioned that in terms of P-C the dependence of different values of n_{eo} did not show any significant difference in the overpotential losses if the operating conditions do not change. Medina and Santarelli [79] investigate the matter of the water cross-over due to electro-osmotic drag, without measuring the performance of the stack but they measured the water in the cathode due to this phenomenon. Since the model does not contain a mechanism for pressure which influences the drag coefficient, it is expected that one will not see a significant change on the P-C.

The values that were used for n_{eo} are reported in Table 5.1; the value used is equal to 5 from [6] and the value 2.33 solving for **Eq. *3.22***. In Figure 5.4, as mentioned before, the electro-osmotic drag does not show any change at the P-C, in fact the difference was on the O.M of 10^{-10}, so practically zero. It is useful to refer here to an important issue that may arise as shown in this figure. The water transport through the membrane is not strongly related to the performance of the stack but it is related to the whole process. The more water there is in the cathode, the more H_2 is needed to dry it during the purification stage. The efficiency of the process is strongly related with the water transport and thus the cost of it. So, it is very important to know how much water is obtained on the cathode side due to the fact that this amount in terms of a day can be a significant amount. An example can be seen in Figure 4.4 where the production of H_2 is increasing in order to perform the purification.

The next step is to do a sensitivity analysis on the pressures. Even if this is considered as steady since the model is thermally driven, it will be useful to see the change on the P-C for future investigation on their influence. Note here that the trend is to have high pressure PEMEC to minimize the compress work of the H_2 when the need is to store it (storage pressure 200 bars, T = 25 ^{o}C).

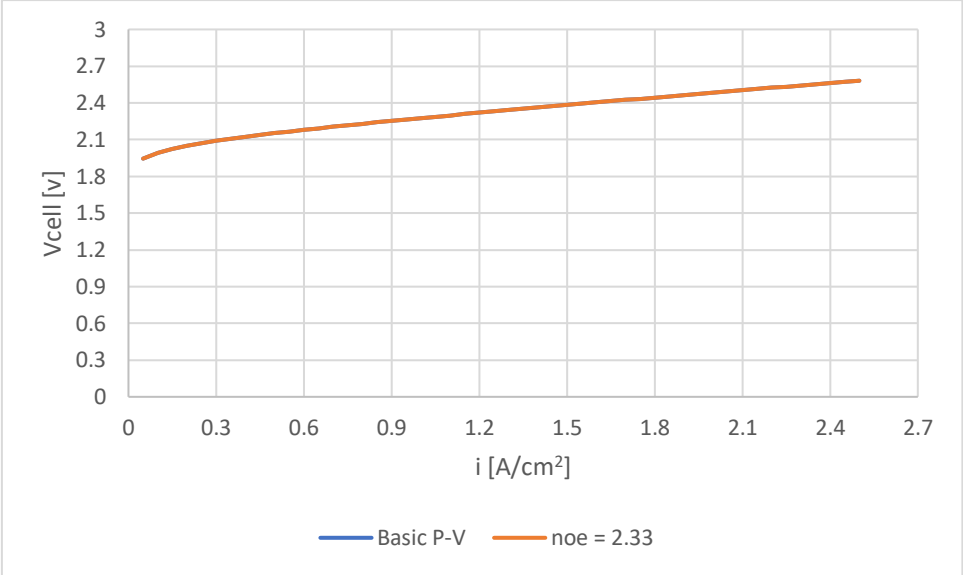

Figure 5.4: The influence of n_{eo} on the P-C. Two values were used and reported in Table 5.1

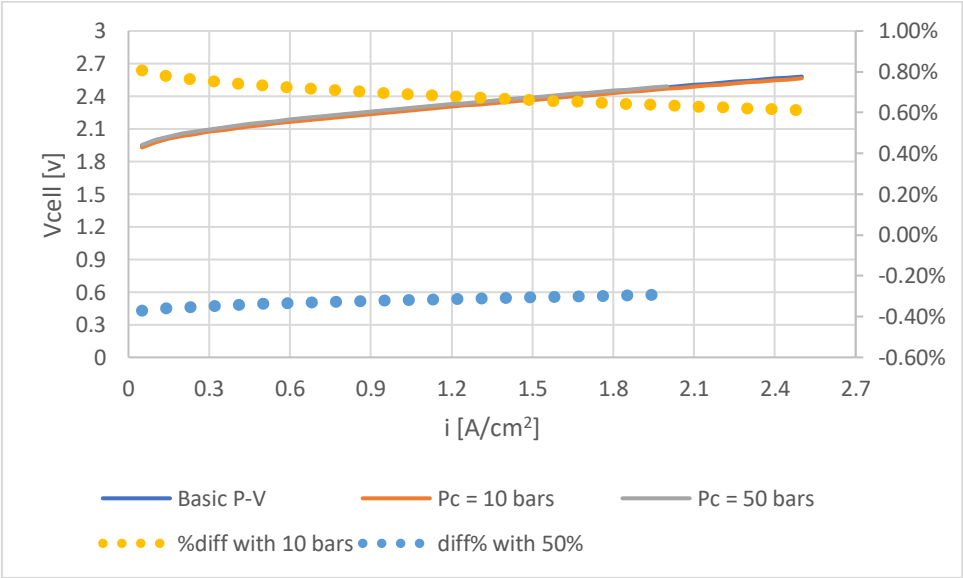

Figure 5.5: Pressure's dependence on P-C for 10 and 50 bars.

The pressure is related with more than one thing in the performance of the stack. The pressure appears on the mass balance but also in the electrochemistry since Nernst's equation is calculated with it. So, the analysis on zero-dimension models need to be carefully analysed because they may lead one to wrong conclusions. Figure 5.5, shows that the higher the pressure the higher are the losses that are obtained. When the simulation is run for different current densities, it is noticed that the system fails to predict the value of Vcell when i is higher than 2.1 A/cm^2. The problem is the way the mass balances equation was calculated by the simulation. The gradient of the concentration between anode and cathode in **Eq. *3.23*** become zero and reach its lower limited value. When Pressure (Pc= 50 bars) is increasing the losses are also increasing, as the negative % values of the right y-axis prove in Figure 5.5. Increasing the pressure, may not affect liquid water volume but decrease the concentration of H_2 in cathode; thus, the concentration of water will also increase. The pressure also affects the

electro-osmotic flow so there will be more water in the cathode. Lastly, the increase of pressure leads also to the rise of the Vid. This is the reason why pressurized electrolyzers are combined with elevated temperatures. For Pc =10 bars the trend is the opposite. The %diff is relatively high (0.8%) at low current densities and tends to decrease as current density is increasing. Nevertheless, for the current analysis the contribution of pressure is less than 1% and it was considered Pc as a fixed parameter and equal to 30 bars.

Anode pressure and pressure drop affect even less the P-C, so both of them are chosen to be held as fixed parameters with the values that were introduced in Table 5.1.

5.1.3 Electrochemistry Parameters

The electrochemistry parameters are related with the activation and the ohmic losses. Their values are related with the material that was used to build the stack. In section Electrochemical 3.4, the importance of these parameters was analyses and compared to their values that were found in the bibliography. It was expected that the activation losses will appear at low current densities. The parameters that are related with the Vact are the exchange currents of anode and cathode ($i_{o,an}$, $i_{o,c}$) and the transfer coefficients both again for anode and cathode (α_{an}, α_c). Vact has a significant impact on the performance of the stack even if it is remaining almost constant when the current density rises (see Figure 5.1). On the other hand, the parameters that are related with the ohmic loss are the resistivities (ρ), that were assumed as equal, meaning that there is the same material. The values which chosen to test the activation losses are taken from Table 3.4. The values of the resistivities were chosen arbitrarily assuming +/-10% on the value of 7.5 μΩ cm.

In Figure 5.6, the results of the sensitivity analysis are depicted, applying a different current densities and transfer coefficients. The sensitivity analysis was divided into four cases. Each case has four different transfer coefficients. With this way, it was possible to understand how these parameters act on the Vcell. In Table 5.2 are summarized the cases that were used to obtain Figure 5.6

In Figure 5.6, the basic P-C that were used as an indicator is the orange line (1-b). In the case 1 varying the transfer coefficient an improvement on the Vcell is seen. In the (1-a) case where there is an increase in the anode transfer coefficient and a decrease in the cathode transfer coefficient the activation losses are improving significantly, around 9% (i=0.05 A/cm^2). Then keeping constant the cathode transfer coefficient and moving to case (1-c) where there is a lowering of the anode transfer coefficient (0.8) and the grey P-C is generated which means that the losses are higher than in case (1-a) but still better than the basic case (1-b). (1-d) shows the lowest loses with respect to the other three (yellow line). Thus, the higher is the transfer coefficient of the anode side, the better is for the losses. It seems that the cathode transfer coefficient does not affect the performance of the cell as the anode transfer coefficient does.

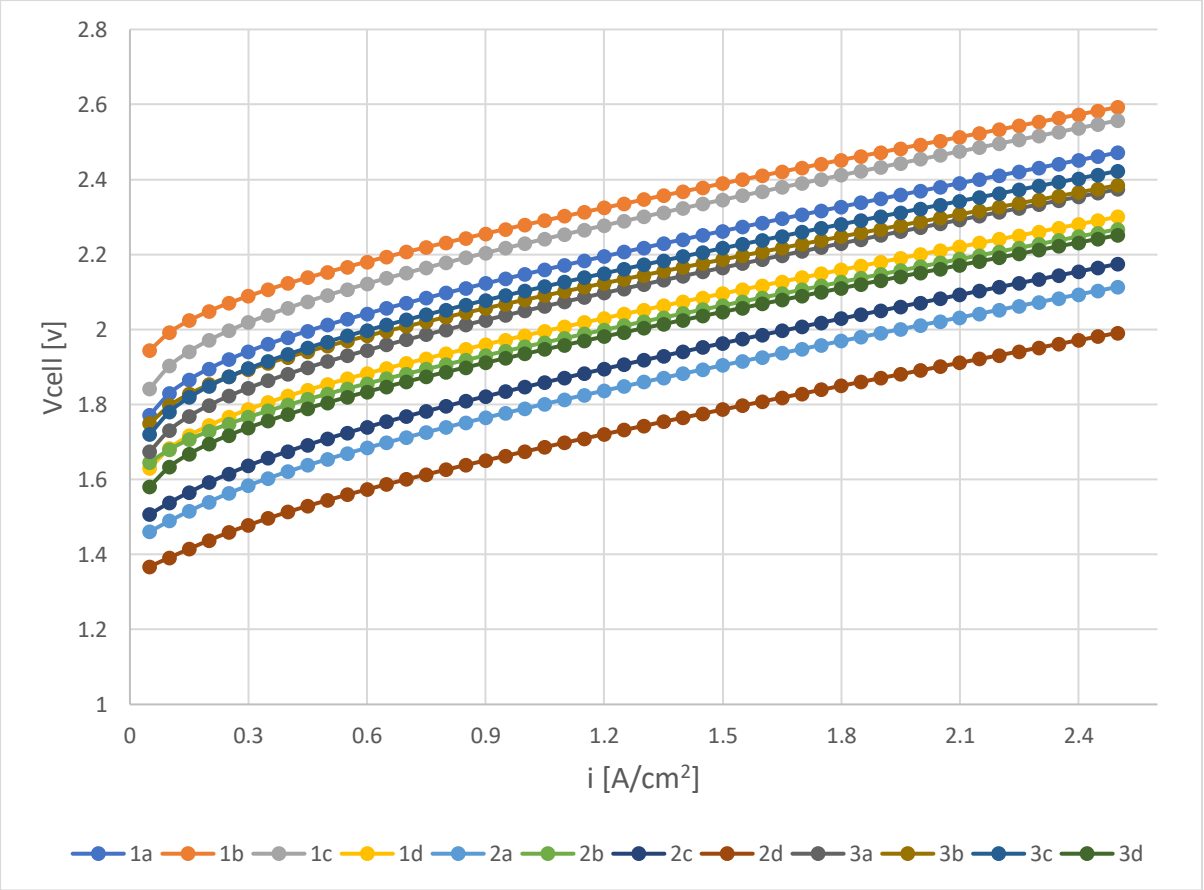

Figure 5.6: Different i_o and α were tested to obtain the dependence of Vcell

Table 5.2: The values of i_o and α that are used for Figure 5.6

Exchange Current		Transfer Coefficient			
		a	b	c	d
1.	$i_{o,an}$: 1e-10 $i_{o,c}$: 1e-3	α_{an} = 1 α_c = 0.25	α_{an} = 0.5 α_c = 0.5	α_{an} = 0.8 α_c = 0.25	α_{an} = 2 α_c = 0.25
2.	$i_{o,an}$: 1e-7 $i_{o,c}$: 1e-1				
3.	$i_{o,an}$: 1e-7 $i_{o,c}$: 1e-3				

Moreover, when moving to case 3, where the exchange current of the anode becomes 1000 times higher than case 1 the results follow the same trend as before, but the improvement is much better than in the case 1. Comparing (1-b) with the (3-b), the gain is around 10% for current density 0.05 A/cm^2.

Acting now on the exchange current of the cathode, increasing the latter by 100 times keeping constant the anode's exchange current, again lower losses are noticed. In fact, comparing (1-b) with (2-b), the improvement is 15%. The best case is by far case (2-d) in which the activation losses improved by 30%. Although, case (2-d) it is an extreme condition, it shows the trend on these parameters. The physical meaning on the advance performance of the cell when the transfer

coefficient and the exchange current are increased is that the kinetics of the electrochemistry reaction improve. The latter was achieved either increasing the load of the catalyst (but also the cost) or utilized the geometry of the electrode near to the membrane or change the catalyst for example from Pt to Ir. Lastly, all the curves are parallel with each other and only move up or down, the slope does not change, since there is no change in the ohmic losses. For the calibration the four parameters will be considered as fitting parameters to adjust the experimental data to the model.

The last parameter which will be analyzed is the resistivity of the electrode. The resistivity will affect the slope of the curve meaning that if material with lower resistivity is used the slope will decrease. The problem with the ohmic losses is that there are too many parameters to be assumed, the resistivity and the width of the electrode, which both are used to calculate the Rohm. The ohmic losses also include the resistance of the separate plates which are made by the same material as the electrode. The values of the resistivity that were tested are 6.75 μΩ cm and 8.25 μΩ cm.

In Figure 5.7, it is shown that the resistivities do not affect the P-C. The three curves are almost equal and the relative change at its maximum value is 0.03%. In this case, even if it is observed that there is a small dependence, the resistivities will be used as fitting parameters in model because there is only one parameter that counts for the ohmic losses and this is the width of the membrane. The physical meaning of the results during the calibration will be discussed in the Calibration section.

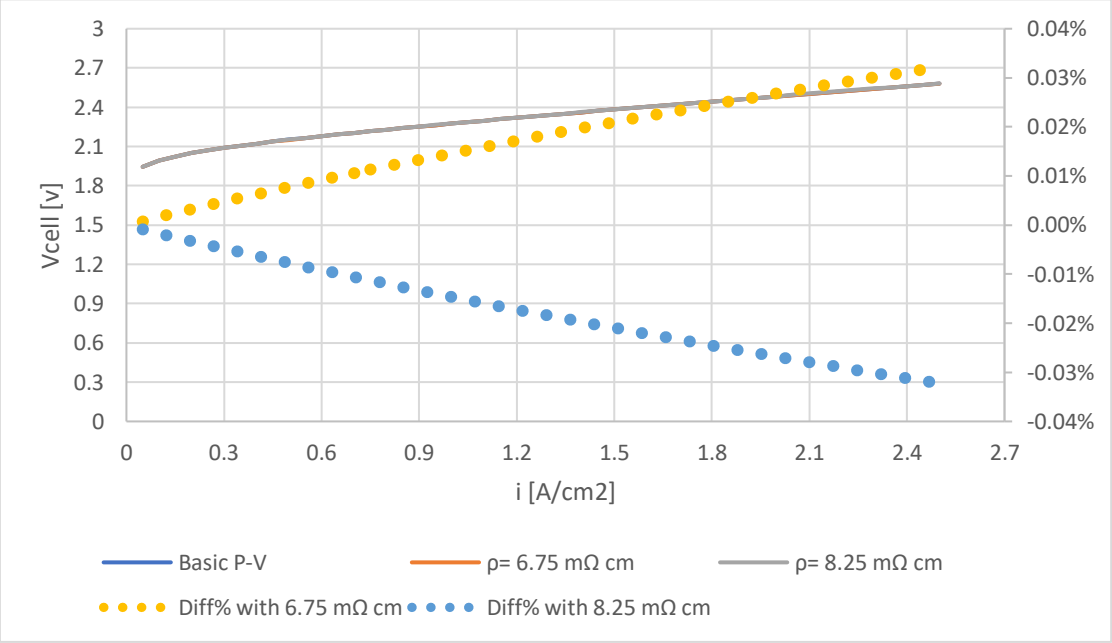

Figure 5.7: The figure shows the dependence of the resistivities on the Vcell

5.2 Model's Calibration

In order to estimate the parameters which were presented in the previous section, a proper mathematical methodology is needed to ensure that the results are valid. The calibration was performed in Aspen Custom Modeler. Aspen has a mathematical way to fit the parameters that were

imposed on its software when the experimental data were introduced. The experimental data was presented in Table 4.2.

The mathematical methodology of the estimator that was used is called "Least Squares". According to Aspen, the latter method minimizes the weighted absolute squared error between the observed and predicted values of the experimental data. The solver that was chosen to run the estimation is called "FEASOPT". FEASOPT, evaluates the objective variable the maximum likelihood function at the current point and moves the estimated variables to take the objective variable towards its set value. After solving with the new estimated variables, FEASOPT re-evaluates the objective variable. In this way, FEASOPT steps towards the optimum solution.

In Table 5.3 the parameters that were used to calibrate the model are illustrated and, the upper and the lower limits are reported. The latter is requested by ACM in order to know the range on which the parameters can change. The ranges were obtained from the literature, except of the resistivities of the anode and cathode for which random values were chosen for the upper limit. The validity of the latter selection will be discussed when the results will be introduced.

Different cases for the estimation were performed, considering different procedures for each one of them. It has been noticed that the estimator of ACM is depending on the initial conditions that was set on the fitting parameters. So, the solutions obtained were not unique but were corresponding to the values that were set at the begging.

Table 5.3: The Lower and Upper values of the fitting parameters

Parameters	Upper value	Lower Value	units
ρ_{an}	0.01	0	Ω cm
ρ_{c}	0.01	0	Ω cm
$i_{o,c}$	0.1	1e-3	A/cm^2
$i_{o,a}$	1.e-6	1e-12	A/cm^2
α_{an}	2	0.5	-
α_{c}	0.8	0.25	-
t_{mem}	0.00025	0.000175	m

For example, if for the transfer coefficient a value close to two was set, the obtained value after the calibration was very close or equal to two. Then, the same simulation was applied keeping the same values for the other parameters but changing only the α_{an} but now with a value close to 0.8, the resulting parameter of α_{an} was not close to two but close to 0.8. Between the two simulations the results weren't the same also for the other parameters, since if there was a lower α_{an} the estimator was fixing for example the exchange current density of the anode (it was increasing). When this behavior was noticed, it was chosen to set a base on the parameters and not change the initial values.

In ACM a weight factor can be set in the experimental data considering the parameters that are expected to be found. The latter was used when the simulation was run in the range of current densities [0.456- 1 A/cm^2] where the activation losses are more important than the ones of the ohmic losses. The opposite procedure was followed for the range of current densities [1- 1.919 A/cm^2]. In this point, it is useful to show the difference of the basic P-C and the P-C of the experimental data.

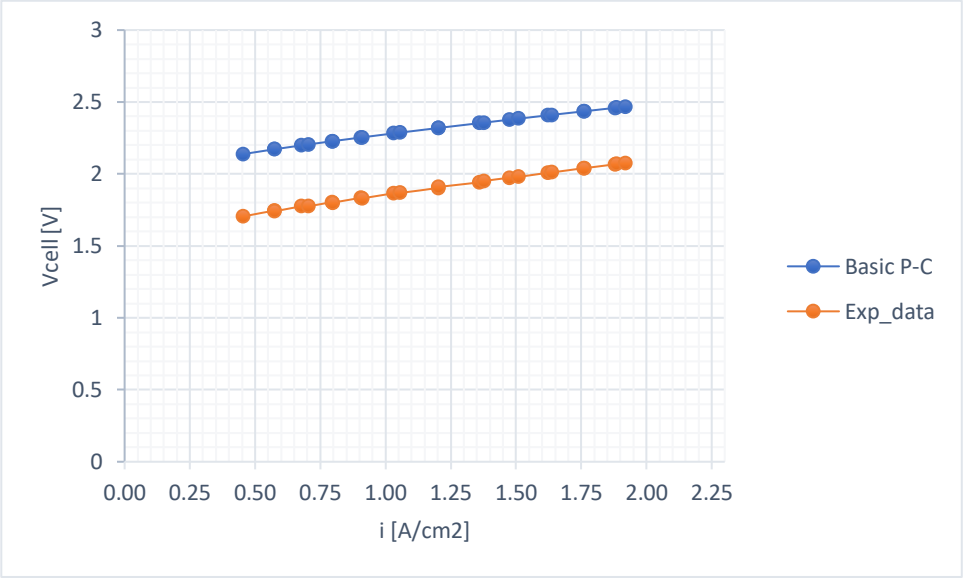

Figure 5.8: Comparison of the basic P-C and the experimental data

In Figure 5.8, it is observed that the basic P-C has higher losses according to the results that are obtained from the experimental data. The Vcell is 20% higher for basic P-C in the range [0.46- 0.92 A/cm^2] densities and the difference is lower up to 16% for the range [1.76 – 1.92 A/cm^2]. This means that the electrochemistry parameters are worse than the reality so during the estimation it is expected to have higher values for the exchange current densities and probably higher transfer coefficient. Moreover, the slope of the experimental is higher than the basic P-C, which means that the ohmic losses should be increase during the estimation.

The results of each case were evaluated comparing them with the experimental data and as indicator to test which case is fitting better the experimental data, MARD (Mean Absolute Relative Deviation) was used:

$$MARD = \frac{1}{N}\sum_{i=1}^{N}\left|\frac{y(i)_{pred} - y(i)_{exp}}{y(i)_{exp}}\right| \qquad \textbf{Eq. 5.1}$$

Taking into account all the above the results are depicted in terms of different P-C in the same figure.

In Figure 5.9, it is understood that all the estimations that were performed, almost fit the experimental data. But no practical conclusion can be derived using the figure with P-C. So, it is better to evaluate the MARD (see. **Eq. *5.1***). In Table 5.4, the results of the MARD are depicted, each case fits the experimental data with an error less than 1%. The higher percentage is on Est15 (0.94%). In this case, the porosity (**Eq. *3.45***), was neglected and Rel was calculated directly with **Eq. *3.44***.These results prove that the porosity is important for calculating the electrode resistance. Est12, Est14 and Est15 have the same results in terms of the fitting parameters. In the Est14 Tafel's equation is used instead of B-V's equation. The difference is minor, only 0.001%. Thus, to the use of Tafel 's equation seems to be a good approximation.

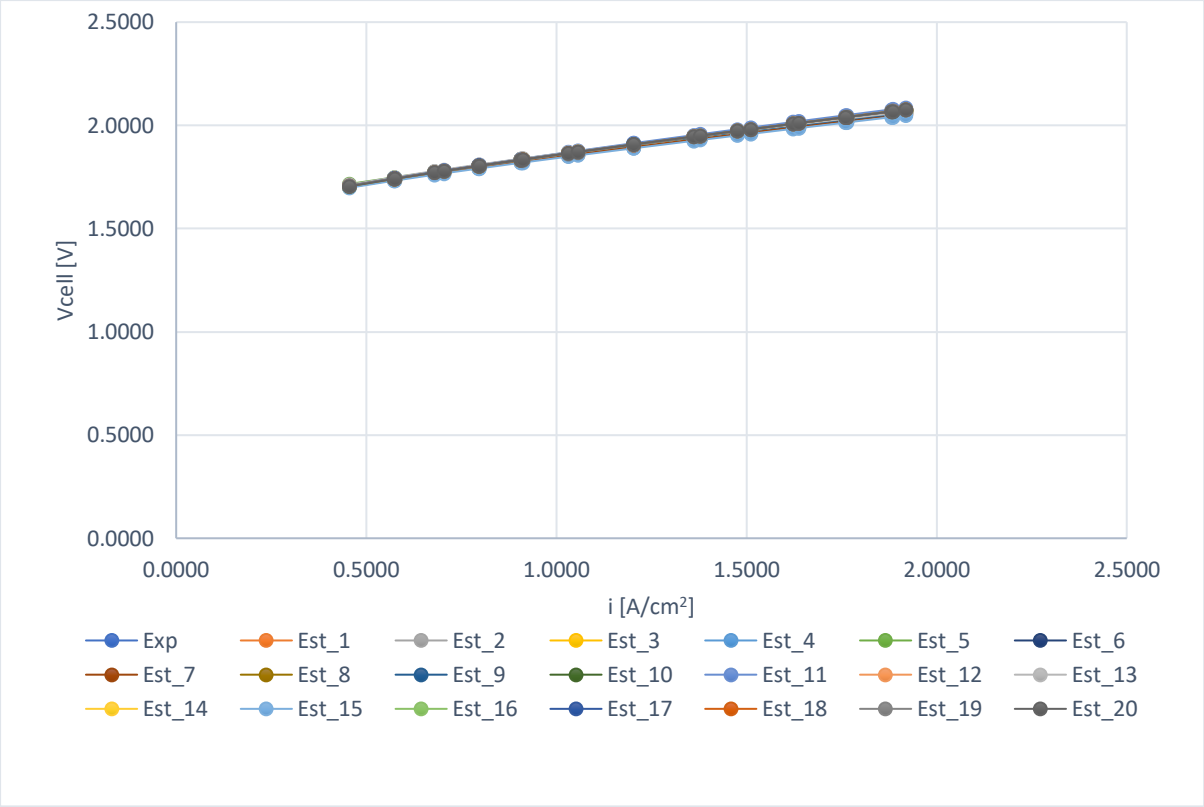

Figure 5.9: Comparison of different estimated P-C respect to the P-C of the experimental data

For the Est1 and Est7, the resistivities ware treated as fixed values and not as fixed parameters. Also, for the Est7 Tafel's equation was used instead of the B-V. Here, the error was increased, with respect to the previous comparison (Est12 and Est14). In both cases the simulation had only one parameter to fit the ohmic losses, the t_{mem} which reached its highest value (2.5e-4 m). So, in order to fit the data, the cathode exchange current density have changed. In both cases the exchange current was 0.1 and 0.65 A/cm^2 for the Est1 and Est7, respectively.

In the Est2 and Est5 the width of the membrane (t_{mem}) was treated as fixed parameter. The value which imposed, was 2.5e-4 m meaning the upper bound of the width, that most of the estimations were reached. The only difference between the two simulations was on the initial values of the resistivities, the Est5 was used that was obtained from Est4. So, for the Est2 the ρ was 0.0075 Ω cm and for the Est4 the initial value was 0.0721 Ω cm. The results confirm the observation, that the estimation simulation depends on the initial values. For the Est.2 the resistivities were 0.0456 Ω cm while for the Est.5 were 0.1 (Upper limit see Table 5.3). For the other parameters the two estimations results were also different, but between them, Est2. was better predicting the experimental data.

All the above was done to find the best combination of group of parameters, even though the simulation from the very first estimation was fitting the experimental data with less than 1% error. The best solution is apparently between Est12 and Est18 0.104% and 0.107%, respectively. The best

Table 5.4: The table shows the MARD of each estimator case

Est	MARD
1	0.206%
2	0.121%
3	0.123%
4	0.124%
5	0.226%
6	0.108%
7	0.648%
8	0.111%
9	0.311%
10	0.205%
11	0.347%
12	0.104%
13	0.317%
14	0.105%
15	0.939%
16	0.107%
17	0.117%
18	0.105%
19	0.116%
20	0.106%

From the Est16 until Est20, a different procedure was applied to calculate the R_{el}. The latter was done since in the R_{el} is calculated by three geometrical ($t_{el,a}$, $t_{el,c}$, t_p) and three electrochemist parameters ($\rho_{el,an}$, $\rho_{el,c}$, ρ_p) that their values have been assumed. The plate width and their resistivities weren't included in the model since the losses related with them are minor. The ρ_{el} of the Est12 reached a value of 0.081 Ω cm, which according to the literature, no material, which was used to build the electrode of the PEMEC, fitted with this value, the value was high. So, during the fitting process the additional resistivities of the plate and the width were included in the resistivities of the electrode. So physically, it would not be proper to show as a result, unrealistic values. Keep in mind that also the boundaries of the resistivities were imposed randomly.

To solve the problem, the procedure was changed on how the R_{el} is calculated in the model. Instead of calculating it from **Eq. *3.44*** and **Eq. *3.45***. it was assumed as a Fixed parameter with a value of 0.001 Ω cm. This value comes up from the results of the Est12. The upper and lower values were kept the same as the one of resistivities. Running the Est16. the Rel now reaches the value of 0.147 mΩ cm. The cathode transfer coefficient and exchange current are become lower and simultaneously the anode transfer coefficient and exchange current are increased. Then as initial value for the Rel in the Est17 the result that was obtained from the Est16 was used. Also, for the Est.17 Tafel's equation was used. The results become worse in terms of MARD. Moreover, the Rel that was obtained was lower than Est16, and further increase in the other parameters was noticed, except of the α_{an}, that was decreased. Following the same procedure, B-V's equation was used this time and as an initial value was assigned the one that was obtained from Est17. The results of the Est18 were better both from Est16, Est17. The same pattern was implemented for Est19 and Est20 but MARD was increased in both cases.

Table 5.5: The table depicts the different values of the parameters with the best fitted estimation results.

Est	Parameters	Value	units
18	R_{el}	1.76e-4	Ω cm
	$i_{o,c}$	0.0423	A/cm^2
	$i_{o,a}$	9.27e-07	A/cm^2
	α_{an}	0.634	-
	α_c	0.5335	-
	t_{mem}	2.5e-4	m

Est	Parameters	Value	units
12	ρ_{an}	0.081	Ω cm
	ρ_c	0.081	Ω cm
	$i_{o,c}$	0.056	A/cm^2
	$i_{o,a}$	1.04e-07	A/cm^2
	α_{an}	0.772	-
	α_c	0.394	-
	t_{mem}	2.46e-4	m

Between the two best fitted estimations the Est.18, was chosen because as it was explained the results need to have a physical correspondence. It should be noted also that the transfer coefficients have both almost symmetrical values for Est.18 which correspond with the literature's models. The exchange current for the anode is in the order of magnitude of 1e-7 which coincides with the papers of Z. Abdin et. al,[83] , Yigit et. al, [84] , Garcia- Valverde et. al,[74] and with Marangio et.al,[72], who said that this O.M. corresponds to the Pt catalyst.

In Figure 5.10 is depicted the final P-C that was best fitted with the experimental data. The two lines are almost equal, which means that the calibration on the fitting parameters is representing the real stack; this also means that it can be used for further investigation in building a process that includes other parts of the real process, like the heat exchangers, pump, separators etc. The latter will be analyzed in the next chapter.

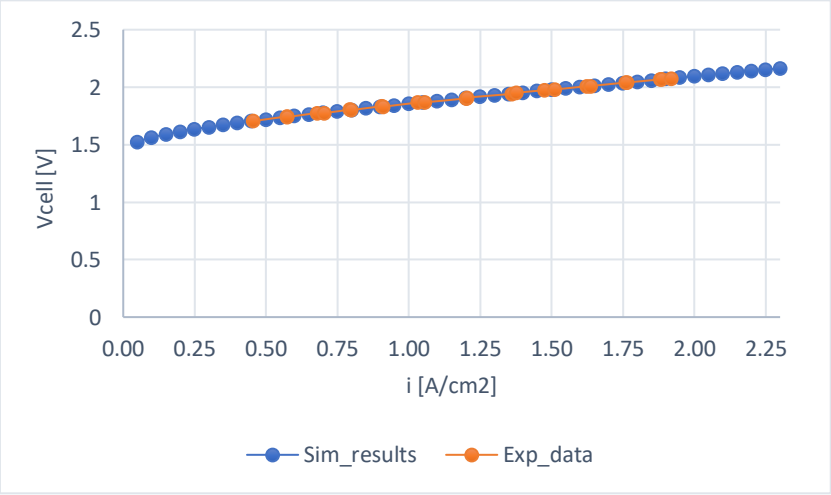

Figure 5.10: The figures shows the result of the Est18 in terms of P-C, the experimental data are almost equal with the simulation results

5.3 Model's Validation

The model validation was performed considering experimental data different from the one that was used for the calibration but from the same commercial electrolyzer. In chapter 4, it was mention that there were two different sets of data running two different days. The one that was used to perform the calibration in the previous session was demonstrating partial load, peak load and again partial load. For the validation of the model, the PEMEC was operated for a day in peak load with some minutes of start-up and shut down during the end. Figure 5.11, represents the load profile of the current density and voltage for one day. The peak load electric power is around 55 kW, while the voltage and the current density profiles are almost constant with only some small fluctuations that are not high, if they are compared with the profiles that was used for the calibration (see. section 4).

The validation will be performed using a random sample from the data in the peak load. The current density and the temperature of the stack was placed to the simulation as input parameters, and as an output parameter voltage was calculated. Again, the validity of the results was tested using the MARD that was introduced in **Eq. *5.1***. The sample, that was used, has a range time from [0-200s] where the current density at the start had values 0.143 to 0.247 for the first 3s. Temperature was varied between 52 to 59 °C. In Table 5.6 it is depicted the temperature and the current densities of some points of the sample since, it will not be practical to show all the two hundred of points.

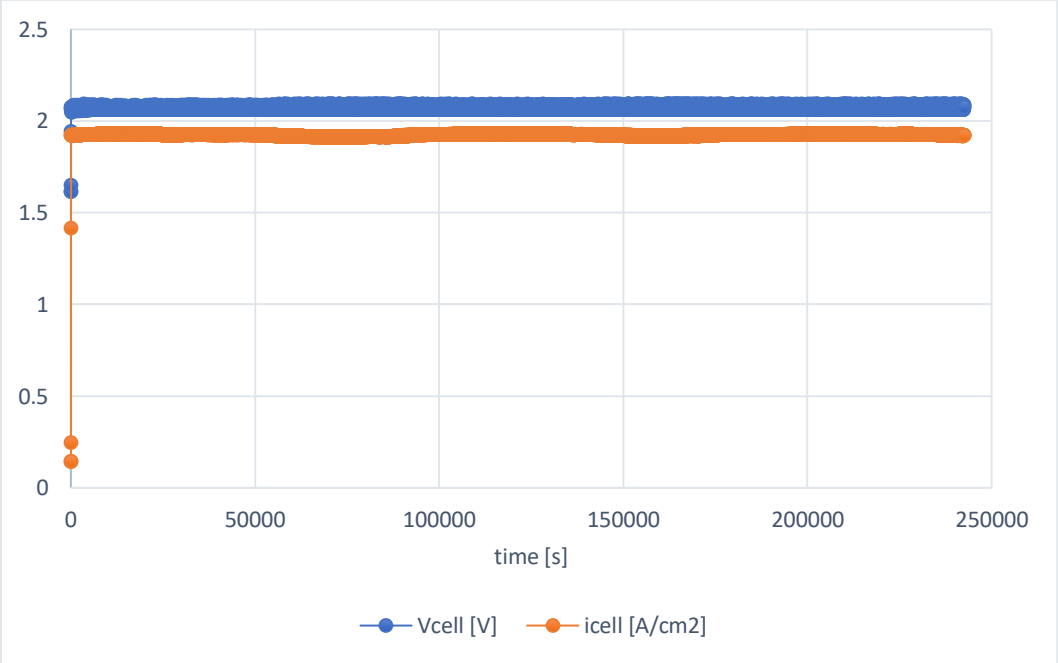

Figure 5.11: The peak load profiles of current and voltage for one day

Figure 5.12 shows that the simulation predicts very well the experimental data even if there are some scatter points (yellow dots). For example, if the experiment voltage is 2.053 V and if the error is zero then in the y axis, it will show the same value, but if the simulated result has different value, in the y axis it will appear this value. The MARD that was calculated over the sample of the 200s was 0.3%. Comparing the MARD of the Est18, 0.105% with the validating MARD, it is confirmed that the

model almost perfectly predicts the voltage of the cell under various Top and i. In this point, the stack can be used as a component to simulate a process that will represent a simplified process compared to the real one.

Table 5.6: Random values of i and Top that was used to validate the model

Current density [A/cm^2]	Top [°C]
0.14	52.48
0.15	52.45
0.25	52.57
1.42	52.82
1.92	53.88
1.92	55.38
1.92	56.69
1.92	57.91
1.92	59.14
1.92	58.17
1.92	55.99
1.92	56.31
1.92	57.71
1.92	59.10
1.92	57.82
1.92	55.34
1.92	55.70
1.92	57.09
1.92	58.27
1.92	58.90
1.92	57.55

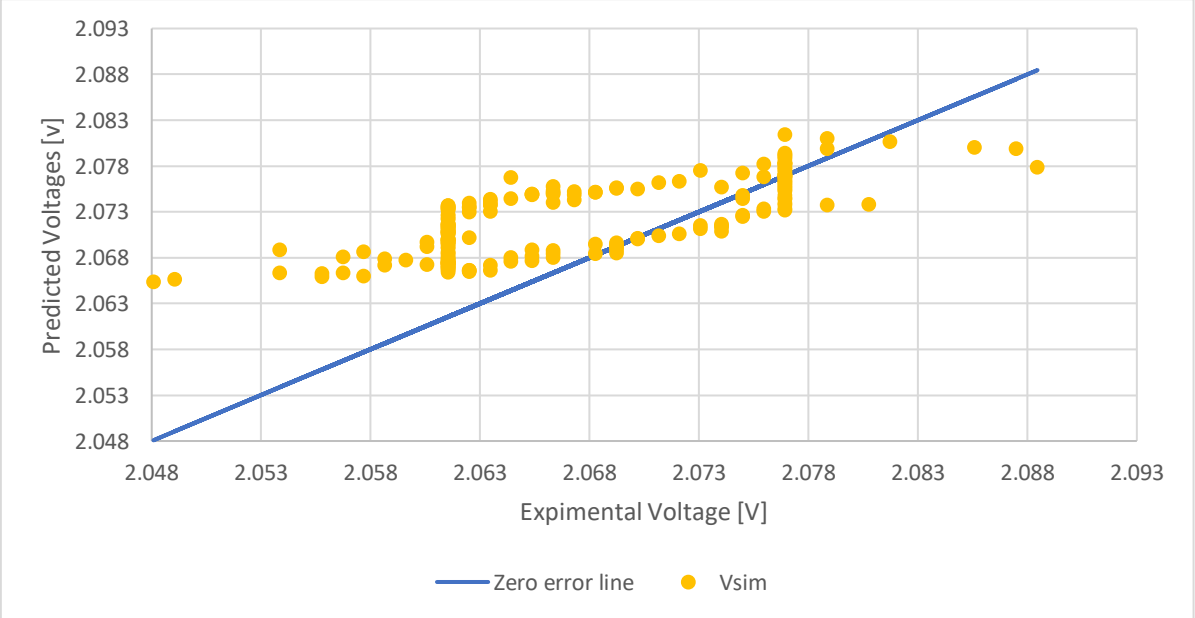

Figure 5.12: The figure compares the results of the simulation (yellow dots) with the zero error line (Blue straight line 45[9])

6. Preliminary Dynamic Model of the System

It appears useful to integrate the dynamic model of the stack into a simulation of the entire system. Hence, a dynamic model of the electrolysis plant has been developed to investigate the performance. The behavior of the PEM electrolyzer stack depends on the electricity input and, through the model equations, it determines the current and the voltage. The stack model is thermally oriented, which means, the dynamic performance of the stack is dependent on how the temperature (T_{op}) changes with time. To simulate the system in a proper way, the stack needs to relate to other components that correspond with the real process. The experimental setup of the system has been introduced in section 3.2 (see Figure 3.2). In this section, a simplified version of the overall system is built using Aspen Plus Dynamics (APD).

6.1 System's and Model's Description

Figure 6.1 shows the layout of the investigated PEM electrolysis system. The electrolyzer (A) is a serial stack of 65 electrolysis cells, in which the reactions occur as shown in section 2.5. Deionized feed water (E) enters into the system by mixing with the water that is recirculated from the oxygen/water separator (B); from here the liquid phase is pumped (G) to the anode side of the electrolyzer after passing through a heat exchanger (D) for temperature control. As the electrons are drawn by an external DC power supply, water is decomposed into oxygen and protons on the surface of the anode electrode, and the protons are attracted to the negatively charged cathode through the MEA. The protons are converted to hydrogen on the cathode electrode through a combination with the electrons supplied by the DC power source. Hydrogen leaves the cathode with water and it is sent to the hydrogen/water (F) separator while unreacted water and oxygen from the anode outlet are sent to the oxygen/water separator (B). Then the hydrogen leaves the separator and enters the purifications columns (C) to separate from the remaining humidity and reach purity around 99,98%.

Figure 6.1, depicts the real process with the related components being assigned with an alphabetic letter, with the following association:

A) Stack
B) Separator column of O_2/H_2O
C) Purification column of H_2
D) Plate heat exchanger in the inlet of the stack
E) Water tank
F) Separator column of H_2/H_2O
G) Pump

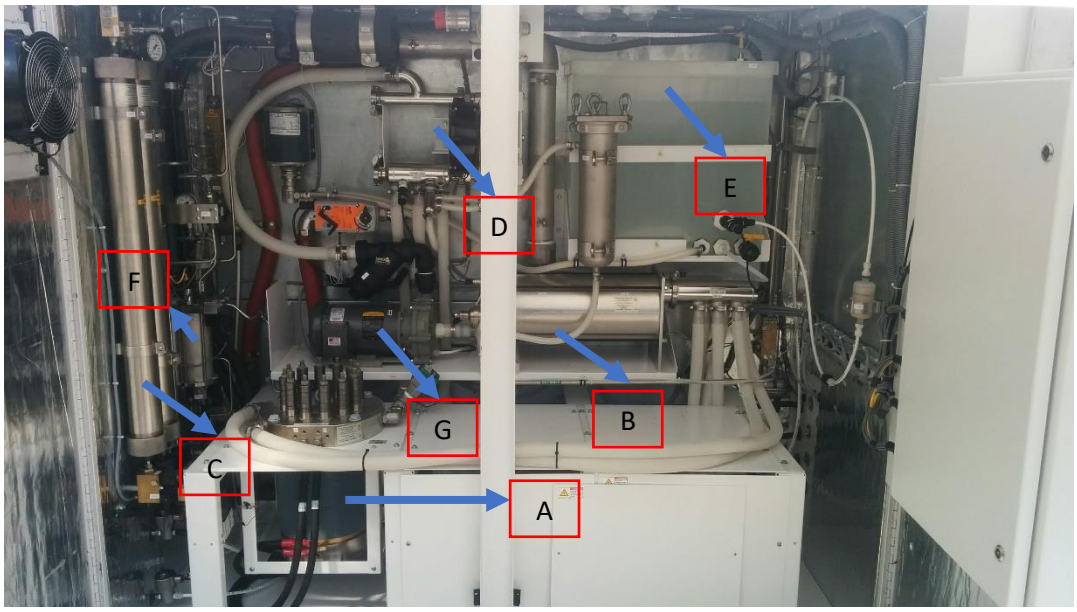

Figure 6.1: Photograph of the system's components

The system has other components like converter, valves upstream and downstream the anode and the cathode to control the pressure, venting valves, sensors, safety devices, fans and a variety of control systems that are not described in Figure 6.1, but they are adapted to control and monitor the system. The latter choice was done to focus more on the most crucial components that also will be used to build the simplified model. Although, a simple control system will be introduced, related to temperature and power input because they are important to the system when the electrical input varies with time.

Figure 6.2 shows the system's flow chart as it was designed in APD. One of the main components, that it was not simulated, is the purification columns (C). The purification is important when the process is integrated for hydrogen storage. The current model does not test this part of the system for two reasons; 1) the purification stage would need a detailed model that accounts for the mass transport mechanisms in the column, 2) the compression of H_2 needs further modelling. Both reasons are relevant but out of the scope of the current thesis. Table 6.1, depicts the descriptions of each component that is introduced in Figure 6.2.

The two PID controllers are introduced in the system for different reasons. The PIDel is connecting the stack with the electrical input. It reads the electrical input and generates a current density to the stack, which behaves as an input to the system to solve the equations of the stack's model. The variation of the electrical input has impact to the Top of the stack through the thermal sub-model. It is either increasing or decreasing the temperature of the system. The control of this behavior is done through the PIDtemp. The PIDtemp controls the Top by fixing the inlet temperature of water in the anode side. The set point of the controller is fixed to 56.6 ^{o}C, then the PIDtemp reads the temperature of the stack (Top) and as output signal gives signal to the HX1 to fix the temperature on the outlet stream S6, which is the inlet on the anode side of the stack. With these two controllers the simulated process tries to approach the real behavior of the system when the electrical input varies with time.

The detail description and the main aspect of the simulated process will be introduced in the section 6.2.

Table 6.1: Description of the simulated components of the system

Component	Description
Stack	The PEM electrolyzer stack (A)
SEPO2	The separator of O_2/H_2O (B)
HX1	The heat exchanger in the inlet of the anode (D)
SEPH2	The separator of H_2/H_2O (G)
Pump	The pump of water in the anode side
MIX1	The mixture of the recirculated water with the makeup water from the tank (F) plus the water from the SEPO2
MIX2	The mixture of the water from SEPO2 and the make makeup water
PowerIN	The electric power input respect to time
PIDel	The PID controller of the electrical input
PIDtemp	The PID controller of the operation temperature

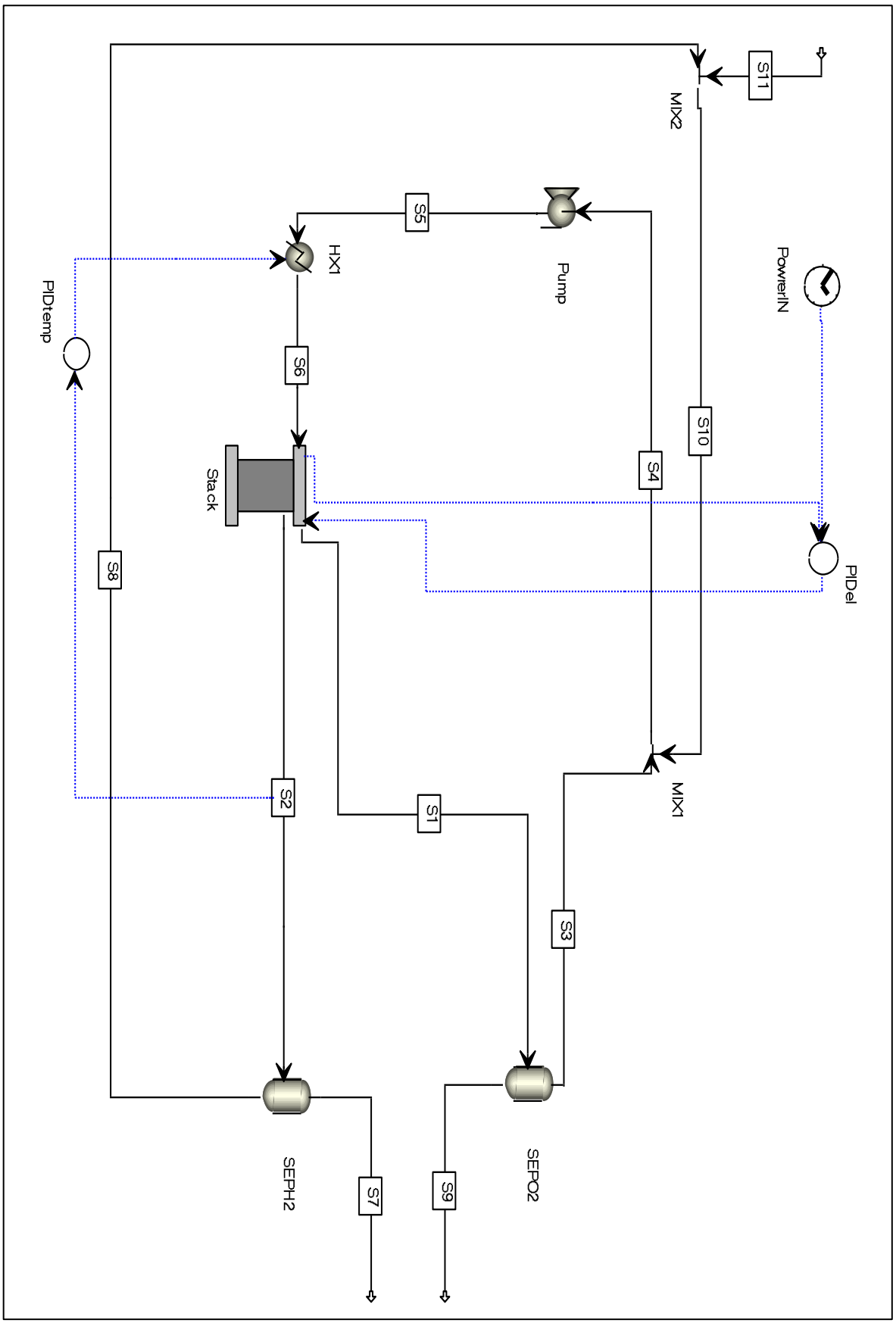

Figure 6.2: Scheme of the simulated system configuration in APD

6.2 Setup of Dynamic Simulation

This section will analyze the setup of the dynamic simulation in terms of the components of the system and the strategy that was followed to evaluate the global thermal capacity of the system which is the only parameter that was not calibrated in section 5.2, since the calibration was held in the steady state conditions.

- **Stack**

The stack setup in the dynamic system was prepared differently than in the steady state simulations. Some values that were characterized as fixed parameters in the steady state condition, in the dynamic are evaluated by externals flows or inputs. Accordingly, the model itself did not change in structural terms. The flow inlet of water is not anymore fixed for the stack, but it is calculated by the stream S4. The flow remains constant all over the streams S4, S5 and S6. For the overall system, the flow of water remained constant when the dynamic simulation was performed. As mentioned in section 6.1, the Top is not any more fixed, but it is controlled by the PIDtemp and varies when the current density is changed. As for the current density, in steady state it was assumed as input fixed parameter; in this case it is controlled by the PIDel. At the same time, the electrical power is not any more calculated as the product of current and voltage, but it is generated by the block named PowerIN. All the other parameters of the stack remain the same as in the steady state.

- **SEPO2 and SEPH2**

When simulating the two separators of the system in APD, they were assumed as flash separators of gas-liquid equilibrium. The APD block that was the most suitable for the model was called “Flash2”. In this block a perfect mixing was assumed, and the two phases are always in equilibrium. For this block it was assumed that the pressure remains constant since the stack model is not built with a pressure driven format (zero-dimensions). Both pressures of the two separators were assigned by the flows coming from the anode at 2.5 bars (S1), and cathode, at 30 bars (S2), respectively. The temperature was assumed again constant but this time the temperature is not assigned from the S1 and S2. An external fluid was assumed to control the temperature for the SEPH2, while for the SEPO2 not heat transfer was occurred internally, so the SEPO2 keeps the temperature of 56.6. The fluid, which was assigned for the SEPH2, is not mentioned in Figure 6.2, since it is not in the control volume of the system that is tested and the effect of it is not related with the dynamic model. In the real process, the separators have the same temperature of the outlet streams of anode and cathode. Moreover, after SEPH2, there is an air-cooled heat exchanger that cools down- the hydrogen around 20 to 30 ^{o}C. So, the block of SEPH2 combine the two effects (separation and exchange heat) into one component. For the SEPO2, there was no information concerning a heat exchanger after the separation to lower the temperature of the water and oxygen, so a zero-heat duty was assigned to focus only on the separation of the oxygen with water. Despite of what is the temperature of the separators, the temperature of the flows at the outlet do not have any significal effect on the process. The SEPO2 in the reality is a horizontal vessel much larger than SEPH2 (see (B) in Figure 6.1) and it is

described as a gravitation separator [94]. Since data does not exist on the size of the vessel both separators were designed with the same manner. The only difference was in the temperature of SEPH2 that was assumed 38 ^{o}C in terms of medium temperature (i.e. it is the temperature that is regulated by the other fluid with overall heat transfer coefficient 5 kW/K).

- **Heat Exchanger (HX1)**

The heat exchanger regulates the Top of the stack through the stream S6. Like the separators which work with an external fluid, the same concept is followed with the heat exchanger. The external fluid of the heat exchanger is not included in the control volume of the tested system, only its own output is important, which is to cool or heat the stack according to the temperature of the stack. Since its size is unknown, its design is related to its thermal duty, which is to absorb or generate heat to the system. The temperature of the HX1 is fixed from the PIDtemp and no pressure drop occurs in it. The HX1 was chosen to be countercurrent with the option to work in a dynamic operation in order to have the corresponding temperature outlet according to the needs of the stack. The flow rate of the HX1 is the same flowrate as in the recirculated streams (S1, S3, S4, S5 and S6) where the flow is only water. For the dynamic option it was asked to add some additional information related to the volume of the flow, the mass of the HX and the thermal capacity of the materials. HX is the only component in the system with the stack that changes its operation temperature in the dynamic system. In order to have an inertial of the system also in the other components, the volume and the mass of the HX were overestimated. The volume was calculated by the product of the volume flow rate of water (i.e. 2 m^3/h) and assuming that the residence time of water in the recirculated stream and the SEPO2 is 15 min. The mass was calculated by some very rough assumptions of the weight of each component, SEPO2 (around 30 kg), pump (around 15 kg) and HX (around 15kg) totally 60 kg. The specific heat C_p was equal to 0.5 kJ/kgK close to the value of the stainless steel.

- **Pump**

The Pump is used in the system to regulate the pressure of the anode. It has been assumed that the only pressure drop in the system is introduced in the anode part in the stack (ΔP% =10%). Again, no information was given related to technical specification of the pump, so the efficiency was assumed 72% (default value of APD). The design of the pump in the system was done by regulating the pressure at the outlet stream (S5). Since the system is not pressure driven, the inlet pressure is 2.25 bars and the outlet pressure is 2.5 bars, equal to the anode pressure.

- **MIX1 and MIX2**

The MIX1 and MIX2 represent the mixture valves of the system. Both were designed in the same way. The type and size of the mixtures are not specified by the manufacturer but in this case the design is simple since the only species that is involved in them is liquid water. So, the properties of the outlet streams are weighted averages of the inlet streams. The MIX2 mixes the makeup water and the water that comes from the SEPO2, then this mixed water is sent to MIX1 where it mixes with the recirculated

water. No pressure drop was assumed throughout the mixing process nor external heat transfer fluid. In contrast the temperature of the stream is changing as it was mentioned before by weighing it according to the mass flow rates of each stream.

- **Stream S11 (makeup water)**

The makeup water is the water that is added to the system to balance the fixed flow (100 kmol/h). The water is added to the system from a water tank (F), which is not depicted in the APD because it does not affect the system performance. The temperature of this stream is fixed at 25 ^{o}C and the flow rate is changing according to the loss of water during the electrochemistry reaction in the stack. No leakages are assumed, and no water is lost due to evaporation.

- **PID controllers**

The PID controllers are adapted to the system to regulate and fix the parameters that are of crucial importance when the system operates under dynamic conditions. Two PID were introduced; one for the power and one for the temperature. The description of them was done in section 6.2, where the setup of the controllers is described. The latter was made by running the dynamic system without fitting the global thermal capacity but only introducing arbitrary step wise electrical input. Then the tuning of each controller was performed separately. First, the PIDel was tuned, since the electrical input generates the current and thus the current introduces a perturbation on the Top. Then the system accumulates the perturbation by fixing the Tin through the HX1.

In the PID control should be assigned three parameters: 1) the process variable (PV), the operation variable (OP) and the set point (SP). Table 6.2, shows the assigned variable for the two types of PID controllers of the simulated system.

Table 6.2: Assigned variables in the PID controllers

Controller	OP	PV	SP
PIDel	i [A/cm^2]	Pel [kW]	Pel [kW]
PIDtemp	Tin [K]	Top [K]	Top, set [K]

Every PID controller is based on three parameters that are shown in the next equation:

$$OP = Bias + Gain \left\{ E_p + \frac{1}{Integraltime} \int E_I + Derivtime \frac{d(E_d)}{dt} \right\} \quad \textbf{Eq. 6.1}$$

Where E_p is the proportional mode error, E_I is the integral mode error and E_d is the derivative mode error. All of these errors are derived from the standard error E, which is defines as:

$$E = SP - PV \quad \textbf{Eq. 6.2}$$

The bias value is the OP that before the perturbation (t -1 s)

In the simulation in order to tune the controllers, it is needed to change the values of Gain (a), the integraltime (b) and the derivtime (c).

In the real process there is a controller that is represented by the simulated system with PIDel. The experimental data that were measured did not reported the real Pel. The Pel was obtained by the product of the measured current and voltage. The problem in this, is that there is a delay on the real controller that is needed to take into account when the system is simulated. But since there are no data either for the real Pel in time t or about the controller's delay, it was assumed that the real controller does not have any delay. The latter was simulated by tuning the PIDel with very fast respondence in the stepwise power electricity input. The system starts from a power input equals to 40 kW and at t = 60s the power input becomes 50 kW.

Figure 6.3a, depicts the response of the PID when varying the b of the integral error, the a is equal to 0.1 % (Gain X Ep) and c is equal to zero. In

Figure 6.3b, is depicted the behavior of PID when a of the Gain is varying, b is equals to 50 min and c is equal to zero. Practically, the PID is a PI since the derivative time is accounted as zero. The latter was chosen since the derivative part is introducing perturbation before reaching the SP. So, the parameters to tune the PIDel are: a equal to 0.5%, b equal to 30 min and c equal to zero. In this case the Elpower will reach the stepwise variation in less than 15s which is the time steps that the experimental data of power input are recorded.

For the PIDtemp, the tuning of the parameters is a little more complex than the PIDel. The difficulty is that the temperature variation is not depending only on the PID controller but also on the C_{th} (see section 3.5). The real system appears to have temperature perturbation even if it operates in almost constant power input (i.e. in the peak load profile see section 5.3). The strategy that was followed for tuning the PIDtemp was to make reasonable assumptions for the values of a, b and c, considering that the PID will not control ideally the inlet temperature to correspond closer to the real profile. The results that were obtained are: a equal to 0.06%, b equal to 2 hr and c equal to 10 min. The c was added to introduce some fluctuations on the Top before reaching the SP.

a)

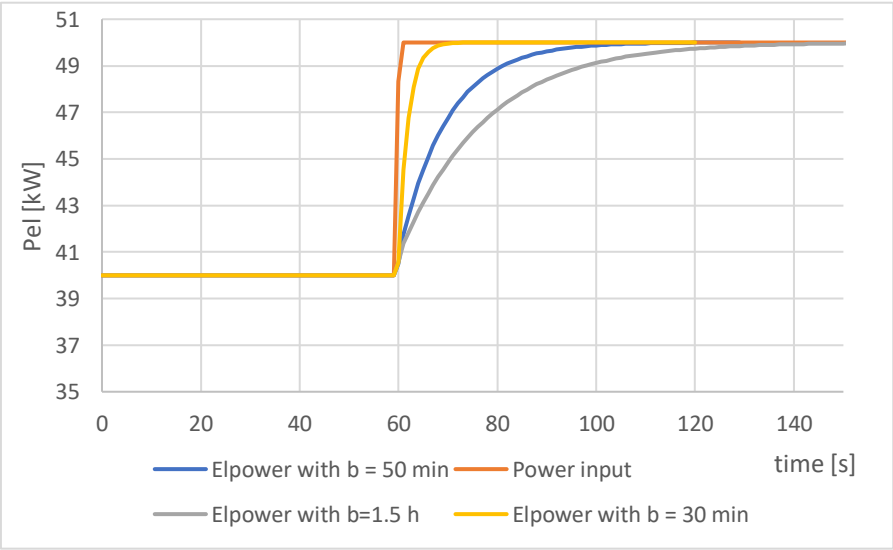

b)

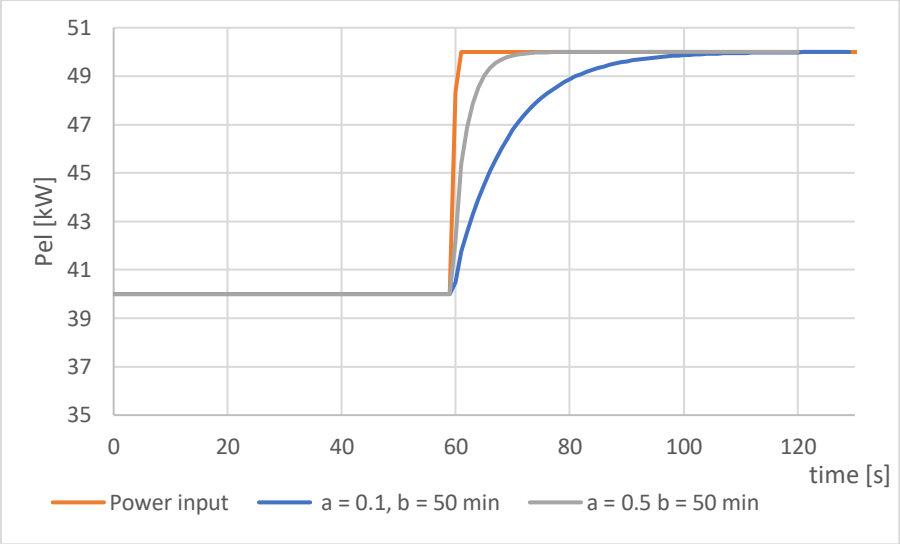

Figure 6.3: a)The behaviour of PIDel when b is varying b) The behaviour of the PID when a is varying

6.3 Results

Before showing the results of the preliminary profile of the involved parameters, it was useful to do an analysis to calculate the value of C_{th}. Due to the lack of the geometrical parameters of the stack, reasonable assumptions based on the dimensions and the materials of the components were considered. Furthermore, it was assumed that the anode and the cathode of each cell is flooded with water, thus the water fills the void volume of the gas diffusion layer. The C_{th} can be calculated as follows:

$$C_{th} = \rho_w V_w C_{p,w} + \rho_s V_s C_{p,s} + \rho_{MEA} V_{MEA} C_{p,MEA} + \rho_{s,ext} V_{s,ext} C_{p,s,ext} \quad \textbf{Eq. 6.3}$$

where ρ_w, ρ_s, ρ_{MEA} and $\rho_{s,ext}$ are the densities [kg/cm^3] of water, GDL/plates, membrane and external material, respectively. V_w , V_s, V_{MEA} and $V_{s,ext}$ are the volumes [cm^3] of water, GDL/plates, membrane and external material, respectively. $C_{p,w}$, $C_{p,s}$, V_{MEA} and $C_{p,ext}$ [kJ/kgK]are the specific heats of water, GDL/plates, membrane and external material, respectively. It was assumed that the GDL/plates are made from carbon (graphite) and the external material is stainless steel. Their properties are depicted in Table 6.3.

For the calculation of water and GDL/plates width, the geometrical parameters of Table 5.1 were used. For the MEA's width, the calibrated value t_{mem} was used ($2.46 \cdot 10^{-4}$ m). Taking into account that the Acell is 213.67 cm^2 for 65 cells, the total volume of the internal stack was obtained.

Table 6.3: Physical properties of the material that are used for the calculation of C_{th} [95, 96]

Material	Density ρ [kg/cm^3]	Specific heat [kJ/kgk]
Water	10^{-3}	4.186
Carbon	$2.6 \cdot 10^{-3}$	0.71
Stainless steel	$8.05 \cdot 10^{-3}$	0.49
MEA	$1.98 \cdot 10^{-3}$	1.5

A representative drawing model is depicted in Figure 6.4, where the internal volume of the stack is the red volume. For the external diameter of the stack was assumed, D_{ext} equal to 20 cm and subtracting the internal volume of the stack it was calculated the volume of the external ring of stack. For the upper and bottom support plates, reasonable values were obtained from the Figure 6.1. For the upper support plate, a D_{upper} equals to 30 cm and h_{upper} (height) equal to 5 cm were used, while for the bottom D_{bottom} equals to 22 cm and h_{bottom} equal to 3 cm. All the external materials were stainless steel. Lastly for the void volume, which is equal to the volume of the water, a value of 46 cm^3/cell for the anode and cathode was assumed (based on the porosity). A thermal capacity equal to 50.1 kJ/K was calculated.

The stack and the HX1 until this point are the only components that are considered to add an inertial in the system when a perturbation on temperature is introduced. This consideration, for a preliminary dynamic model of the system seems reasonable due to lack of data on the size of the real process components.

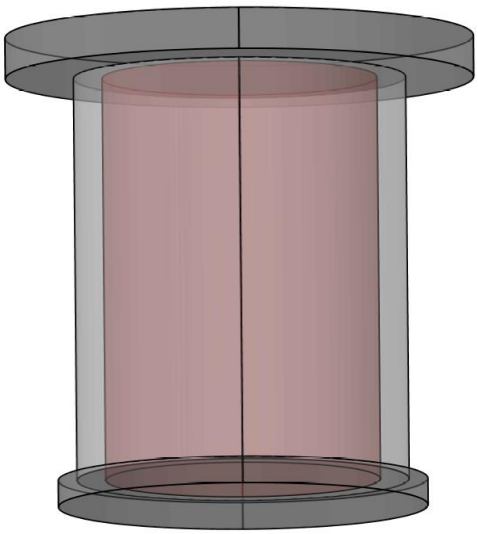

Figure 6.4: Drawing model of the stack

It was chosen to run the simulation with the electrical power that corresponds to the peak load of the system. The same profile that was chosen to validate the steady state simulation (see. section 5.3). The time that the simulation was run was 990 s, where the first 90 s are characterized as start-up period. The simulation displayed the results every 15 s in order to be consistent with the real display time of the measurements. Between two times steps the simulation is running as in steady state

condition. Each perturbation of the electrical input is set to be a step wise variation and then the PIDel reads the signal and introduces the step wise variation with a delay of 2s. Figure 6.5 depicts the results that were obtained for the electrical input and current density, while Figure 6.6 shows the variation of the Tin ,Top and the Texp respect to time .

Once again like the validation of the model in steady state condition, the measured current density is predicted well by the simulation with a MARD 4% (Figure 6.5). The difference on the current densities probably is mainly due to the purification stage and to the tuning of the PIDel. Nevertheless, they are almost equal, and it can be stated that the model of the whole system and not only the stack is able to have good approximation results on the current densities. The same will stand for the voltage, which is not depicted since it can be calculated by the power and the current density.

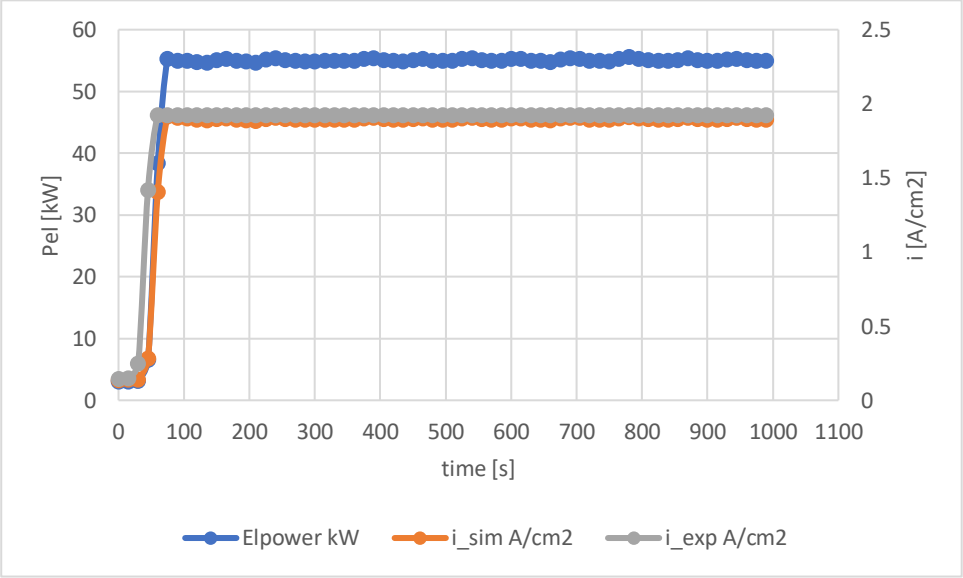

Figure 6.5: The dynamic profile of the electrical input, the simulated current density and the experimental current density.

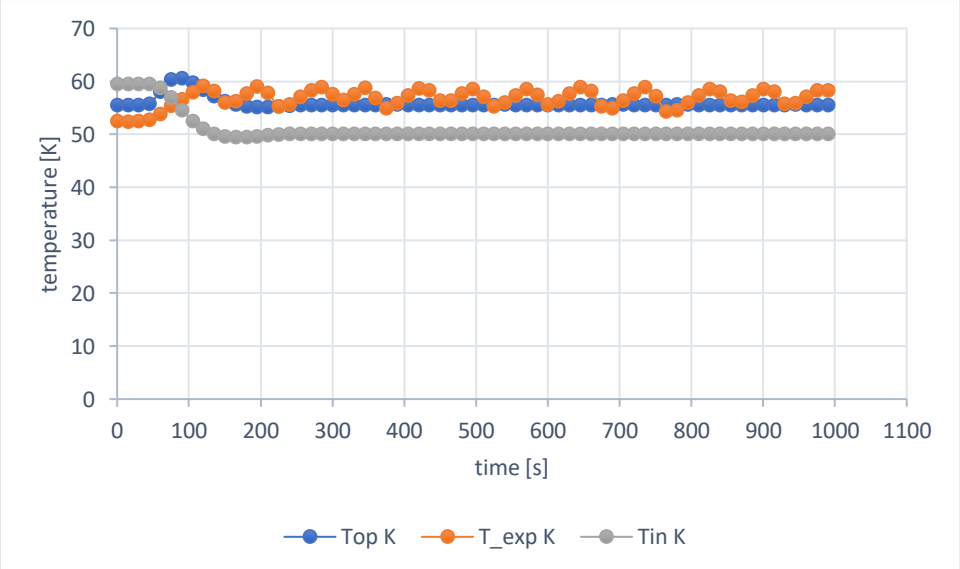

Figure 6.6: The dynamic profiles of inlet, operation and experimental temperatures

For the temperature profiles, in Figure 6.6, the simulation can predict up to point the measured temperature, but it is constrained by the PIDtemp, even if the latter was not tuned with the best way to have some fluctuations. For small perturbation in the electrical input almost periodically there are some small peaks on the Texp which the Top from the simulation cannot predict. The cause of this, probably is related with the zero-dimensional model of the stack which is not calculate the change of the pressure in the anode and in the cathode side which. Moreover, the simulated system is not built based on the real geometrical and material characteristics of the real process but from reasonable assumptions, which may lead to this temperature difference. Lastly, the dynamic system was not calibrated to validate the assumption that were made due to lack of experimental data.

As far as the Tin, at the beginning of the simulation is higher than the Top meaning that the HX1 heats the water which enters the anode side of the stack. This behaviour was noticed generally when the system was working with a power input less than 20 kW, both in steady state and in the dynamic model. Generally, the heat exchanger on an PEMEC systems is designed to cool the stack. Probably, the latter was caused again on the implementation of a zero-dimension model in a simulated system. In the literature does not exist any zero-dimension model apply to a simulated process, so no comparison was able to be done. Furthermore, at the begging of the operation, the experimental temperature is starting from around 52 ^{o}C, while the simulation temperature starts from the SP (56 ^{o}C). This phenomenon, is related with the start period of the electrolyzer which starts to heat up for the first 100 s until it reaches the SP. The simulation temperature follows this increase almost parallel but in higher temperature and it reaches the peak temperature (61 ^{o}C) in time equal to 80 s. The MARD again in this case is small 3%, but it cannot be a good indicator that the system will work perfectly for other applications for the reasons that were explained above.

It was interesting to study the behaviour of the system when it was operated in partial load and especially when the power input changed according to the time steps that were introduced in Table 4.1. Especially, the power input was obtained between step 10 and step 11, from 36510 s to 37050 s (see. Figure 6.7).

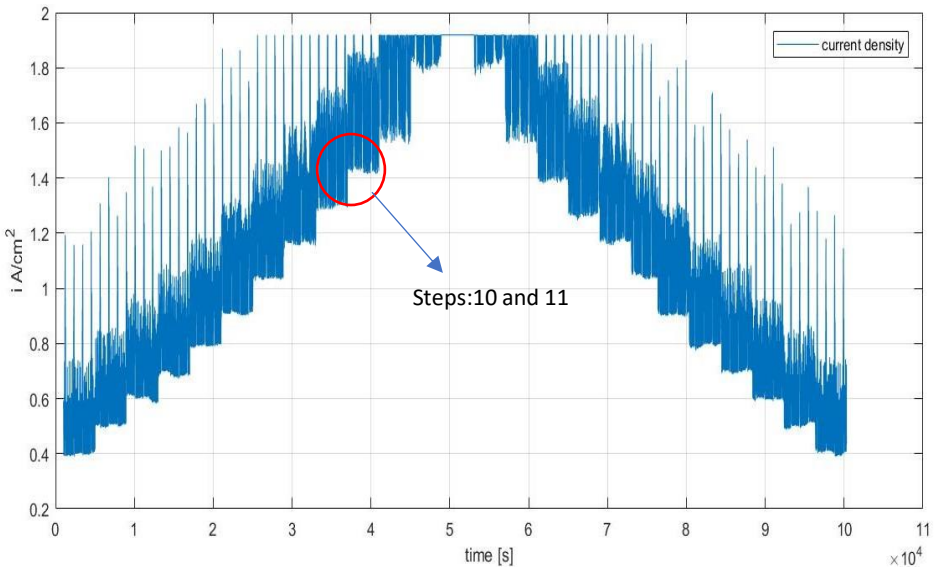

Figure 6.7: The steps that were used from the partial load to study the temperature variation

Figure 6.8, depicts the behaviour of the temperatures when the system operates in partial load. The situation is quite similar as before, the experimental temperature has more perturbation than the simulated temperature. It is interesting to comment when the system moves from step 10 to step 11. The system faces a transient time for 135 s where both Top and Texp are increasing, but the Texp does not change a lot the pattern that was followed before and after the transient time. It tries to reach the SP with a steep decrease in temperature from 54.14 °C to 53 °C at 36750 s. In the transient period the Top follows a smoother profile than Texp by increasing its value to 57.06 °C and then gradually decreases to reach the set point. This behaviour is mainly depending on how the PIDtemp has been tuned. The MARD is lower than the previous situation and has a value of 2%.

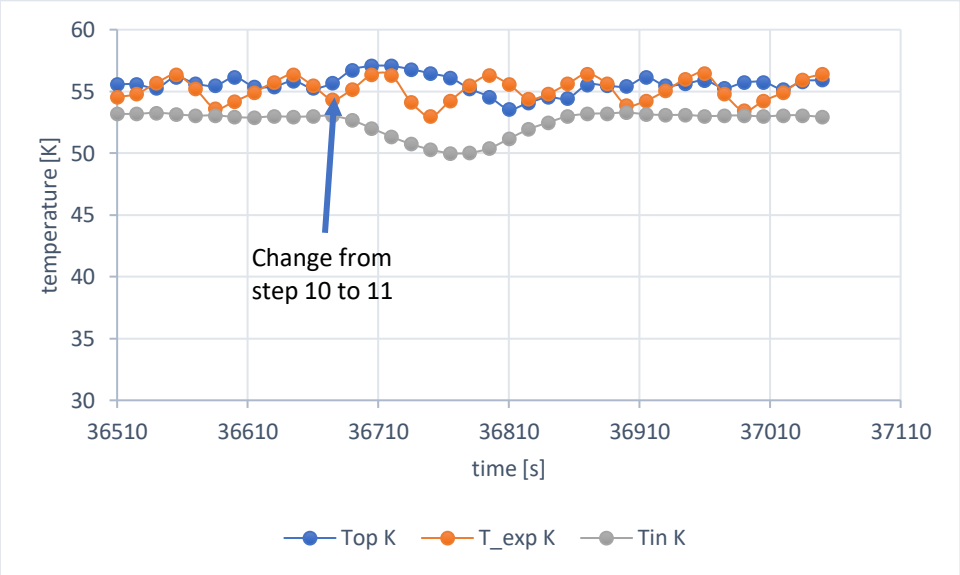

Figure 6.8: The dynamic profiles of the inlet, operation and experimental temperatures in partial load

The main reason to apply a dynamic simulation for a PEMEC system, is to calculate the H_2 production which in this case cannot be comparable with the real H_2 production since in the model is not included the purification stage. On the contrary, it can be compared with the theoretical H_2.

For the comparison of the flows of H_2, it was applied the power input that was used for the evaluation of the temperature (step 10 and step 11). Figure 6.9 shows the variation of hydrogen production among theoretical, simulated and experimental one. It is also depicted the variation of the electrical input. Both the theoretical and simulated H_2 production follow the profile of the electrical input, since they have direct connections with it. Although, the simulated production shows a small delay to adopt the change in the electrical input, and this is a good indicator for the simulated system since it appears to have an inertial on the change which approach better a real operation's behaviour. In the contrary the experimental H_2 , it cannot be predicted as it was expected since the purification stage is not implemented. The MARD between simulated and experimental is 11% and between the simulated and theoretical production is 19%. Generally, the simulated is predict better the real production since in the model there is a small amount of H_2 that due to permeability of the Hydrogen through the membrane is lost in the anode side, also there are some parasitic losses in the current

which are 1% (Faraday's efficiency) and lastly the delay of the system in the change of the electrical input. So, in a point the simulation can be used to give some reasonable results on the production of hydrogen before the purification stage.

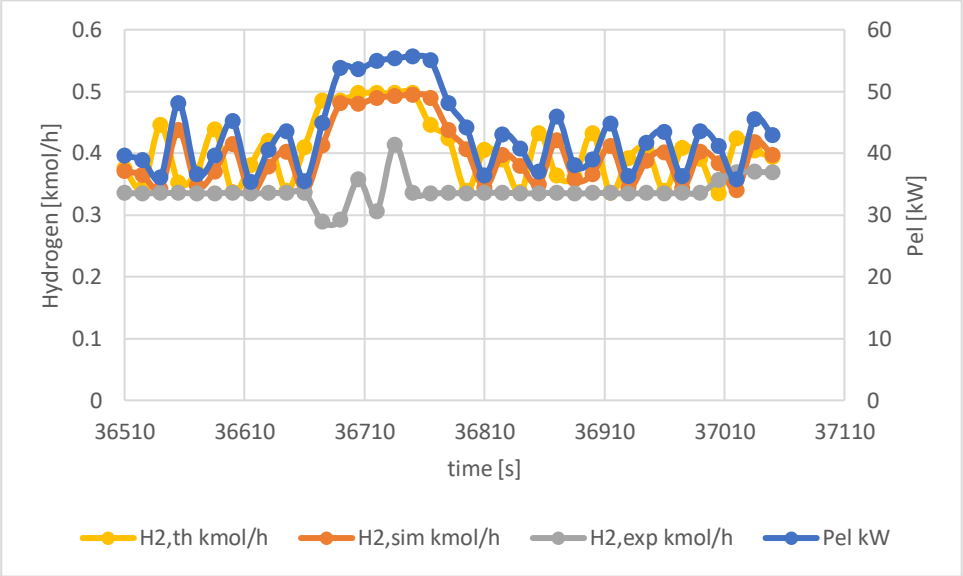

Figure 6.9: Dynamic profiles of the power, theoretical, simulated and experimental Hydrogen production.

In Figure 4.11, depicted the difference between the theoretical and the experimental production of hydrogen for the step 10 and 11 (608 to 618 mins), MARD was almost 15%. For the simulation when it was running on this time step was 11%. According to Proton On site company the Hydrogen that they lose in the purification stage in the peak load is almost 10%, very close with the result on the sample that the simulation was chosen to run.

7. Conclusions and Future Work

7.1 Conclusions

The current thesis succeeds to develop a stationary zero-dimension model for PEMEC which was implemented in a simulated system configuration based on a real process to analyze its behavior in a dynamic mode.

In section 3 an extended literature review was applied to identify reasonable values on the involved parameters that were used to set the stationary model. With this review, the thesis provides a simple model of mass balance equations, electrochemical relations and energy balance that can easily adapt with real electrolyzer stacks. The model offers a flexibility in terms of adding more complex equations based on a high order models (i.e.1-D 2-D) and test the results in terms of current-voltages figures (polarization curves).

In section 4, an analysis on experimental data was performed obtained by a commercial PEM electrolyzer system built by the company 'Proton On Site'. The experimental data of the current density, the voltage and the temperature were chosen to be tested. With this analysis, it was able to obtain suitable average values that were used for the calibration of the current model. Moreover, the analysis shows that the real system has a lot of perturbation in terms of current density, voltage and temperature when the electrical power varies. Since the electrical input profile was comparable to a typical solar panels electrical output for one day, the depicted and analyzed profile in Figure 4.1, Figure 4.2, Figure 4.3,Figure 4.4, Figure 4.9,Figure 4.10 and Figure 4.11 give additional information on how a PEM electrolyzer system will behave when couple with renewables to produce H_2 for energy storage. It is worth mentioning the profiles of Figure 4.10 and Figure 4.11 which show that the production of hydrogen (kmol) turns to be steady for each time step in partial load, but in peak load some hydrogen is lost in the purification stage since the electrolyzer works in the peak power where the system cannot demand more power to clean the purification columns. In the contrary, the system was penalized more in the partial load in terms of hydrogen loss, 28% to 45% comparing with the theoretical hydrogen production, while for power input from 25 kW to 55 kW the system has almost steady hydrogen loss around 15%. This may lead to the conclusion that for the system, it will be better to operate in the peak load range of power for the whole day due to the fact that the loss of hydrogen is strictly related with the efficiency of the system.

In section 5, it was found that the parameters which affect more the performance of the stack in a stationary model are: the exchange current and transfer coefficients in the Butler-Volmer's equation (see. **Eq. *3.32***) which are related with the activations losses, the resistance of the membrane which was related in the current model with the width of the membrane (t_{mem}) and lastly the ohmic losses which for the current thesis were related with the resistances of the electrodes and plates. For the cross-over of water from the anode to the cathode due to the electro-osmotic flow rate, the parameter of the electroosmotic drag coefficient did not appear to have any significant effect in the performance of the stack in terms of polarization curve, although it is important when the stack is tested in a real process. Cathode pressure did not appear to have any significant effect in terms of the

polarization curve when it changes from: a) 30 bars to 50 bars and b) from 30 bars to 10 bars. The increase of the cell voltage was 0.4% from 30 to 50 bars and was gradually increasing when current density was increased, while the decrease of cathode pressure (from 30 to 10 bars) leads to lower cell voltage. The relative difference was 0.8% at low current densities and was tended to decrease as current density was increased. The overall effect of both anode and cathode pressure change was less than 1%, but pressure needs more attention when the operation pressure is sufficiently high (100 bars) [77]. The model was calibrated based on the parameters by executing different calculations and comparing the results. The best result obtain, was when MARD was equal to 0.105%. The tested PEM electrolyzer has low activation losses since the exchange currents both in anode and cathode were closed to the lower limited values that was found in the literature. The transfer coefficients were almost symmetrical as most of the references had suggested. Moreover, the stack appears to have high ohmic losses, as indicated by the total electrical resistance of the electrodes and the plates. In addition, the width membrane reaches its upper limits which compounds the ohmic losses.

In section 6, the preliminary dynamic model, that was developed, predicts with good approximation the temperature and the current density profiles of the tested system. The dynamic performance of the components that were chosen to be added at the dynamic simulation (separators, pump and mixers) were not able to be tested due to lack of data on their size. However, a thermal inertial was added in the simulated system by sizing the heat exchanger respect to its volume and mass. The current model was not able to predict instantaneous hydrogen production flow rates due to the absence of a model for the purification section, which introduced oscillations in the outlet hydrogen flow rate. A model of the purification section would have required detailed information about the components and the control logics of that part of the process, which were not available. However, the simulated hydrogen production was calculated with a MARD 11% higher than the experimental hydrogen production. The latter results was roughly equal to the manufacturer's specification of hydrogen loss (10%) in the purification stage when the PEMEC operates in a peak load.

7.2 Future Work

The future works that need to be done are:

- ***Improvements on zero-dimension model:***

I. Some assumptions that were made in the model related to the geometrical parameters need to be verified or more data for this manner should be obtained.
II. A more analytical model can be performed in higher dimension analysis (1-D) and to be verified with the experimental data from the current work.
III. The model to be calibrated and validated with different experimental data sets of other commercial electrolyzers.

- ***Improvements on the preliminary dynamic system:***

I. Simulate the dynamic performance of the components concerning their size and materials.
II. Adding in the dynamic system a simulated block that represents the purification columns of hydrogen and test its validity with experimental data.
III. Apply different electrical input profiles and test the performance of the system.
IV. Adding in the dynamic system a simulated block that represents the compressed hydrogen for storage.
V. Perform a first and second law analysis in each component and to the whole system.
VI. Perform a complete validation of the model against a sufficient dataset of dynamic readings concerning reactant temperatures and flow rate.

8. Bibliography

[1] International Energy Agency, "Energy and climate change," 2015.

[2] *World Energy Balances*. Available: https://www.iea.org/statistics/balances/.

[3] *The Paris Agreement * Available: https://unfccc.int/process-and-meetings/the-paris-agreement/the-paris-agreement.

[4] International Energy Agency, "Energy access outlook 2017 from poverty to prosperity," IEA, 2017.

[5] *Sustainable Development Goals*. Available: https://sustainabledevelopment.un.org/?menu=1300.

[6] A. Awasthi, K. Scott and S. Basu, "Dynamic modeling and simulation of a proton exchange membrane electrolyzer for hydrogen production," *International Journal of Hydrogen Energy,* vol. 36, *(22),* pp. 14779-14786, 2011.

[7] K. Rajeshwar, R. McConnell and S. Licht, "Solar hydrogen generation," *Toward a Renewable Energy Future,* 2008.

[8] A. Ursua, L. M. Gandia and P. Sanchis, "Hydrogen Production from Water Electrolysis: Current Status and Future Trends," *Proceedings of the IEEE,* vol. 100, *(2),* pp. 410-426, 2012.

[9] B. Sørensen and G. Spazzafumo, *Hydrogen and Fuel Cells: Emerging Technologies and Applications.* Academic Press, 2018.

[10] J. D. Holladay, J. Hu, D. L. King and Y. Wang, "An overview of hydrogen production technologies," *Catalysis Today,* vol. 139, *(4),* pp. 244-260, 2009.

[11] C. Winter, "Hydrogen energy — Abundant, efficient, clean: A debate over the energy-system-of-change," *International Journal of Hydrogen Energy,* vol. 34, *(14, Supplement 1),* pp. S52, 2009.

[12] F. A. Felder and A. Hajos, "Using Restructured Electricity Markets in the Hydrogen Transition: The PJM Case," *Proceedings of the IEEE,* vol. 94, *(10),* pp. 1864-1879, 2006.

[13] J. O. Jensen, V. Bandur, N. J. Bjerrum, S. H. Jensen, S. Ebbesen, M. Mogensen, N. Tophoj and L. Yde, "Pre-investigation of water electrolysis," *Technical University of Denmark, Lyngby,* pp. 196, 2008.

[14] F. M. Sapountzi, J. M. Gracia, C. J. (. Weststrate, H. O. A. Fredriksson and J. W. (. Niemantsverdriet, "Electrocatalysts for the generation of hydrogen, oxygen and synthesis gas," *Progress in Energy and Combustion Science,* vol. 58, pp. 1-35, 2017.

[15] K. Zeng and D. Zhang, "Recent progress in alkaline water electrolysis for hydrogen production and applications," *Progress in Energy and Combustion Science,* vol. 36, *(3),* pp. 307-326, 2010.

[16] D. Todd, M. Schwager and W. Mérida, "Thermodynamics of high-temperature, high-pressure water electrolysis," *Journal of Power Sources,* vol. 269, pp. 424-429, 2014.

[17] J. C. Ganley, "High temperature and pressure alkaline electrolysis," *International Journal of Hydrogen Energy,* vol. 34, *(9),* pp. 3604-3611, 2009.

[18] M. Carmo, D. L. Fritz, J. Mergel and D. Stolten, "A comprehensive review on PEM water electrolysis," *International Journal of Hydrogen Energy,* vol. 38, *(12),* pp. 4901-4934, 2013. Available:

[19] A. H. Abdol Rahim, A. S. Tijani, S. K. Kamarudin and S. Hanapi, "An overview of polymer electrolyte membrane electrolyzer for hydrogen production: Modeling and mass transport," *Journal of Power Sources,* vol. 309, pp. 56-65, 2016.

[20] W. Nicholson and A. Carlisle, "Account of the new electrical or galvanic apparatus of Alessandro Volta and experiments performed with the same," *Journal of Natural Philosophy,* pp. 179-187, 1801.

[21] M. Faraday, "Experimental researches in electricit," Richard and John Edward Taylor, London, 1849.

[22] W. Kreuter and H. Hofmann, "Electrolysis: The important energy transformer in a world of sustainable energy," *International Journal of Hydrogen Energy,* vol. 23, *(8),* pp. 661-666, 1998.

[23] P. Millet, F. Andolfatto and R. Durand, "Design and performance of a solid polymer electrolyte water electrolyzer," *International Journal of Hydrogen Energy,* vol. 21, *(2),* pp. 87-93, 1996.

[24] P. Millet, T. Alleau and R. Durand, "Characterization of membrane-electrode assemblies for solid polymer electrolyte water electrolysis," *J. Appl. Electrochem.,* vol. 23, *(4),* pp. 322-331, 1993.

[25] H. Takenaka, E. Torikai, Y. Kawami and N. Wakabayashi, "Solid polymer electrolyte water electrolysis," *Int J Hydrogen Energy,* vol. 7, *(5),* pp. 397-403, 1982.

[26] M. Yamaguchi, K. Okisawa and T. Nakanori, "Development of high-performance solid polymer electrolyte water electrolyzer in WE-NET," in *IECEC-97 Proceedings of the Thirty-Second Intersociety Energy Conversion Engineering Conference (Cat. no. 97CH6203),* 1997, pp. 1958-1965.

[27] P. Millet, D. Dragoe, S. Grigoriev, V. Fateev and C. Etievant, "GenHyPEM: A research program on PEM water electrolysis supported by the European Commission," *International Journal of Hydrogen Energy,* vol. 34, *(11),* pp. 4974-4982, 2009.

[28] D. Bessarabov, H. Wang, H. Li and N. Zhao, *PEM Electrolysis for Hydrogen Production: Principles and Applications.* CRC press, 2016.

[29] Ø Ulleberg, "Modeling of advanced alkaline electrolyzers: a system simulation approach," *International Journal of Hydrogen Energy,* vol. 28, *(1),* pp. 21-33, 2003.

[30] Matthew A. Pellow,*a Christopher J. M. Emmott,bc Charles J. Barnhartd and Sally M. Bensonaef, "Hydrogen or batteries for grid storage? A net energy analysis," .

[31] A. Ursua, L. M. Gandia and P. Sanchis, "Hydrogen Production from Water Electrolysis: Current Status and Future Trends," *Proceedings of the IEEE,* vol. 100, *(2),* pp. 410-426, 2012. . DOI: 10.1109/JPROC.2011.2156750.

[32] Dmitri Bessarabov, Haijiang Wang, Hui Li and Nana Zhao, *PEM Electrolysis for Hydrogen Production. Principles and Applications.* London, New York: CRC Press Taylor & Francis Group, 2016.

[33] M. Ni, M. K. H. Leung and D. Y. C. Leung, "Technological development of hydrogen production by solid oxide electrolyzer cell (SOEC)," *International Journal of Hydrogen Energy,* vol. 33, *(9),* pp. 2337-2354, 2008.

[34] Jan Pawel Stempiena, Qiang Sunc and Siew Hwa Chan, "Solid Oxide Electrolyzer Cell Modeling: A Review," *Journal of Power Technologies,* vol. 4, pp. 216-246, 2013.

[35] Stefano Campanari, "High temperature fuel cells–MCFC, SOFC and SOEC " June 2017.

[36] M. N. Manage, D. Hodgson, N. Milligan, S. J. R. Simons and D. J. L. Brett, "A techno-economic appraisal of hydrogen generation and the case for solid oxide electrolyser cells," *International Journal of Hydrogen Energy,* vol. 36, *(10),* pp. 5782-5796, 2011.

[37] M. Ni, M. K. H. Leung and D. Y. C. Leung, "Technological development of hydrogen production by solid oxide electrolyzer cell (SOEC)," *Int J Hydrogen Energy,* vol. 33, *(9),* pp. 2337-2354, 2008.

[38] J. H. Russell, L. J. Nuttall and A. P. Fickett, "No title," *Hydrogen Generation by Solid Polymer Electrolyte Water Electrolysis.,* vol. 18, *(3),* pp. 24e40, 1973.

[39] W. T. Grubb, "Ionic migration in ion-exchange membranes," *J. Phys. Chem.,* vol. 63, *(1),* pp. 55-58, 1959.

[40] W. T. Grubb, "Batteries with Solid Ion Exchange Electrolytes," *J. Electrochem. Soc.,* vol. 106, *(4),* pp. 275-278, 1959.

[41] C. A. Martinson, G. van Schoor, K. R. Uren and D. Bessarabov, "Characterisation of a PEM electrolyser using the current interrupt method," *International Journal of Hydrogen Energy,* vol. 39, *(36),* pp. 20865-20878, 2014.

[42] B. Lee, J. Heo, S. Kim, C. Sung, C. Moon, S. Moon and H. Lim, "Economic feasibility studies of high-pressure PEM water electrolysis for distributed H2 refuelling stations," *Energy Conversion and Management,* vol. 162, pp. 139-144, 2018.

[43] M. Yamaguchi, M. Horiguchi and T. Nakanori, "Development of large-scale water electrolyser using solid polymer electrolyte in WE-NET," in 2000, pp. 274-281.

[44] Tsutomu Oi and Yoshinori Sakaki, "Optimum hydrogen generation capacity and current density of the PEM-type water electrolyzer operated only during the off-peak period of electricity demand," *Power Sources 129,* pp. 229-237, April, 2004.

[45] R. Savinell, "A Polymer Electrolyte for Operation at Temperatures up to 200°C," *Journal of the Electrochemical Society,* vol. 141, *(4),* pp. L46, 1994. . DOI: 10.1149/1.2054875.

[46] A. Ghielmi, P. Vaccarono, C. Troglia and V. Arcella, "Proton exchange membranes based on the short-side-chain perfluorinated ionomer," *Journal of Power Sources,* vol. 145, *(2),* pp. 108-115, 2005.

[47] Kirt A. Page, Kevin M. Cable and Robert B. Moore, "Molecular Origins of the Thermal Transitions and Dynamic Mechanical Relaxations in Perfluorosulfonate Ionomers," *American Chemical Society,* vol. 38(15), pp. 6472-6484, June, 2005.

[48] K. Kreuer, S. J. Paddison, E. Spohr and M. Schuster, "Transport in proton conductors for fuel-cell applications: simulations, elementary reactions, and phenomenology," *Chem. Rev.,* vol. 104, *(10),* pp. 4637-4678, 2004.

[49] G. A. Luduena, T. D. Kühne and D. Sebastiani, "Mixed Grotthuss and vehicle transport mechanism in proton conducting polymers from ab initio molecular dynamics simulations," *Chemistry of Materials,* vol. 23, *(6),* pp. 1424-1429, 2011.

[50] R. Parsons, "The kinetics of electrode reactions and the electrode material," *Surface Science,* vol. 2, pp. 418-435, 1964.

[51] S. Trasatti, "Electrocatalysis in the anodic evolution of oxygen and chlorine," *Electrochimica Acta,* vol. 29, *(11),* pp. 1503-1512, 1984.

[52] J. Gatineau, K. Yanagita and C. Dussarrat, "A new RuO4 solvent solution for pure ruthenium film depositions," *Microelectronic Engineering,* vol. 83, *(11-12),* pp. 2248-2252, 2006.

[53] Y. Koda, "Boiling points and ideal solutions of ruthenium and osmium tetraoxides," *Journal of the Chemical Society, Chemical Communications, (17),* pp. 1347-1348, 1986.

[54] S. Siracusano, V. Baglio, S. A. Grigoriev, L. Merlo, V. N. Fateev and A. S. Aricò, "The influence of iridium chemical oxidation state on the performance and durability of oxygen evolution catalysts in PEM electrolysis," *Journal of Power Sources,* vol. 366, pp. 105-114, 2017.

[55] E. Anderson, K. Ayers and C. Capuano, "R&D focus areas based on 60,000 hr life PEM water electrolysis stack experience," in *Proceedings of the First International Workshop on Durability and Degradation Issues in PEM Electrolysis Cells and its Components,* 2013, pp. 11-12.

[56] K. E. Ayers, E. B. Anderson, C. Capuano, B. Carter, L. Dalton, G. Hanlon, J. Manco and M. Niedzwiecki, "Research advances towards low cost, high efficiency PEM electrolysis," *ECS Transactions,* vol. 33, *(1),* pp. 3-15, 2010.

[57] T. Swamy, E. C. Kumbur and M. M. Mench, "Investigation of bipolar plate and diffusion media interfacial structure in PEFCs: A fractal geometry approach," *Electrochimica Acta,* vol. 56, *(8),* pp. 3060-3070, 2011.

[58] S. A. Grigoriev, P. Millet, S. A. Volobuev and V. N. Fateev, "Optimization of porous current collectors for PEM water electrolysers," *International Journal of Hydrogen Energy,* vol. 34, *(11),* pp. 4968-4973, 2009.

[59] A. Marshall, B. Børresen, G. Hagen, M. Tsypkin and R. Tunold, "Electrochemical characterisation of IrxSn1−xO2 powders as oxygen evolution electrocatalysts," *Electrochimica Acta,* vol. 51, *(15),* pp. 3161-3167, 2006.

[60] J. Cheng, H. Zhang, G. Chen and Y. Zhang, "Study of IrxRu1−xO2 oxides as anodic electrocatalysts for solid polymer electrolyte water electrolysis," *Electrochimica Acta,* vol. 54, *(26),* pp. 6250-6256, 2009.

[61] H. Tawfik, Y. Hung and D. Mahajan, "Metal bipolar plates for PEM fuel cell—A review," *Journal of Power Sources,* vol. 163, *(2),* pp. 755-767, 2007..

[62] S. Wang, J. Peng and W. Lui, "Surface modification and development of titanium bipolar plates for PEM fuel cells," *Journal of Power Sources,* vol. 160, *(1),* pp. 485-489, 2006.

[63] H. Jung, S. Huang, P. Ganesan and B. N. Popov, "Performance of gold-coated titanium bipolar plates in unitized regenerative fuel cell operation," *Journal of Power Sources,* vol. 194, *(2),* pp. 972-975, 2009.

[64] Y. Wang and C. Wang, "Transient analysis of polymer electrolyte fuel cells," *Electrochimica Acta,* vol. 50, *(6),* pp. 1307-1315, 2005.

[65] Y. Wang and C. Wang, "Two-phase transients of polymer electrolyte fuel cells," *J. Electrochem. Soc.,* vol. 154, *(7),* pp. B643, 2007.

[66] A. Bıyıkoğlu, "Review of proton exchange membrane fuel cell models," *International Journal of Hydrogen Energy,* vol. 30, *(11),* pp. 1181-1212, 2005.

[67] T. Yalcinoz and M. S. Alam, "Dynamic modeling and simulation of air-breathing proton exchange membrane fuel cell," *Journal of Power Sources,* vol. 182, *(1),* pp. 168-174, 2008.

[68] H. Görgün, "Dynamic modelling of a proton exchange membrane (PEM) electrolyzer," *Int J Hydrogen Energy,* vol. 31, *(1),* pp. 29-38, 2006.

[69] N. V. Dale, M. D. Mann and H. Salehfar, "Semiempirical model based on thermodynamic principles for determining 6kW proton exchange membrane electrolyzer stack characteristics," *Journal of Power Sources,* vol. 185, *(2),* pp. 1348-1353, 2008.

[70] C. Y. Biaku, N. V. Dale, M. D. Mann, H. Salehfar, A. J. Peters and T. Han, "A semiempirical study of the temperature dependence of the anode charge transfer coefficient of a 6kW PEM electrolyzer," *International Journal of Hydrogen Energy,* vol. 33, *(16),* pp. 4247-4254, 2008.

[71] M. Santarelli, P. Medina and M. Calì, "Fitting regression model and experimental validation for a high-pressure PEM electrolyzer," *International Journal of Hydrogen Energy,* vol. 34, *(6),* pp. 2519-2530, 2009.

[72] F. Marangio, M. Santarelli and M. Calì, "Theoretical model and experimental analysis of a high pressure PEM water electrolyser for hydrogen production," *International Journal of Hydrogen Energy,* vol. 34, *(3),* pp. 1143-1158, 2009.

[73] M. E. Lebbal and S. Lecœuche, "Identification and monitoring of a PEM electrolyser based on dynamical modelling," *International Journal of Hydrogen Energy,* vol. 34, *(14),* pp. 5992-5999, 2009.

[74] R. García-Valverde, N. Espinosa and A. Urbina, "Simple PEM water electrolyser model and experimental validation," *International Journal of Hydrogen Energy,* vol. 37, *(2),* pp. 1927-1938, 2012.

[75] K. Onda, T. Kyakuno, K. Hattori and K. Ito, "Prediction of production power for high-pressure hydrogen by high-pressure water electrolysis," *Journal of Power Sources,* vol. 132, *(1),* pp. 64-70, 2004.

[76] P. Choi, D. G. Bessarabov and R. Datta, "A simple model for solid polymer electrolyte (SPE) water electrolysis," *Solid State Ionics,* vol. 175, *(1),* pp. 535-539, 2004.

[77] H. Kim, M. Park and K. S. Lee, "One-dimensional dynamic modeling of a high-pressure water electrolysis system for hydrogen production," *International Journal of Hydrogen Energy,* vol. 38, *(6),* pp. 2596-2609, 2013.

[78] H. Ito, T. Maeda, A. Nakano and H. Takenaka, "Properties of Nafion membranes under PEM water electrolysis conditions," *International Journal of Hydrogen Energy,* vol. 36, *(17),* pp. 10527-10540, 2011.

[79] P. Medina and M. Santarelli, "Analysis of water transport in a high pressure PEM electrolyzer," *International Journal of Hydrogen Energy,* vol. 35, *(11),* pp. 5173-5186, 2010.

[80] H. Görgün, "Dynamic modelling of a proton exchange membrane (PEM) electrolyzer," *Int J Hydrogen Energy,* vol. 31, *(1),* pp. 29-38, 2006.

[81] T. A. Zawodzinski, T. E. Springer, J. Davey, R. Jestel, C. Lopez, J. Valerio and S. Gottesfeld, "A comparative study of water uptake by and transport through ionomeric fuel cell membranes," *J. Electrochem. Soc.,* vol. 140, *(7),* pp. 1981-1985, 1993.

[82] M. Ise, K. D. Kreuer and J. Maier, "Electroosmotic drag in polymer electrolyte membranes: an electrophoretic NMR study," *Solid State Ionics,* vol. 125, *(1),* pp. 213-223, 1999.

[83] Z. Abdin, C. J. Webb and E. M. Gray, "Modelling and simulation of a proton exchange membrane (PEM) electrolyser cell," *International Journal of Hydrogen Energy,* vol. 40, *(39),* pp. 13243-13257, 2015.

[84] T. Yigit and O. F. Selamet, "Mathematical modeling and dynamic Simulink simulation of high-pressure PEM electrolyzer system," *International Journal of Hydrogen Energy,* vol. 41, *(32),* pp. 13901-13914, 2016.

[85] S. Shimpalee, S. Dutta and J. W. Van Zee, "Numerical prediction of local temperature and current density in a PEM fuel cell," *Asme-Publications-Htd,* vol. 366, pp. 1-10, 2000.

[86] G. Lin, W. He and T. Van Nguyen, "Modeling liquid water effects in the gas diffusion and catalyst layers of the cathode of a PEM fuel cell," *J. Electrochem. Soc.,* vol. 151, *(12),* pp. A2006, 2004.

[87] M. M. Tomadakis and S. V. Sotirchos, "Ordinary and transition regime diffusion in random fiber structures," *AIChE J.,* vol. 39, *(3),* pp. 397-412, 1993.

[88] J. H. Nam and M. Kaviany, "Effective diffusivity and water-saturation distribution in single- and two-layer PEMFC diffusion medium," *International Journal of Heat and Mass Transfer,* vol. 46, *(24),* pp. 4595-4611, 2003.

[89] Ν Κουλουμπή, "Ηλεκτροχημεία," *Εκδόσεις Συμεών,* 2002.

[90] C. Marr and X. Li, "An engineering model of proton exchange membrane fuel cell performance," *ARI-an International Journal for Physical and Engineering Sciences,* vol. 50, *(4),* pp. 190-200, 1997.

[91] Z. Ke, L. Cheng-Feng and Z. Zhen-Gang, "Measurement of electrical conductivity of porous titanium and Ti6Al4V prepared by the powder metallurgy method," *Chinese Physics Letters,* vol. 24, *(1),* pp. 187, 2007.

[92] K. E. Ayers, E. B. Anderson, C. Capuano, B. Carter, L. Dalton, G. Hanlon, J. Manco and M. Niedzwiecki, "Research advances towards low cost, high efficiency PEM electrolysis," *ECS Transactions,* vol. 33, *(1),* pp. 3-15, 2010.

[93] T. E. Springer, T. A. Zawodzinski and S. Gottesfeld, "Polymer electrolyte fuel cell model," *J. Electrochem. Soc.,* vol. 138, *(8),* pp. 2334-2342, 1991.

[94] P. Millet, A. Ranjbari, F. de Guglielmo, S. A. Grigoriev and F. Auprêtre, "Cell failure mechanisms in PEM water electrolyzers," *International Journal of Hydrogen Energy,* vol. 37, *(22),* pp. 17478-17487, 2012.

[95] F. Incropera and D. DeWitt, "Introduction to heat transfer," 1985.

[96] *E.I. du Pont de Nemours and Company*. Available: http://www.dupont.com.